325
3/6/64

ORNL-3513
UC-34 – Physics
TID-4500 (26th ed.)

MEASUREMENTS OF RADIATION INTENSITIES IN VERTICAL CONCRETE-LINED HOLES AND AN ADJOINING TUNNEL AT THE TSF TOWER SHIELDING FACILITY

V. R. Cain
C. E. Clifford
L. B. Holland

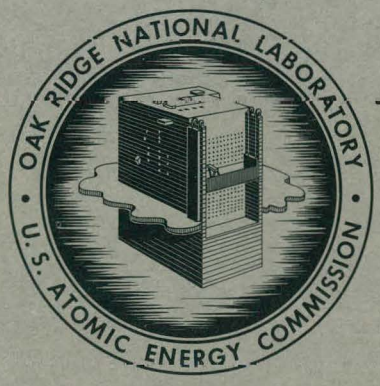

OAK RIDGE NATIONAL LABORATORY
operated by
UNION CARBIDE CORPORATION
for the
U.S. ATOMIC ENERGY COMMISSION

DISCLAIMER

Printed in USA. Price: $2.00 Available from the
Office of Technical Services
U. S. Department of Commerce
Washington 25, D. C.

ORNL-3513*

Contract No. W-7405-eng-26

Neutron Physics Division

MEASUREMENTS OF RADIATION INTENSITIES IN VERTICAL CONCRETE-LINED HOLES AND AN ADJOINING TUNNEL AT THE TOWER SHIELDING FACILITY**

by

V. R. Cain, C. E. Clifford, L. B. Holland
and the Tower Shielding Facility Staff

MARCH 1964

*Referred to in earlier documents as ORNL-TM-285.
**Work performed under Contracts AF-(04-694)-62-2 and OCD-OS-62-145.

OAK RIDGE NATIONAL LABORATORY
Oak Ridge, Tennessee
operated by
UNION CARBIDE CORPORATION
for the
U.S. ATOMIC ENERGY COMMISSION

THIS PAGE

WAS INTENTIONALLY

LEFT BLANK

TABLE OF CONTENTS

THIS PAGE

WAS INTENTIONALLY

LEFT BLANK

ABSTRACT

Fast-neutron and gamma-ray dose rates within 4-ft-diam, 20-ft-deep, concrete-lined holes have been measured at the ORNL Tower Shielding Facility. The radiation source was the Tower Shielding Reactor II (TSR-II) enclosed in a shield which modified the neutron to gamma-ray ratio of the reactor leakage spectrum to more closely resemble that of a weapon spectrum. The holes were located at horizontal distances of 100, 228, and 450 ft from the reactor. From the hole at 100 ft extended a reinforced concrete-lined tunnel, 6 ft high, 2 1/2 ft wide, and 20 ft long,with its ceiling 10 ft below ground level. The experimental measurements consisted of vertical traverses in the three holes and horizontal traverses in the tunnel. The parameters varied included distance from the reactor, the angle of elevation of the reactor with respect to the horizontal at the hole, and the material and thickness of the shield over the hole. Reactor elevation angles ranged from 15 to 90°. The shields over the holes were concrete, iron, and laminated iron and concrete slabs.

INTRODUCTION

In order to solve some of the problems which face the military and civil defense organizations, a thorough understanding must be gained of the transport of prompt radiation, particularly of neutrons, through the atmosphere and subsequently through shields which are required for hardened or radiation-safe installations. An experimental program was undertaken at the Tower Shielding Facility (TSF) to provide measurements of the neutron and gamma-ray intensities in a series of configurations which represent typical installations, with the TSF reactor utilized as a source of radiation. The spectrum leaking from the reactor was somewhat modified by a thin shield of lead and water to give a neutron spectrum more typical of that from fission weapons. Neutron and gamma-ray intensities were measured in three rather deep concrete-lined cylindrical wells. Each well was located at a different distance from the reactor and could be covered by various arrangements of concrete and iron shields. The well nearest the reactor was joined by a horizontal rectangular tunnel which had sufficient earth shielding above it to assure that only radiation scattered down the well would contribute to the dose in the tunnel.

Measurements were taken for both shielded and unshielded well configurations with the reactor at various altitudes and positions to simulate a number of burst configurations. Since a major part of the gamma-ray dose rate in the very high dose-rate time periods immediately after a weapon explosion results from neutron interactions with the atmosphere and with shielding materials, the TSF experimental information is useful for checking the analytical methods for predicting the intensities of the gamma rays as well as the neutron dose rates which are produced in these configurations.

EXPERIMENTAL PROGRAM

The TSF, a general view of which is shown in Fig. 1, is described in detail elsewhere.[1] Its distinguishing features are four 315-ft-high towers and a reactor (the TSR-II) which can be lifted to heights ranging

1. L. B. Holland and C. E. Clifford, Description of the Tower Shielding Reactor II and Proposed Preliminary Experiments, ORNL-2747 (1959).

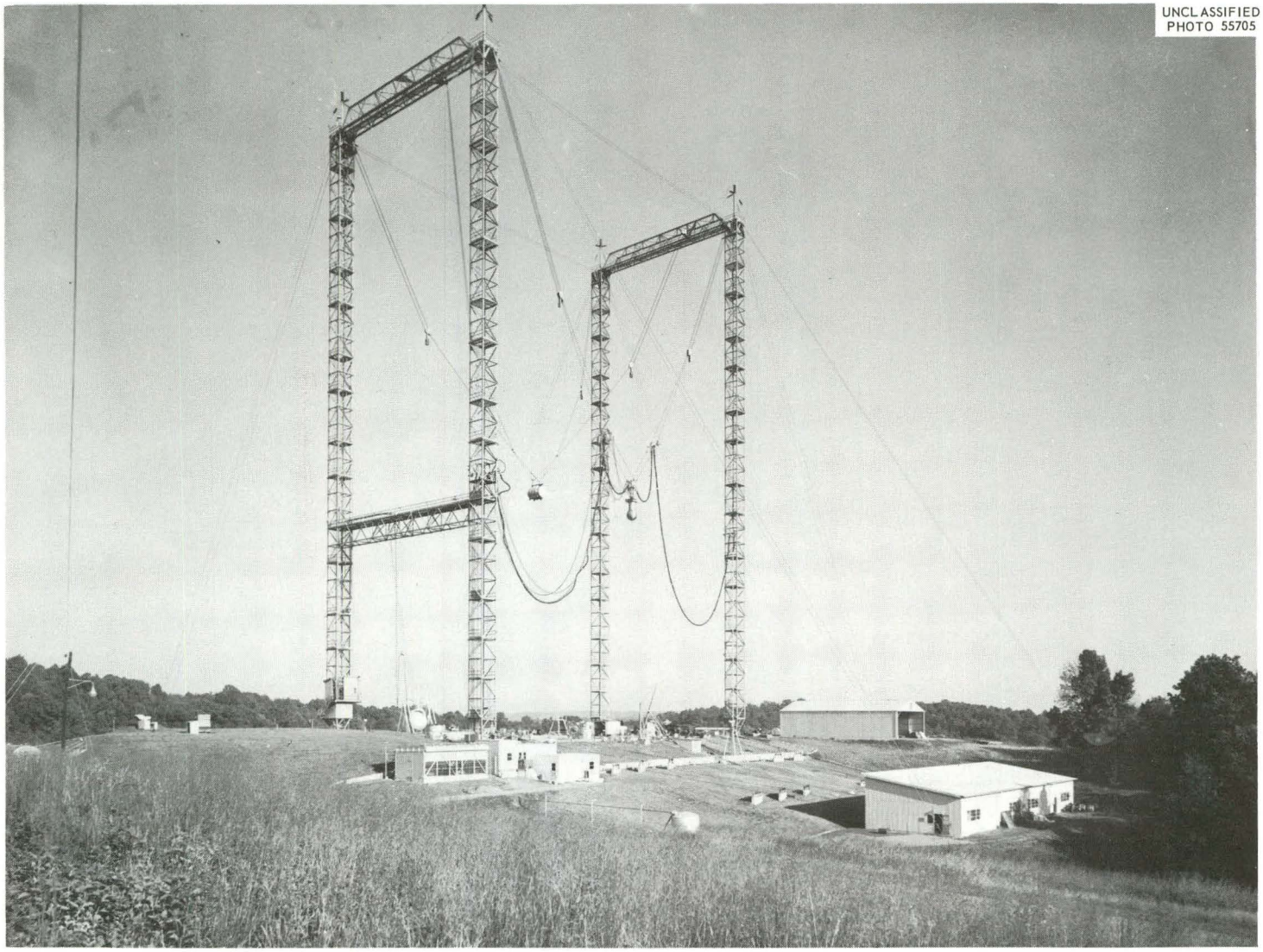

Fig. 1. The ORNL Tower Shielding Facility.

from 0 to 200 ft above the ground. The reactor is always positioned in the plane between the two towers from which it is suspended.

The TSR-II itself is a heterogeneous, light-water-moderated and -cooled reactor in which the fuel plates are shaped to form a spherical core and thus to give a leakage current that is very nearly spherically symmetric. For the present work the TSR-II was enclosed in a shield identified as COOL-I and shown in Fig. 2. The purpose of the shield was to obtain a leakage spectrum having a neutron to gamma-ray ratio more closely resembling that of a weapon spectrum. The neutron spectrum emitted from the COOL-I shield is shown in Fig. 3.

A plan of the experimental site is shown in Fig. 4. Three reinforced concrete-lined holes 4 ft in diameter and 20 ft deep were constructed at the locations shown, and a rectangular reinforced concrete-lined tunnel was constructed to extend horizontally from Hole No. 1. The configuration of Hole No. 1 is shown in Fig. 5; the other two holes were identical in construction but were without tunnels. The tunnel was 6 ft high, 2 1/2 ft wide, and 20 ft long, and its ceiling was 10 ft below ground level.

Most of the experimental measurements were taken within Hole No. 1 and its tunnel, and for these measurements the reactor was maintained at a constant 100-ft distance from the center of the top of the hole. The parameters varied were the reactor elevation angle, γ (the angle which a line from the center of the top of the hole to the center of the reactor made with the horizontal), and the thicknesses and types of shielding covering the hole. Typical elevation angles were 15, 30, 45, 60, and 90° (directly over the hole), although not all angles were used with all hole covers. For the data obtained in Hole No. 2 the reactor was maintained at an altitude of 228 ft and an elevation angle of 45°; for the measurements in Hole No. 3 it was at 450 ft and 15°.

The shields or covers for the holes were of three basic types: slabs of ordinary reinforced portland cement concrete from 3 to 42 in. thick; a 3 1/2-in.-thick slab of iron above concrete slabs of various thicknesses; and an iron-concrete-iron sandwich in which the top layer was always 3 1/2 in. thick, the middle layer varied in thickness, and the bottom layer was either 1 1/2 or 3 1/2 in. thick. In one case an iron-air-iron configuration was used.

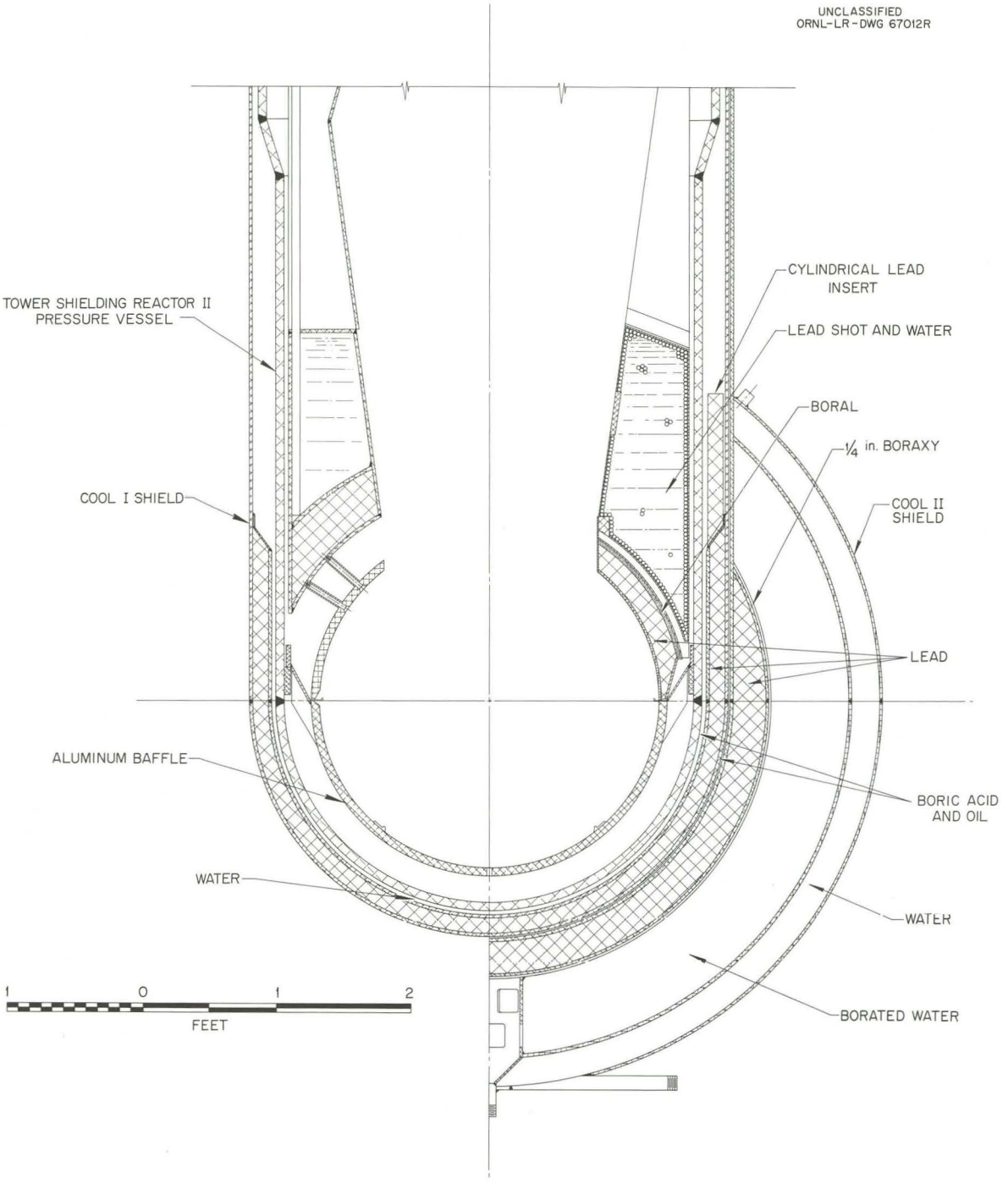

Fig. 2. COOL-I and COOL-II Tower Shielding Reactor II Shields. The COOL-II shield was not used in the present work.

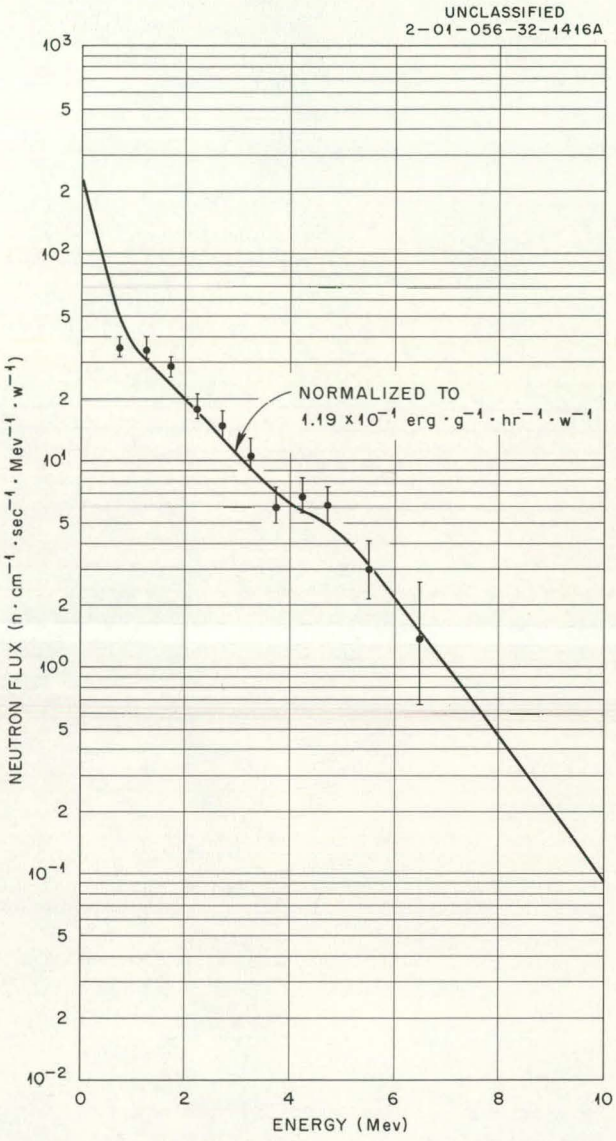

Fig. 3. Spectrum of Neutrons from COOL-I Shield.

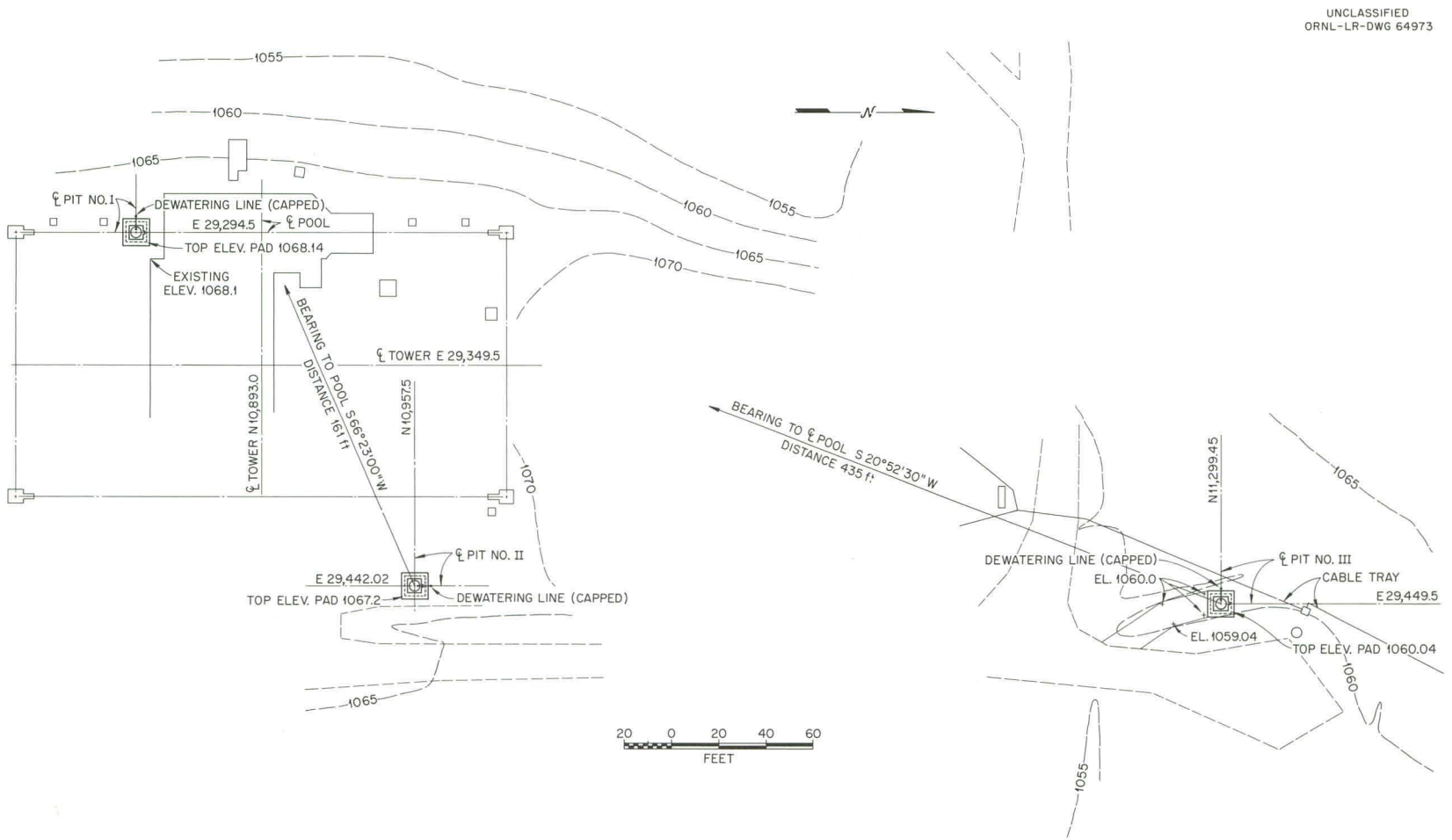

Fig. 4. Relative Positions of Cylindrical Holes at TSF.

UNCLASSIFIED
2-01-056-33D-1218

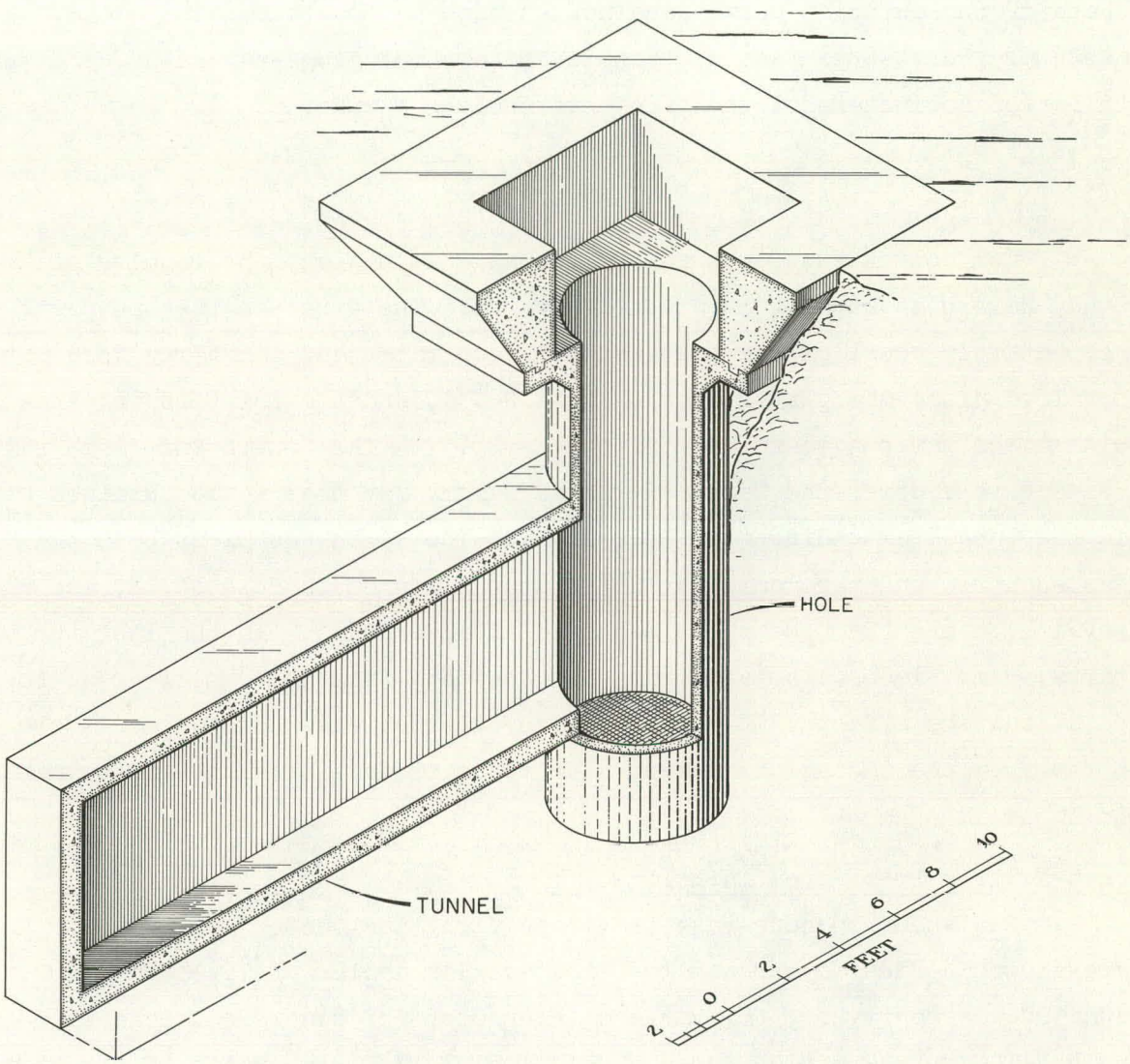

Fig. 5. Cutaway View of Hole No. 1 and Tunnel.

Fast-neutron and gamma-ray dose rates were measured along the axis of each hole and along a horizontal line 27 or 30.5 in. above the floor of the tunnel. Dose rates vs detector position were plotted by automatic equipment and were confirmed by separate counts taken (usually) at the beginning, middle, and end of each traverse and plotted by hand. In analyzing the data, the plotted curve was adjusted to the hand points, with the shape of the autoplot curve retained as much as possible. The detectors used were Hurst-type fast-neutron dosimeters and gamma-ray anthracene scintillation dosimeters of the type described by Maerker et al.[2]

RESULTS

For convenience in presentation and discussion, the results of this study have been separated into seven parts. The first and second parts respectively consider the fast-neutron dose rates and gamma-ray dose rates obtained along the center line of Hole No. 1, and the third is concerned with miscellaneous measurements in Hole No. 1. The fourth and fifth parts respectively cover the fast-neutron and gamma-ray dose rates obtained within the tunnel extending from Hole No. 1. The sixth describes both the fast-neutron and the gamma-ray dose rates measured in Hole No. 2, and the seventh covers the dose rates measured in Hole No. 3. In the last two parts, comparisons also are made with the data from Hole No. 1 so as to point out the effects, if any, caused by the increased distance of Hole No. 3 from the radiation source. The types of data obtained are summarized in Table 1.

Fast-Neutron Dose Rates in Hole No. 1

Fast-neutron dose-rate traverses along the center line of Hole No.1 are shown in Figs. 6 through 10 for elevation angles of 15, 30, 45, 60, and 90°, respectively, for various thicknesses of concrete shield over the hole. The data are plotted as a function of ℓ/D, the ratio of detector depth in the hole to its diameter. The data will be most useful in this form, since Blizard et al.[3] have previously demonstrated that, given

2. R. E. Maerker et al., In-Air Radiation Measurements in the Vicinity of the Tower Shielding Reactor II, ORNL-3288 (1963).
3. E. P. Blizard et al., ORNL-TM-253 (Aug. 30, 1962) (classified).

Table 1. Data Plot Locater

Shield Material	Shield Thickness (in.)	Reactor Elevation Angle (deg)	Figure No.	Notes
	Fast-Neutron Dose Rate vs ℓ/D; Hole No. 1			
Concrete	0,3,6,12,18,24,36	15	6	Figs. 6 through 104 appear at the end of this report
	0,3,6,18	30	7	
	3,6,12,18,24,30	45	8	
	0,6,12,18,30	60	9	
	0,6,12,30	90	10	
	0,6,12,18,24,36	15	11	Fit to $\ell n(1+r^2/\ell^2)^{\frac{1}{2}}$
	0,3,6,18	30	12	
	0,6,12,18,24,36	45	13	
	0,6,12,18,30	60	14	
Fe	$3\frac{1}{2}$	15,45	16	
Fe-concrete	$3\frac{1}{2}$ Fe, 3 concrete	15,45	17	
	$3\frac{1}{2}$ Fe, 6 concrete	15,45	18	
	$3\frac{1}{2}$ Fe, 12 concrete	15,45	19	
Fe-concrete-Fe	$3\frac{1}{2}$ Fe, 3 concrete, $1\frac{1}{2}$ Fe	15,45	21	
	$3\frac{1}{2}$ Fe, 6 concrete, $1\frac{1}{2}$ Fe	15,45	22	
	$3\frac{1}{2}$ Fe, 9 concrete, $1\frac{1}{2}$ Fe	15,45	23	
	$3\frac{1}{2}$ Fe, 12 concrete, $1\frac{1}{2}$ Fe	15,45	24	
	$3\frac{1}{2}$ Fe, 15 concrete, $1\frac{1}{2}$ Fe	15,45	25	
Fe-air-Fe	$3\frac{1}{2}$ Fe, 12 air, $3\frac{1}{2}$ Fe	15,45	27	
Fe-concrete-Fe	$3\frac{1}{2}$ Fe, 3 concrete, $3\frac{1}{2}$ Fe	15,45	28	
	$3\frac{1}{2}$ Fe, 6 concrete, $3\frac{1}{2}$ Fe	15,45	29	
	$3\frac{1}{2}$ Fe, 9 concrete, $3\frac{1}{2}$ Fe	15,45	30	
	$3\frac{1}{2}$ Fe, 12 concrete, $3\frac{1}{2}$ Fe	15,45	31	
	$3\frac{1}{2}$ Fe, 15 concrete, $3\frac{1}{2}$ Fe	15,45	32	

Table 1. (Cont.)

Shield Material	Shield Thickness (in.)	Reactor Elevation Angle (deg)	Figure No.	Notes
	Fast-Neutron Dose Rate vs ℓ/D; Hole No. 2			
Concrete	0,3,6,12,18,24,30	45	80	
Fe	0,1½,5,7	45	82	
Concrete-Fe	15 concrete, 3½ Fe	45	82	
Fe-concrete-Fe	3½ Fe, 15 concrete, 1½ Fe	45	82	
None		45	84	Shows result of varying radial position of dosimeter within Hole 2
Concrete	0,6,12,18	45	85	Comparison with Hole 1 data
	Fast-Neutron Dose Rate vs ℓ/D; Hole No. 3			
Concrete	0,3,6,12	15	95	
	0,3,6,12	15	97	Comparison with Hole 1 data
Fe	0,1½,3½,5,7	15	98	
Fe-concrete-Fe	3½ Fe, 6 concrete, 1½ Fe	15	98	
	3½ Fe, 6 concrete, 3½ Fe	15	98	
	3½ Fe, 15 concrete, 3½ Fe	15	98	With and without 1/4 in. boral

Table 1. (Cont.)

Shield Material	Shield Thickness (in.)	Reactor Elevation Angle (deg)	Figure No.	Notes
		Fast-Neutron Dose Rate vs Shield Thickness		
Concrete	0 to 36	15,30,45,60	15	
Fe-concrete	$3\frac{1}{2}$ Fe, 0 to 12 concrete	15,45	20	Hole No. 1; ℓ/D = 1,2,3
Fe-concrete-Fe	$3\frac{1}{2}$ Fe, 0-15 concrete, $1\frac{1}{2}$ Fe	15,45	26	
	$3\frac{1}{2}$ Fe, 0-15 concrete, $3\frac{1}{2}$ Fe	15,45	33	
Concrete	0 to 30	45	81	Hole No. 2; ℓ/D = 1,2,3
Fe	0 to 7	45	83	
Concrete	0 to 18	45	86	Comparison: Hole 1 vs Hole 2; ℓ/D = 1,2,3
	0 to 12	15	96	Comparison: Hole 1 vs Hole 3; ℓ/D = 1,2,3
Fe	0 to 7	15	99	Hole No. 3; ℓ/D = 1,2,3
		Fast-Neutron Dose Rate vs γ, Reactor Elevation Angle		
None		15 to 85	61	Hole No. 1; ℓ/D = 3, 3.75
		Gamma-Ray Dose Rate vs ℓ/D; Hole No. 1		
Concrete	0,3,6,12,18,24,30	15	34	
	0,3,6,18	30	35	
	0,3,6,18,24,30	45	36	
	0,3,6,12,18,30	60	37	
	0,6,12,30	90	38	

Table 1. (Cont.)

Shield Material	Shield Thickness (in.)	Reactor Elevation Angle (deg)	Figure No.	Notes
		Gamma-Ray Dose Rate vs ℓ/D; Hole No. 1 (Cont.)		
Fe	$3\frac{1}{2}$	15,45	40	
Fe-concrete	$3\frac{1}{2}$ Fe, 3 concrete	15,45	41	
	$3\frac{1}{2}$ Fe, 6 concrete	15,45	42	
	$3\frac{1}{2}$ Fe, 12 concrete	15,45	43	
Fe-concrete-Fe	$3\frac{1}{2}$ Fe, 3 concrete, $1\frac{1}{2}$ Fe	15,45	45	
	$3\frac{1}{2}$ Fe, 6 concrete, $1\frac{1}{2}$ Fe	15,45	46	
	$3\frac{1}{2}$ Fe, 9 concrete, $1\frac{1}{2}$ Fe	15,45	47	
	$3\frac{1}{2}$ Fe, 12 concrete, $1\frac{1}{2}$ Fe	15,45	48	
	$3\frac{1}{2}$ Fe, 15 concrete, $1\frac{1}{2}$ Fe	15,45	49	
Fe-air-Fe	$3\frac{1}{2}$ Fe, 12 air, $3\frac{1}{2}$ Fe	15,45	51	
Fe-concrete-Fe	$3\frac{1}{2}$ Fe, 3 concrete, $3\frac{1}{2}$ Fe	15,45	52	
	$3\frac{1}{2}$ Fe, 6 concrete, $3\frac{1}{2}$ Fe	15,45	53	
	$3\frac{1}{2}$ Fe, 9 concrete, $3\frac{1}{2}$ Fe	15,45	54	
	$3\frac{1}{2}$ Fe, 12 concrete, $3\frac{1}{2}$ Fe	15,45	55	
	$3\frac{1}{2}$ Fe, 15 concrete, $3\frac{1}{2}$ Fe	15,45	56	
		Gamma-Ray Dose Rate vs ℓ/D; Hole No. 2		
Concrete	0,6,12,18,24,30	45	87	
Fe	0,$1\frac{1}{2}$,5,7	45	89	
Concrete-Fe	15 concrete, $3\frac{1}{2}$ Fe	45	89	
Fe-concrete-Fe	$3\frac{1}{2}$ Fe, 15 concrete, $1\frac{1}{2}$ Fe	45	89	

Table 1. (Cont.)

Shield Material	Shield Thickness (in.)	Reactor Elevation Angle (deg)	Figure No.	Notes
		Gamma-Ray Dose Rate vs ℓ/D; Hole No. 2 (Cont.)		
None		45	91	Shows results of varying radial position of dosimeter within Hole No. 2
Concrete	0,6,18,24	45	92	Comparison with Hole 1 data
		Gamma-Ray Dose Rate vs ℓ/D; Hole No. 3		
Concrete	0,3,6,12	15	100	
Fe	$1\frac{1}{2}$,$3\frac{1}{2}$,5,7	15	101	
Fe-concrete-Fe	$3\frac{1}{2}$ Fe, 6 concrete, $1\frac{1}{2}$ Fe	15	101	
	$3\frac{1}{2}$ Fe, 6 concrete, $3\frac{1}{2}$ Fe	15	101	
	$3\frac{1}{2}$ Fe, 15 concrete, $3\frac{1}{2}$ Fe	15	101	With and without 1/4-in. boral
Polyethylene-Fe	2 polyethylene, $3\frac{1}{2}$ Fe	15	101	
Concrete	0,3,6,12	15	102	Comparison: Hole 1 vs Hole 3

Table 1. (Cont.)

Shield Material	Shield Thickness (in.)	Reactor Elevation Angle (deg)	Figure No.	Notes
		Gamma-Ray Dose Rate vs Shield Thickness		
Concrete	0 to 35	15,30,45,60	39	Hole No. 1, ℓ/D = 1,2,3
Fe-concrete	$3\frac{1}{2}$ Fe, 0-12 concrete	15,45	44	
Fe-concrete-Fe	$3\frac{1}{2}$ Fe, 0-15 concrete, $1\frac{1}{2}$ Fe	15,45	50	
	$3\frac{1}{2}$ Fe, 0-15 concrete, $3\frac{1}{2}$ Fe	15,45	57	
Concrete	0 to 30	45	88	Hole No. 2, ℓ/D = 1,2,3
Fe	0 to 7	45	90	
Concrete	0 to 24	45	93	Comparison: Hole No. 1 vs Hole No. 2; ℓ/D = 1,2,3
	0 to 12	15	103	Comparison: Hole No. 1 vs Hole No. 3; ℓ/D = 1,2,3
Fe	0 to 7	15	104	Comparison: Hole No. 1 vs Hole No. 3; ℓ/D = 1,2,3
Fe-concrete-Fe	$3\frac{1}{2}$ Fe, 0-15 concrete, $1\frac{1}{2}$-$3\frac{1}{2}$ Fe	15,45	59	Thickness plotted in g/cm^2 ℓ/D = 2
	$3\frac{1}{2}$ Fe, 0-15 concrete, $1\frac{1}{2}$-$3\frac{1}{2}$ Fe	15,45	60	Thickness plotted in g/cm^2 ℓ/D = 3

Table 1 (Cont.)

Shield Thickness	Shield Thickness (in.)	Reactor Elevation Angle (deg)	Figure No.	Notes
		Gamma-Ray Dose Rate vs γ, Reactor Elevation Angle		
None		15 to 90	62	Hole No. 1; $\ell/D = 3$
		Fast-Neutron Dose Rate vs Distance in Tunnel		
None		15,45,90,	64	Dosimeter at 30.5 and 66.3 in. from tunnel floor
None		15,30,45,60,90	65	Modifications in Hole 1 and tunnel.
Fe	$\frac{1}{2}$ Fe on Hole 1	15,30,45,60,90	66	Comparison with no-shield data
	1 Fe on Hole 1	15,30,45,60,90	67	Modifications in Hole 1 and tunnel
	1 Fe on Hole 1	45,90	68	Brick wall across tunnel
	3 Fe on Hole 1	45,90	69	Comparison with no-shield data
	3 concrete on Hole 1	15,30,45,60	70	
Fe-concrete	1 Fe, 3 concrete on Hole 1	60,90	71	

Table 1. (Cont.)

Shield Material	Shield Thickness (in.)	Reactor Elevation Angle (deg)	Figure No.	Notes
		Gamma-Ray Dose Rate vs Distance in Tunnel		
None		15,45,90	72	Dosimeter at 27 and 61 in. from tunnel floor
None		15,30,45,60,90	73	Modifications in Hole 1 and tunnel
Fe	$\frac{1}{2}$ Fe on Hole 1	15,30,45,60,90	74	Comparison with no-shield data
	1 Fe on Hole 1	15,30,45,60,90	75	Modifications in Hole 1 and tunnel
	1 Fe on Hole 1	45,90	76	Brick wall across tunnel
	3 Fe on Hole 1	15,45,90	77	Comparison with no-shield data
Concrete	3 concrete on Hole 1	15,30,45,60,90	78	
Fe-concrete	1 Fe, 3 concrete on Hole 1	60,90	79	Comparison with 3-in. concrete data

Table 1. (Cont.)

Shield Material	Shield Thickness (in.)	Reactor Elevation Angle (deg)	Figure No.	Notes
		Thermal-Neutron Flux vs Distance from Top of Shield		
Fe-concrete-Fe	$3\frac{1}{2}$ Fe, 15 concrete, $3\frac{1}{2}$ Fe	15,30	58	Au and Dy foil data; Hole 1
Concrete	Traverse through 12 in.	45	94	Also in nearby gravel; Hole 2
		Thermal-Neutron Flux vs γ, Reactor Elevation Angle; Hole 1		
None		15 to 90	63	$\ell/D = 3, 3.75$

the same source, the direct and reflected doses measured in this experiment can be applied to any geometrically similar cylinders having detectors placed in geometrically similar positions (that is, at the same ℓ/D positions). Initial study of these data[3] had placed the point at which the ℓ/D ratio should be zero at the bottom of the shield slab, but it now appears that the best fit to simple theory is achieved by placing the zero point at ground surface. In other words, the dose rate behaves as though the source were spread over the top surface of the shield. In using the data of these figures it should be observed that for compactness most curves have been displaced by 1, 2, or 3 factors of 10, which has been indicated on each curve.

Analysis of the data plotted in Figs. 6-10 shows that the variation in neutron dose rate with depth in the hole can be represented by an expression of the form

$$D_N = k \ln(1 + r^2/\ell^2)^{1/2} \quad , \qquad (1)$$

where D_N is the fast-neutron dose rate in $erg \cdot g_{tissue}^{-1} \cdot hr^{-1} \cdot w^{-1}$, r is the radius of the hole, ℓ is the distance from the ground surface to the detector position, and k is a normalizing constant. Such fits are shown in Figs. 11 through 14. In each case k was chosen by inspection to give the best fit to the data. The discrepancies seen at $\ell/D < 1$ are, of course, due to the large contribution of the direct beam from the reactor at these shallow depths.

Fast-neutron dose rates as a function of concrete shield thickness are plotted in Fig. 15 for the various elevation angles and three values of ℓ/D. The data have been arbitrarily normalized to curves representing a relaxation length of 11 cm, which is the relaxation length characteristic of neutrons having energies > 1.5 MeV (ref 4).

The simplest laminated shields studied in the present work consisted of a single 3 1/2-in.-thick iron slab, below which were placed concrete slabs ranging in thickness from 0 to 12 in. The fast-neutron dose

4. R. Aronson and C. N. Klahr, chap 9 in Reactor Handbook, 2d ed., vol 3, part B (E. P. Blizard and L. S. Abbott, eds.), Interscience, New York, 1962, p 95.

rates measured below these shields for reactor elevation angles of 15 and 45° are shown in Figs. 16 through 19. The data have been cross-plotted in Fig. 20 to show the variation in dose rate with concrete thickness. The curves have been fitted by inspection, and show a relaxation length of roughly 9 cm, indicating a considerable softening of the neutron energy spectrum in these shields.

A more complicated version of the laminated shield consisted of a 3 1/2-in.-thick top layer of iron followed by a middle layer of concrete ranging in thickness from 3 to 15 in. and a bottom layer of iron 1 1/2 in. thick. Measurements obtained below this shield are plotted in Figs. 21 through 25. The data are cross-plotted in Fig. 26 as dose rate vs concrete thickness, and again curves are drawn by inspection. The relaxation length fitting the data appears to be about 8.64 cm, slightly shorter than that of the two-layer shields discussed above.

The final arrangement of the laminated slab shield to be tested in these experiments consisted of two 3 1/2-in.-thick iron slabs separated, in one case, by 12 in. of air and in other cases by concrete ranging in thickness from 3 to 15 in. Fast-neutron dose rates measured beneath these configurations, for reactor elevation angles of 15 and 45°, are shown in Figs. 27 through 32. These data, plotted as dose rate vs concrete thickness, are repeated in Fig. 33, where the curves show a relaxation length of 8.13 cm, just slightly shorter than that of Fig. 26. The small difference may be due solely to experimental errors.

All the data recorded above were obtained on the axis of Hole No. 1. The possible effect upon the dose rate of detector displacements from this axis was experimentally evaluated. A series of traverses was run beneath a 6-in.-thick concrete shield with the detector offset radially 1 and 1.5 ft from the hole axis at angles of 0, 90, and 180° from a line connecting the hole and the reactor. If any effect existed, it was so small as to be hidden in the experimental error, since the curves from these measurements fall upon each other and upon the curve obtained from measurements along the axis.

Gamma-Ray Dose Rates in Hole No. 1

Gamma-ray dose-rate measurements obtained in Hole No. 1 covered practically the same configurations as the fast-neutron measurements. The dose rates measured below simple concrete shields of various thicknesses for five different angles of reactor elevation are shown in Figs. 34 through 38. The dose rates are plotted as a function of ℓ/D, analogous to the presentation of the fast-neutron data and for the same reason. The data from these curves were fitted by an arbitrary normalization to the curves drawn in Fig. 39 to show the variation in the gamma-ray dose rate with thickness of concrete. The three curves, each representing a particular ℓ/D ratio and thus a particular depth in the hole, give a relaxation length of 15.4 cm.

Gamma-ray dose rates below two-layer iron and concrete shields are shown in Figs. 40 through 43 for reactor elevation angles of 15 and 45°. The dose rate as a function of the thickness of concrete below a 3 1/2-in.-thick iron slab is shown in Fig. 44 for the two elevation angles and three hole depths. At distances of 8 and 12 ft (ℓ/D = 2 and 3) below the top of the slab the data appear to fit a relaxation length of ~18.5 cm, about 20% longer than that obtained for all-concrete shields.

Gamma-ray dose rates below shield sandwiches consisting of 3 1/2 in. of iron, a variable thickness of concrete, and 1 1/2 in. of iron are shown in Figs. 45 through 49, again for reactor elevation angles of 15 and 45°. A plot of these data as dose rate vs concrete thickness (Fig. 50) yields a relaxation length of about 15.5 cm, or approximately the same as that observed behind the simple concrete shields.

The results of the measurements made below two 3 1/2-in.-thick iron slabs separated by air or by various thicknesses of concrete are given in Figs. 51 through 56. A plot of these values as a function of the concrete thickness, given in Fig. 57, shows so much dispersion in the data as to preclude assignment of a single relaxation length to this configuration.

Since much of the gamma-ray dose rate measured below the shields stems from thermal-neutron captures in the shield, the behavior of the

thermal-neutron flux within the shield is of interest. A plot of the thermal (subcadmium) flux through the shield consisting of 3 1/2 in. of iron, 15 in. of concrete, and 3 1/2 in. of iron is shown in Fig. 58 for two reactor elevation angles. It should be observed, however, that the 30° curve was plotted from gold-foil data, while the 15° curve resulted from dysprosium exposures. Thus the relation of the two curves is not necessarily significant. Also shown is the cadmium ratio, that is, the ratio of bare-foil activation to cadmium-covered-foil activation, for the 30° gold-foil measurements.

In Figs. 59 and 60 are shown the variations in dose rates as a function of the thickness (in g/cm^2) of the multilayer shields. It is evident from these data that a shield of 3 1/2 in. of iron plus concrete is comparable, on a g/cm^2 basis, with a shield consisting of a 3 1/2-in. top layer of iron, a layer of concrete, and a 1 1/2-in. bottom layer of iron. When the bottom layer is replaced by a 3 1/2-in. thickness of iron, however, a sharp change in slope is observed, as well as a considerable increase in the gamma-ray dose rate at comparable thicknesses. This is due to the increased production of capture gamma rays in the lower iron slab.

Miscellaneous Gamma-Ray and Neutron Measurements in Hole No. 1

During the analysis of both the gamma-ray and the fast-neutron data, attempts were made to determine a correlation between the angle of elevation of the reactor and the dose rate observed at a given location in the hole. No simple relation was obtained for the data obtained below the shields, but data taken in the open hole show a smooth and reasonable variation with elevation angle. In Fig. 61 is plotted the variation with the elevation angle of the fast-neutron dose rate on the hole axis at depths of 12 ft ($\ell/D = 3$) and 15 ft ($\ell/D = 3.75$) from ground level. A reference curve, the dose rate measured 40 in. above the top of the hole, is shown for comparison. At a depth of 12 ft the dosimeter sees the direct beam from the reactor at an elevation angle of about 80.5°; at a depth of 15 ft the angle is just under 82.5°. The curves seem to inflect accordingly.

Gamma-ray dose rates measured under essentially the same circumstances as the fast-neutron data are shown in Fig. 62, and thermal-neutron fluxes are given in Fig. 63.

In addition to the data discussed above, a somewhat heterogeneous set of measurements were made for Hole No. 1 to more or less explore the possibilities of configurations other than those examined in detail. In the following discussion of these data all dose rates are in ergs·g_{tissue}^{-1} hr^{-1}·w^{-1}.

The effect of the disposition of iron within a sandwich-type shield was explored with a lamination of 3 1/2 in. of iron, 15 in. of concrete, and 1 1/2 in. of iron. When placed so that the thicker iron slab was on top, the fast-neutron dose rate directly behind the shield was 4.8×10^{-7}. Inverting the configuration so that the thinner iron slab was on top increased the fast-neutron dose rate nearly 40%, or to 6.65×10^{-7}. A reverse result was obtained, however, when the gamma-ray dose rate was observed: For gamma rays the higher dose rate, 4.1×10^{-6}, occurred when the thicker iron slab was on top; when the thinner iron slab faced the beam, the gamma-ray dose rate was lower by a factor of nearly 2, or 1.9×10^{-6}.

The addition of 1/4 in. of boral on top of a shield consisting of two 3 1/2-in.-thick iron slabs separated by 15 in. of concrete reduced the capture gamma-ray production in the shield considerably. The dose rate just beneath the shield without the boral was 1.20×10^{-6}, whereas with the boral the dose rate was lower by 14%, or 1.05×10^{-6}. When the boral was replaced by a 2-in. thickness of polyethylene, the original dose rate was reduced by a factor of about 3, or to 3.80×10^{-7}.

Fast-Neutron Dose Rates in Tunnel

Fast-neutron dose rates in the tunnel extending from Hole No. 1 were usually measured along a horizontal line 30.5 in. above the floor of the tunnel and midway between its walls. This height was chosen somewhat arbitrarily, however, and in order to evaluate the importance of the vertical positioning of the detector, a set of traverses were made to compare the dose rate at the 30.5-in. height with that at a height of 66.3 in., the latter being less than 6 in. below the roof of

the tunnel. The data, obtained with no shield over Hole No. 1 and at reactor elevation angles of 15, 45, and 90°, are shown in Fig. 64. The influence of the vertical position of the detector within the tunnel is seen to be the greatest at a reactor angle of 15°, and to be the least at 90°. In all cases the dose rate was less along the upper traverse.

The fast-neutron dose rates 30.5 in. above the floor of the tunnel with Hole No. 1 unshielded are repeated in Fig. 65, where they are compared with the dose rates observed after the hole was modified by construction of a concrete block floor at the same elevation as the tunnel floor. The only data in which the addition of the floor seems to make a significant difference are those taken with the reactor directly over the hole ($\gamma = 90^{\circ}$). In this case the increased scattering from the concrete resulted in an increase of approximately 75% in the dose rate within the tunnel. A further modification of the environment, introduced by blocking the tunnel with a concrete wall built 13.1 ft from the center line of the hole and intended to alter the backscattering, did not appear to have any observable effect on the fast-neutron dose rate in the tunnel.

Although Fig. 65 utilizes data obtained after the hole and tunnel were modified, the modifications were actually made rather late in the experimental program. The measurements that follow, in which various shields were employed on Hole No. 1, were made in the original, unmodified configuration unless specifically noted otherwise.

Figure 66 shows the fast-neutron dose rates within the tunnel, for various reactor elevation angles, after Hole No. 1 had been capped with a 1/2-in.-thick iron slab. When compared with the dose rates measured in the tunnel with Hole No. 1 unshielded, these data exhibit a curious behavior. For reactor elevation angles of 15, 45, and 60° the dose rates measured under the shielded condition are higher than those for the unshielded condition, but for 30 and 90° they are lower. Whether this result is due to unidentified errors in the experimental measurements or to an actual physical effect is presently not clear.

Very little change in the dose rate in the tunnel was obtained by increasing the thickness of the iron slab over the hole to 1 in. (Fig. 67). The curves for 15, 30, 45, and 60° nearly coincide with their counterparts for the 1/2-in.-thick iron shield, although the curve for 90° is lower by a factor of about 1.5.

Figure 67 also shows the effect on the dose rate of modifications of the tunnel-hole environment. In all except the 90° case the modifications had little or no effect. In the 90° case, addition of a concrete floor to the hole increased the dose rate in the tunnel by about 75%, bringing the dose rate up to about that measured when the shield over the hole was 1/2-in.-thick iron. As was observed in the open-hole data, no effect was produced when the previously described concrete wall was added to the tunnel.

A further modification of the tunnel conditions was made by constructing a low, 8-in.-thick brick wall, first 12 in. high and later 24 in. high, across the tunnel at a point 49 in. from the hole center line (25 in. from the tunnel mouth). The curves are plotted as Fig. 68. Neither wall had much effect on the dose rate when the reactor elevation angle was 45°. With the reactor directly above the hole ($\gamma = 90^{\circ}$) the wall apparently lowered the dose rate in the tunnel by a small amount, the higher wall giving the larger decrease.

Fast-neutron dose rates in the tunnel with and without Hole No. 1 covered by a 3-in.-thick iron shield are shown in Fig. 69 for reactor elevation angles of 15, 45, and 90°. The 3-in. thickness produced only a small diminution of the dose rate in the tunnel, except at $\gamma = 90^{\circ}$, where the dose rate was decreased by a factor of about 4.5.

Fast-neutron dose rates within the tunnel with a 3-in.-thick concrete slab capping Hole No. 1 are compared in Fig. 70 with those resulting from the open-hole condition. The results do not differ markedly from those shown in Fig. 69, nor does the addition of 1 in. of iron on top of the 3-in.-thick concrete slab seem to have much effect (see Fig. 71).

Gamma-Ray Dose Rates in Tunnel

In the preceding section it was noted that, principally for convenience, the fast-neutron dose rates were measured along a line 30.5 in. above the tunnel floor. In the case of gamma rays the convenient distance turned out to be 27 in., and so most of the data reported below were taken at that height. Again, however, the effect of detector vertical positioning was evaluated, with the results shown in Fig. 72 (no shield over the hole). In this figure gamma-ray dose rates at the usual height of 27 in. are compared with rates measured at a height of 61 in. Since the tunnel is 72 in. high, the latter rates are relatively close to the tunnel ceiling (11 in.). The apparent effect of the change in height differed with the horizontal position. In and just beyond the hole proper the effect was, logically enough, that of increased dose rate with increased height. At a point just inside the tunnel mouth, the exact location depending on reactor elevation angle, the curves cross, and for the remainder of the tunnel length the dose near the tunnel roof is lower and more rapidly decreasing than the dose at 27 in. above the floor.

The gamma-ray dose rates measured in the tunnel at a height of 27 in. are repeated in Fig. 73, where they are compared with curves resulting from the addition of the concrete floor to the hole and from the further addition of a concrete wall blocking the tunnel 13.1 ft from the center line of the hole (see above). As was the case with the neutron data, the floor made little difference until the reactor elevation angle reached 90°. In contrast to the neutron data, which indicated that the wall in the tunnel had no noticeable effect on the dose rate, the gamma-ray dose rate shows a slight but definite increase as the wall is approached. This is due to an increase in the capture gamma rays generated in the wall.

The positioning of a 1/2-in.-thick iron slab over Hole No. 1 produced a noticeable reduction in the gamma-ray dose rate within the tunnel. The measurements shown in Fig. 74 indicate a 30 to 50% reduction in dose for the various reactor positions.

In Fig. 75 are shown the gamma-ray dose rates observed in the tunnel when a 1-in.-thick iron slab covered the hole. Also shown are the effects, for reactor elevation angles of 15, 45, and 90°, of the addition of the concrete floor to the hole, and for 45 and 90° the effects of the concrete wall at 13.1 ft. The same upturn of the data at large distances within the tunnel that occurred in the unshielded case with the wall added is again seen.

Another variation on the basic hole-tunnel configuration was the introduction of the brick wall within the tunnel mouth 49 in. from the center line of the hole (see above). Neither the concrete floor in the hole nor the concrete wall in the tunnel was in place during these measurements, shown in Fig. 76. The 12-in.-high wall produced a small reduction in dose rate when the reactor was directly over the hole, but produced no effect when the reactor was at 45°. The 24-in.-high wall resulted in a decreased dose rate for both the 90 and 45° cases.

Gamma-ray dose rates measured when a 3-in.-thick iron slab covered the hole are shown in Fig. 77. In comparison with the open-hole data, the dose rate is reduced a factor of about 4 and is roughly the same for all three angles shown. Placing a 3-in.-thick concrete slab over the hole reduced the dose rate a factor of about 2 for the $\gamma = 15^{\circ}$ case and of about 3 for the $\gamma = 90^{\circ}$ case (Fig. 78).

The final hole-shield configuration tested in this series consisted of a 3-in.-thick concrete slab topped by 1 in. of iron. The curves shown in Fig. 79 indicate that the 60 and 90° data are nearly coincident, only a factor of about 1.1 separating them when the detector loses sight of the top of the hole.

Measurements in Hole No. 2

As the distance from the source (the TSR-II) to the hole in which the detector is positioned is increased, the principal change to be expected is a difference in the relative importance of the various components of the radiation striking the top of the hole. The relative importance of the direct beam from the reactor should be lessened, and the contribution due to air-scattered radiation should assume greater

importance. The total effect of these variations was examined in a series of measurements made in Hole No. 2, 228 ft from the reactor, at a reactor elevation angle of 45°. At this angle the reactor was approximately 161 ft from the ground, more than twice the approximately 71-ft elevation required for the 45° data from Hole No. 1.

In Fig. 80 are shown the fast-neutron dose rates as a function of ℓ/D measured below six concrete slabs of various thicknesses, compared with the dose rate measured in the open hole. From these data evolves Fig. 81, showing the fast-neutron dose rate in Hole No. 2 as a function of concrete slab thickness.

Figure 82 shows fast-neutron dose rates in Hole No. 2 below several thicknesses of iron shield, as well as below two composite shields of iron and concrete. From a comparison of the composite shield data with those for simple concrete slabs (i. e., a comparison of Fig. 82 with Fig. 80), it is seen that an advantage exists in the use of the composite shields if minimum thickness is a goal. The advantage would be reversed if total weight were the criterion. The information for simple iron slabs from Fig. 82 is replotted in Fig. 83 to show dose rate as a function of iron thickness. The relaxation length associated with these data is 13.7 cm.

As was the practice at Hole No. 1, all the measurements of Hole No. 2 were made along the center line of the hole. The influence of radial position within the hole was investigated by a series of traverses within the open hole in which the detector was displaced successively 1 and 1 1/2 ft in the direction of the reactor and 1 1/2 ft at 180° from the direction of the reactor. The results are shown in Fig. 84. A small effect, appreciable only near the top of the hole, was most noticeable for the case in which the detector was moved away from the reactor direction.

Fast-neutron dose rates in Hole No. 2 are compared in Fig. 85 with those measured in Hole No. 1. In both cases the reactor elevation angle was 45°, and the concrete shield thickness was varied. The data are cross-plotted to show the fast-neutron dose rates as a function of concrete thickness in Fig. 86.

Gamma-ray dose rates in Hole No. 2 are plotted in Fig. 87 as a function of ℓ/D for various thicknesses of concrete shield, and in Fig. 88 as a function of shield thickness.

Figure 89 presents the results of gamma-ray dose-rate measurements in Hole No. 2 below various thicknesses of simple iron slabs and below two composite configurations. Curves for the latter two configurations strongly emphasize the importance of the iron placement in such configurations, since 3 1/2 in. of iron below 15 in. of concrete is more effective in lowering the dose rate in the hole than is a total of 5 in. of iron and 15 in. of concrete when 3 1/2 in. of the iron is above the concrete and 1 1/2 in. is below it. The gamma-ray dose rates below the iron slabs alone are plotted in Fig. 90 as a function of the iron thickness.

As was the case with the fast-neutron data in Hole No. 2, the effect of shifting the radial position of the detector was explored for the gamma-ray dose rate. The results, which are for the case of no shield over the hole, are shown in Fig. 91.

Gamma-ray dose rates in Hole No. 2 for a reactor angle of 45° and various thicknesses of concrete shields are compared in Fig. 92 with corresponding data for Hole No. 1. The Hole No. 1 gamma-ray dose rate, normalized by a factor of 0.20, is cross-plotted, along with the Hole No. 2 data, as a function of concrete thickness in Fig. 93. The data for ℓ/D values of 2 and 3 appear to be fitted by curves representing a relaxation length of 15.0 cm, but the $\ell/D = 1$ data for both holes seem to be best fitted by a relaxation length of 17.5 cm.

The only thermal-neutron data obtained at Hole No. 2 were from a pair of foil traverses, one though a 12-in.-thick concrete slab and the other through the gravel adjacent to the hole. Both gold and dysprosium foils were used for each traverse, with the gold-foil results being uniformly higher than the dysprosium exposures (see Fig. 94).

Measurements in Hole No. 3

Hole No. 3, which was 450 ft from the reactor, should be far enough from the reactor to bring out, in comparison with data from Hole No. 1, effects peculiar to increased air-scattered radiation since

the separation distance is roughly equivalent to 1 mean free path for energetic neutrons in air. The reactor angle of elevation used for the Hole No. 3 measurements was 15°, placing the reactor at an elevation of about 116 ft.

The fast-neutron dose rates measured in Hole No. 3 below various thicknesses of concrete are shown in Fig. 95, and are replotted as a function of concrete thickness in Fig. 96. A direct comparison is made in Fig. 97 of the Hole No. 3 dose rates below concrete with similar measurements in Hole No. 1.

Fast-neutron dose rates measured as a function of ℓ/D in Hole No. 3 below various simple iron shields and composite iron-concrete shields are shown in Fig. 98. The fast-neutron dose rates below the simple iron slabs are plotted vs iron thickness in Fig. 99.

Gamma-ray dose rates in Hole No. 3 are shown in Fig. 100 for concrete shields and in Fig. 101 for iron and iron-concrete composite shields. In the composite shield measurements a test of the usefulness of a 1/4-in.-thick boral sheet showed that, regardless of its position in the composite, the boral had negligible effects in reducing the gamma-ray dose rate in the hole. The effectiveness of an air gap was also negligible.

The gamma-ray dose rates in Hole No. 3 are compared in Fig. 102 with those in Hole No. 1 as functions of depth within the hole, and in Fig. 103 as functions of concrete thickness. The gamma-ray dose rates in Hole No. 3 below simple iron slabs are plotted in Fig. 104 as functions of slab thickness.

ERRORS

The assignment of accurate and defensible limits of error to the work reported above is difficult. Not only are there many sources of error, but the magnitude of each source and even the method of estimation are not yet firmly determined. The principal sources of error are considered to be the error in determining the reactor power, inaccuracy in reactor positioning relative to the experiment holes, inherent errors in instrument calibration, and errors stemming from counting statistics.

A TSR-II power calibration was made in 1961 at the low nominal power of 40 kw. At that time the accuracy with which the power was known was given as about ±5%. The instrument system which determines power levels in the TSR-II is known to have undergone significant nonrandom changes, and therefore ±10% deviations in power level are probable.

The reactor position is determined by a right-triangle procedure in which the reactor height is measured with a calibrated wire and the angle from horizon to reactor is measured with a surveyor's transit set at the detector station. The resulting right triangle is solved for the slant distance from the reactor to the location of measurement. In principle, this method should give positional accuracy to 1% or less. In practice, effects of wind, etc., on the suspended reactor and on the calibrated wire may make an error of ±5% a reasonable assignment. Errors in carrying out the positioning operation can occur, of course, and Wells,[5] in an analysis of part of the data of Hole No. 1, has pointed out an instance in which this may have occurred.

Both the anthracene scintillation gamma-ray dosimeters and the Hurst-type fast-neutron dosimeters used for the present measurements are usually assigned an error of ±5%, justified on the basis of past experience with these counters.

Some feeling for the counting errors is obtained by an examination of the fluctuations shown on the original autoplot curves. Based on this evidence, counting errors should range between ±1 and ±10%, depending upon the particular experimental configuration. In a few cases the so-called hand points were repeated, with a reproducibility of about ±5%. A value of ±8% is arbitrarily adopted for counting errors.

If it can be assumed that the errors described above are random in nature, a total error of ±15% results. Simply adding errors results in a total error of ±28%.

---

5. M. B. Wells, Analysis of the Measurements of Fast-Neutron Dose Rates in Hole No. 1, Research Note No. 63-3, Radiation Research Associates, Fort Worth (February 1963).

APPLICATIONS AND FUTURE NEEDS

Portions of the work reported above have already been used successfully to check the results of two calculational approaches to the weapon burst problem: that of Blizard et al.[3] and, more recently, that of Wells.[5] Also, Cain[6] of ORNL computed dose rates within tunnels and utilized portions of the tunnel data.

Although it is inevitable that some users of the curves will find deficiencies in specific areas, it is felt that the 90-odd data plots represent a rather complete investigation of the problem. A few questions of fact are left unanswered. In future work the validity of the apparent intensification effect observed behind thin iron shields should be examined, and a detailed study of dose rate as a function of reactor elevation angle would be desirable.

6. V. R. Cain, Calculations of Thermal-Neutron Flux Distributions in Concrete-Walled Ducts Using an Albedo Model with Monte Carlo Techniques, ORNL-3507 (in press).

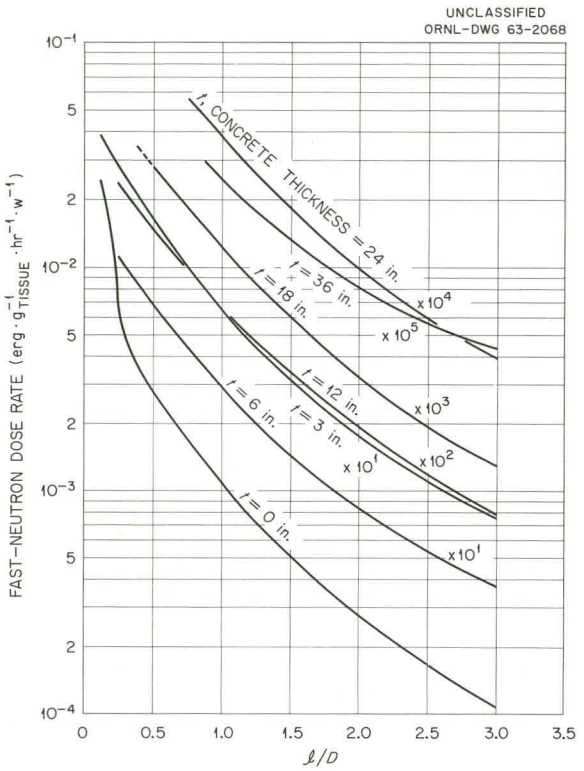

Fig. 6. Fast-Neutron Dose Rate in Hole No. 1 as a Function of ℓ/D for Various Thicknesses of Concrete Shield ($\gamma = 15°$).

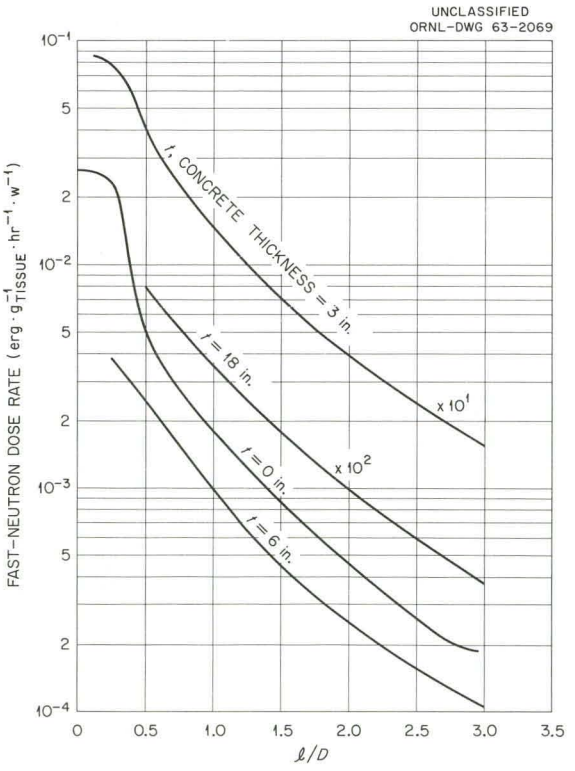

Fig. 7. Fast-Neutron Dose Rate in Hole No. 1 as a Function of ℓ/D for Various Thicknesses of Concrete Shield ($\gamma = 30°$).

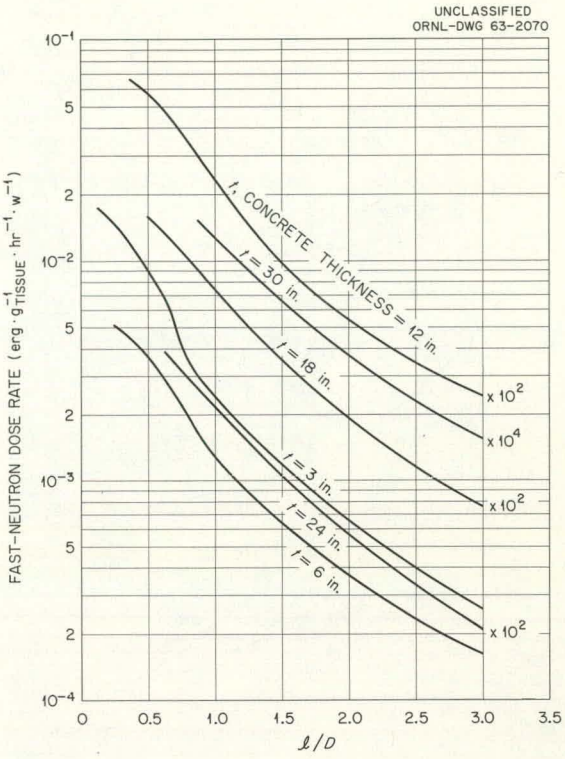

Fig. 8. Fast-Neutron Dose Rate in Hole No. 1 as a Function of ℓ/D for Various Thicknesses of Concrete Shield ($\gamma = 45°$).

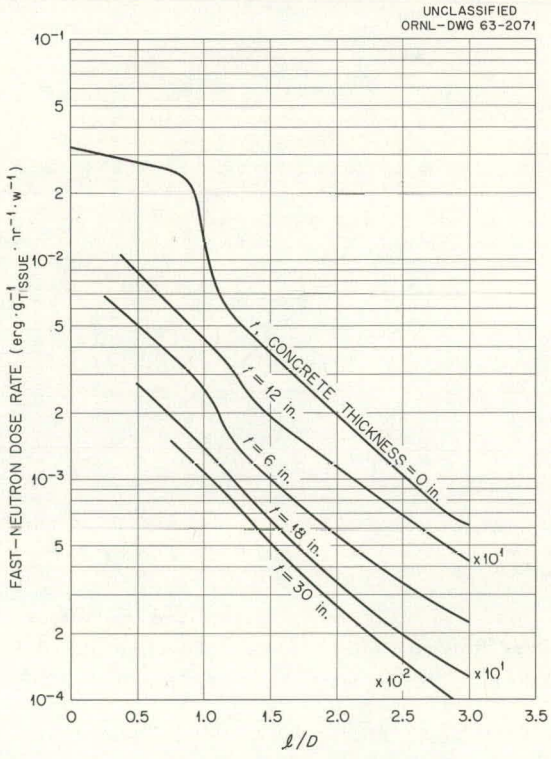

Fig. 9. Fast-Neutron Dose Rate in Hole No. 1 as a Function of ℓ/D for Various Thicknesses of Concrete Shield ($\gamma = 60°$).

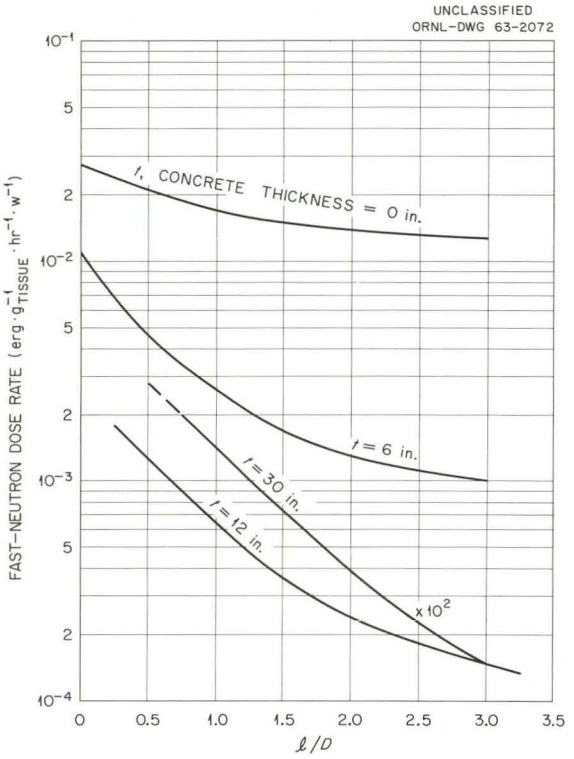

Fig. 10. Fast-Neutron Dose Rate in Hole No. 1 as a Function of ℓ/D for Various Thicknesses of Concrete Shield ($\gamma = 90°$).

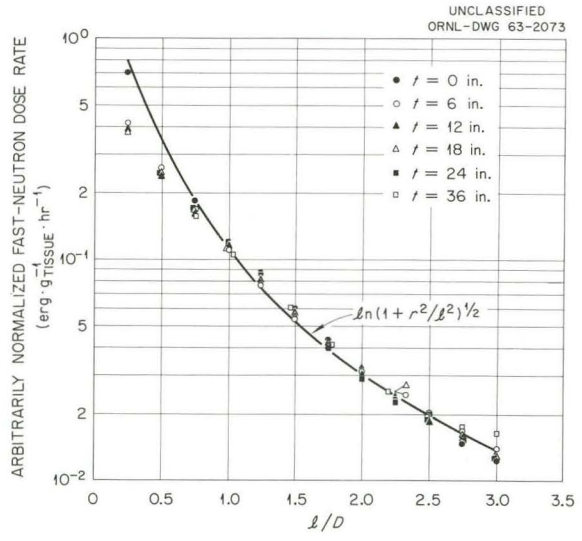

Fig. 11. Arbitrarily Normalized Fast-Neutron Dose Rate in Hole No. 1 as a Function of ℓ/D for Various Thicknesses of Concrete Shield ($\gamma = 15°$).

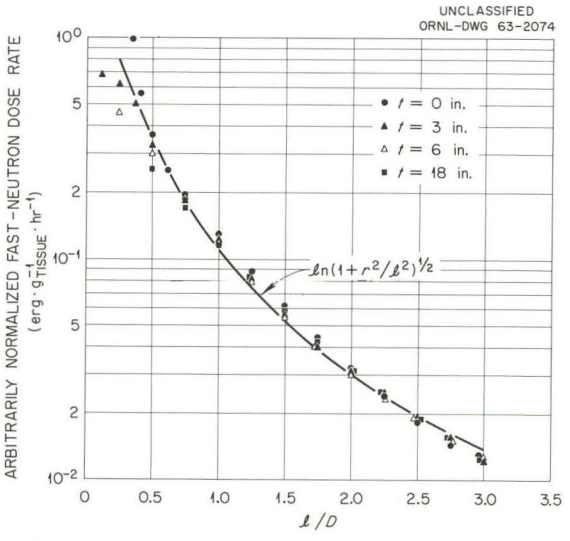

Fig. 12. Arbitrarily Normalized Fast-Neutron Dose Rate in Hole No. 1 as a Function of ℓ/D for Various Thicknesses of Concrete Shield ($\gamma = 30°$).

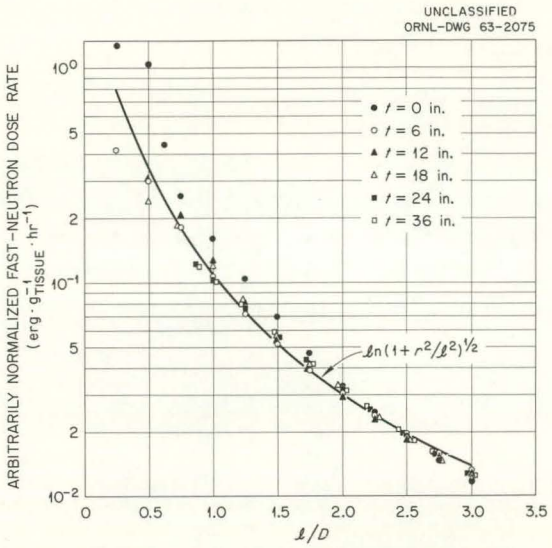

Fig. 13. Arbitrarily Normalized Fast-Neutron Dose Rate in Hole No. 1 as a Function of ℓ/D for Various Thicknesses of Concrete Shield ($\gamma = 45°$).

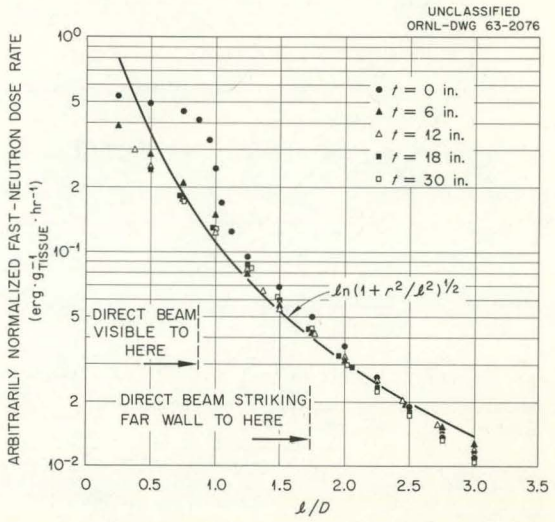

Fig. 14. Arbitrarily Normalized Fast-Neutron Dose Rate in Hole No. 1 as a Function of ℓ/D for Various Thicknesses of Concrete Shield ($\gamma = 60°$).

Fig. 15. Arbitrarily Normalized Fast-Neutron Dose Rate in Hole No. 1 as a Function of the Thickness of Concrete Shield for Various Values of ℓ/D ($\gamma = 15$, 30, 45, and 60°).

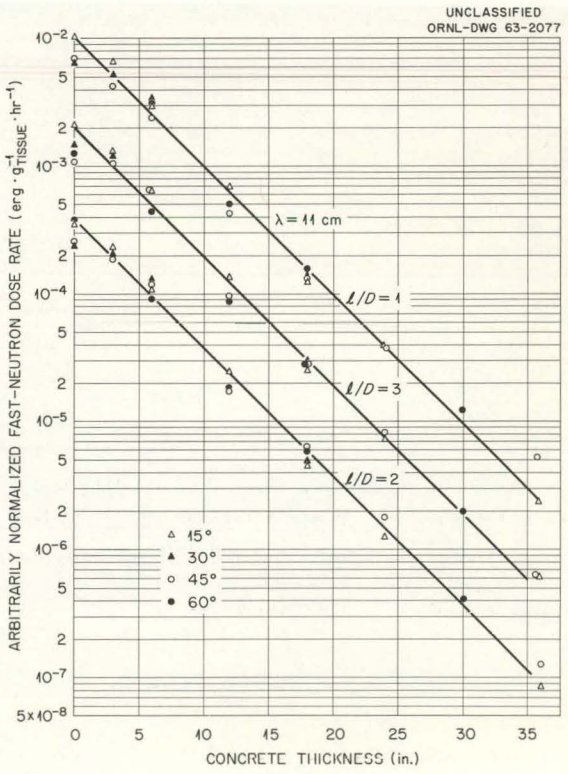

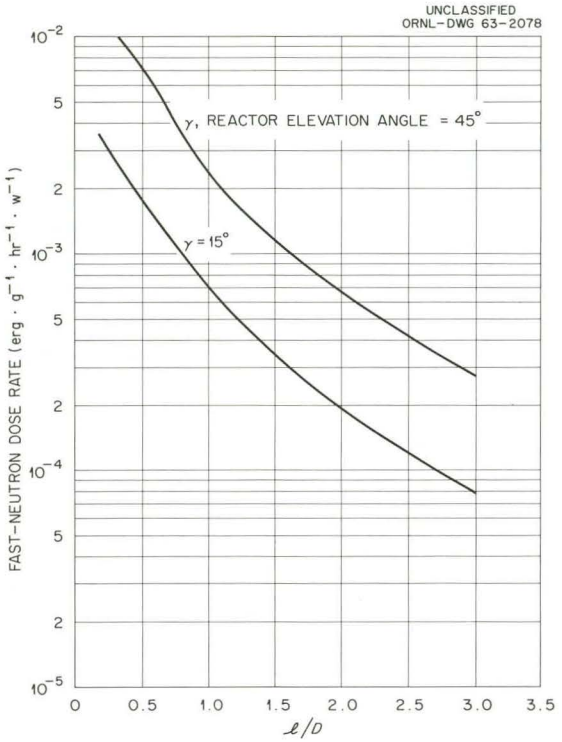

Fig. 16. Fast-Neutron Dose Rate in Hole No. 1 as a Function of ℓ/D for $3\frac{1}{2}$-in.-Thick Iron Shield (γ = 15 and 45°).

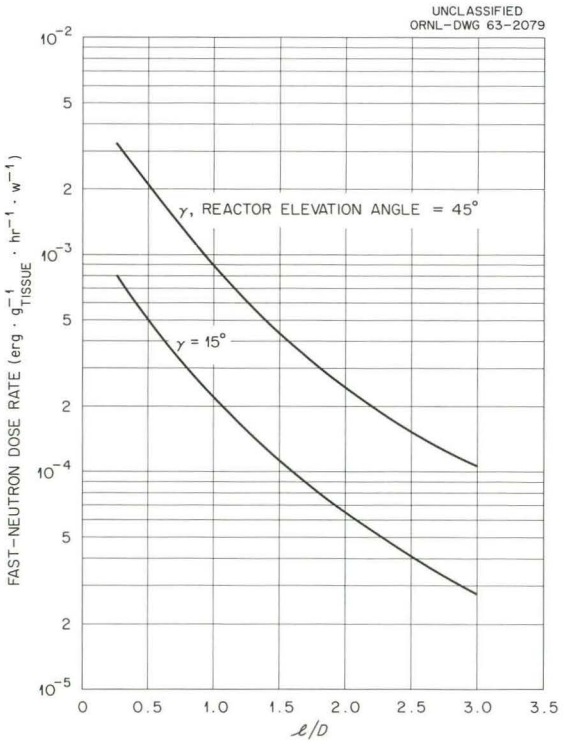

Fig. 17. Fast-Neutron Dose Rate in Hole No. 1 as a Function of ℓ/D for Shield of $3\frac{1}{2}$ in. of Iron and 3 in. of Concrete (γ = 15 and 45°).

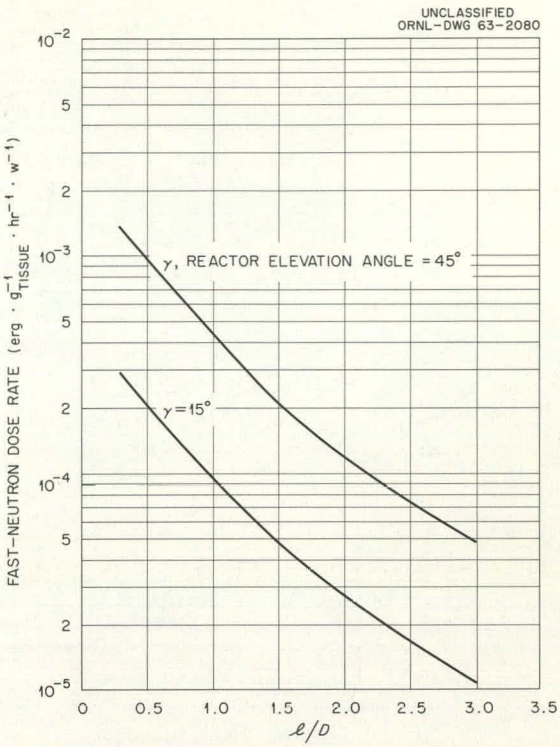

Fig. 18. Fast-Neutron Dose Rate in Hole No. 1 as a Function of ℓ/D for Shield of $3\frac{1}{2}$ in. of Iron and 6 in. of Concrete (γ = 15 and 45°).

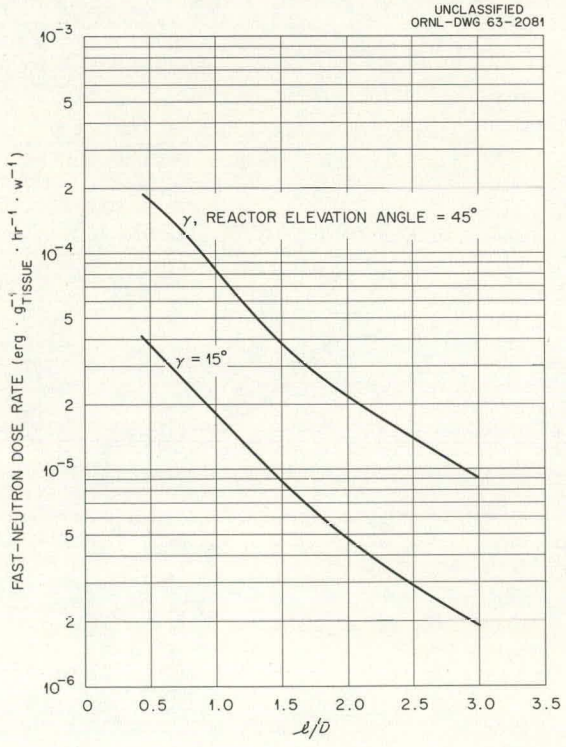

Fig. 19. Fast-Neutron Dose Rate in Hole No. 1 as a Function of ℓ/D for Shield of $3\frac{1}{2}$ in. of Iron and 12 in. of Concrete (γ = 15 and 45°).

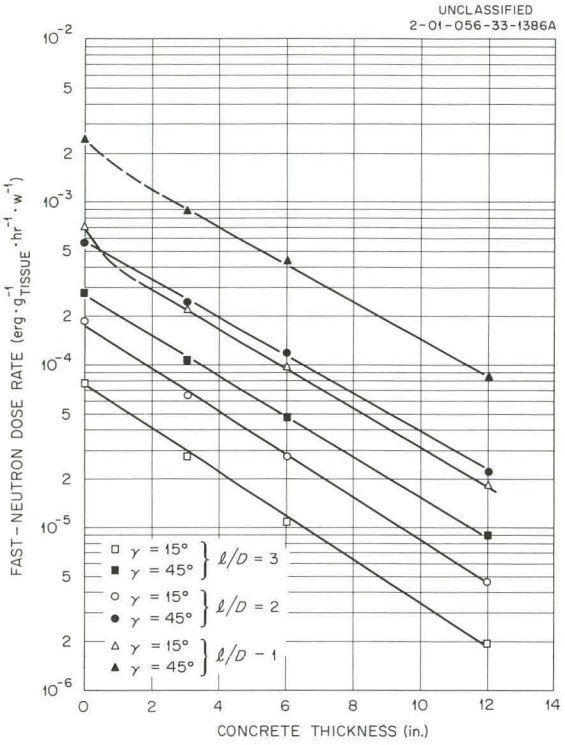

Fig. 20. Fast-Neutron Dose Rate in Hole No. 1 as a Function of the Thickness of Concrete Below $3\frac{1}{2}$ in. of Iron for Various Values of ℓ/D (γ = 15 and 45°).

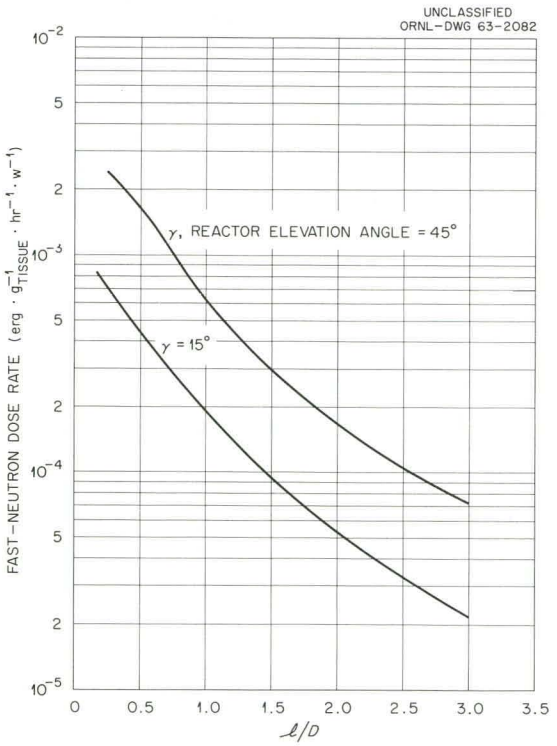

Fig. 21. Fast-Neutron Dose Rate in Hole No. 1 as a Function of ℓ/D for Shield of $3\frac{1}{2}$ in. of Iron, 3 in. of Concrete, and $1\frac{1}{2}$ in. of Iron (γ = 15 and 45°).

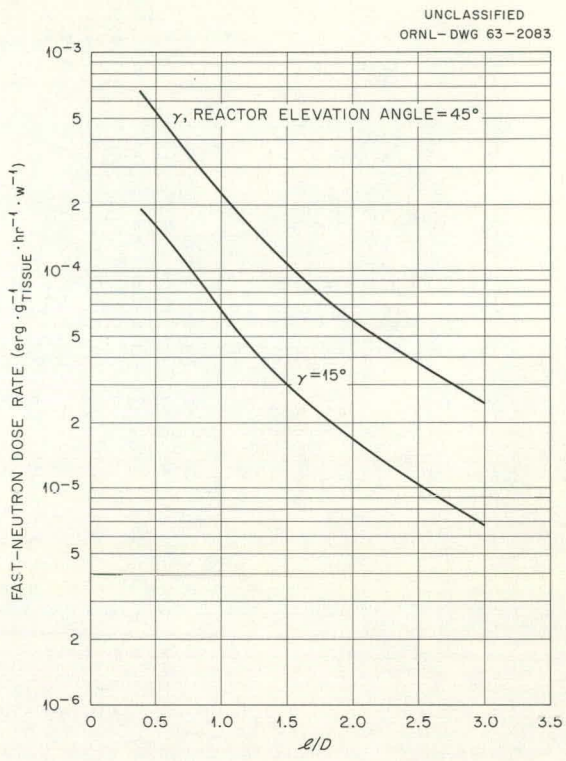

Fig. 22. Fast-Neutron Dose Rate in Hole No. 1 as a Function of ℓ/D for Shield of $3\frac{1}{2}$ in. of Iron, 6 in. of Concrete, and $1\frac{1}{2}$ in. of Iron (γ = 15 and 45°).

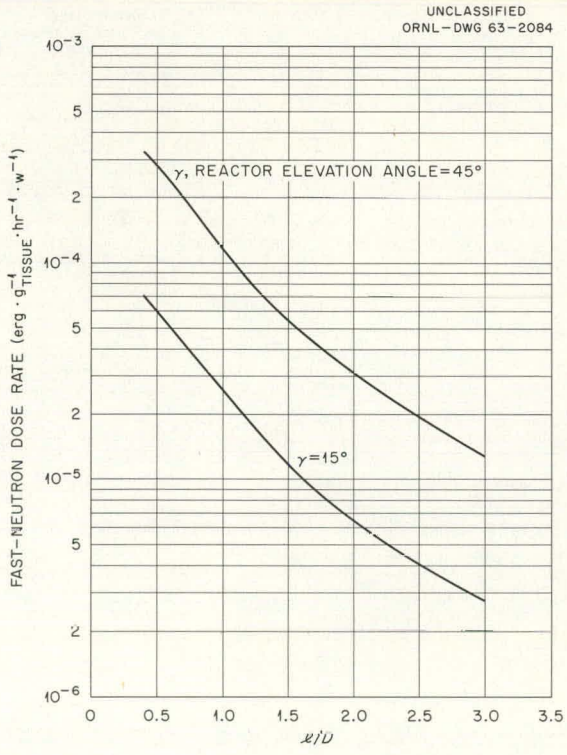

Fig. 23. Fast-Neutron Dose Rate in Hole No. 1 as a Function of ℓ/D for Shield of $3\frac{1}{2}$ in. of Iron, 9 in. of Concrete, and $1\frac{1}{2}$ in. of Iron (γ = 15 and 45°).

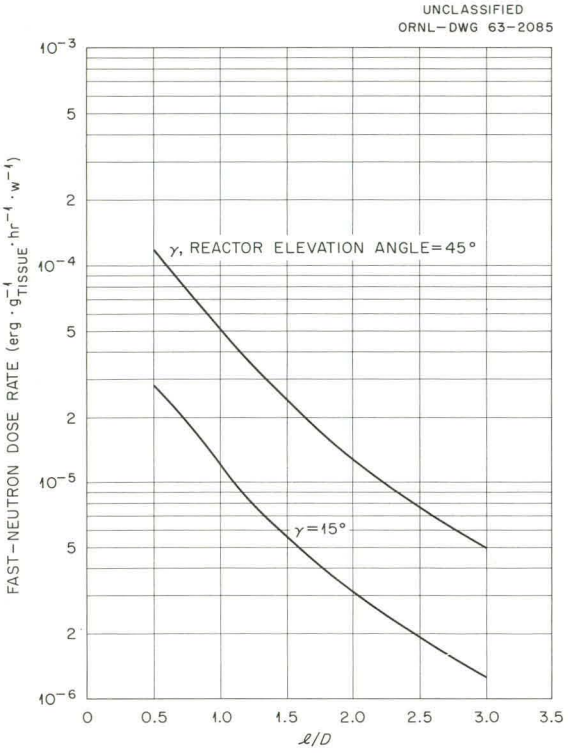

Fig. 24. Fast-Neutron Dose Rate in Hole No. 1 as a Function of ℓ/D for Shield of $3\frac{1}{2}$ in. of Iron, 12 in. of Concrete, and $1\frac{1}{2}$ in. of Iron (γ = 15 and 45°).

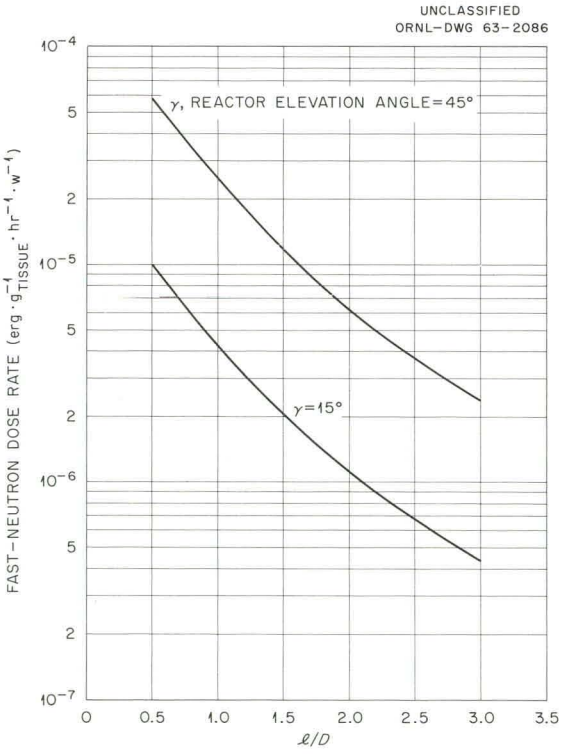

Fig. 25. Fast-Neutron Dose Rate in Hole No. 1 as a Function of ℓ/D for Shield of $3\frac{1}{2}$ in. of Iron, 15 in. of Concrete, and $1\frac{1}{2}$ in. of Iron (γ = 15 and 45°).

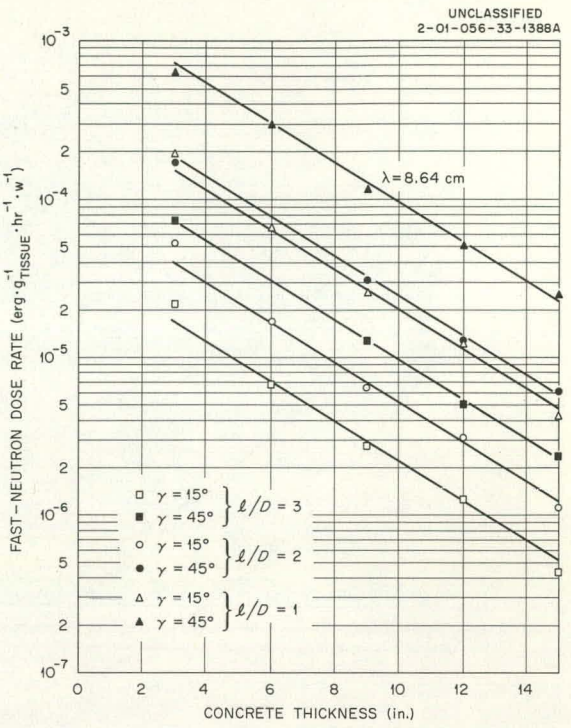

Fig. 26. Fast-Neutron Dose Rate in Hole No. 1 as a Function of the Thickness of Concrete Between $3\frac{1}{2}$-in.-Thick and $1\frac{1}{2}$-in.-Thick Iron Slabs for Various Values of ℓ/D (γ = 15 and 45°).

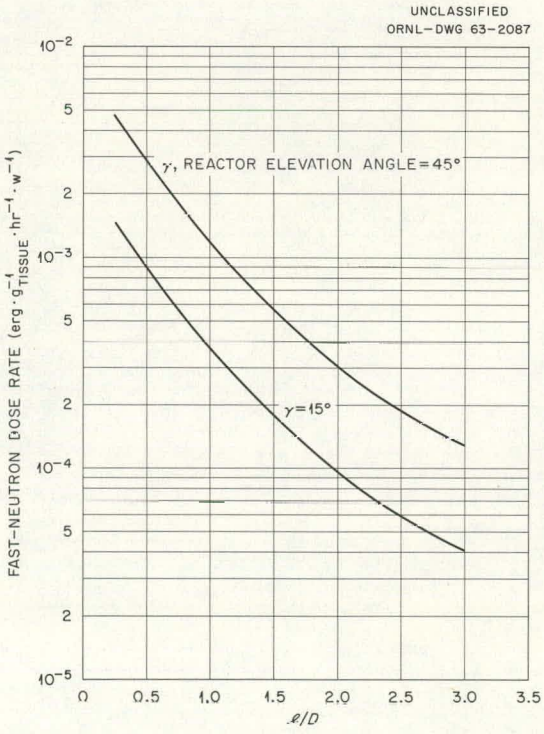

Fig. 27. Fast-Neutron Dose Rate in Hole No. 1 as a Function of ℓ/D for a Shield of Two $3\frac{1}{2}$-in.-Thick Iron Slabs Separated by 12 in. of Air (γ = 15 and 45°).

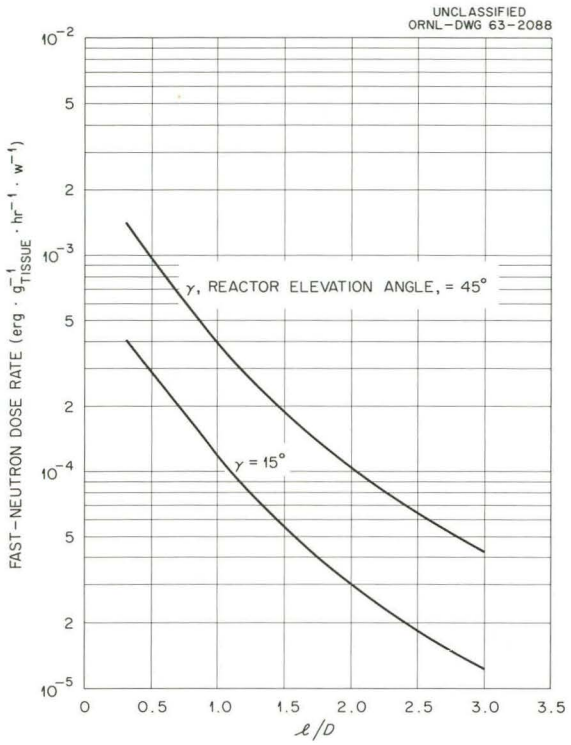

Fig. 28. Fast-Neutron Dose Rate in Hole No. 1 as a Function of ℓ/D for a Shield of Two $3\frac{1}{2}$-in.-Thick Iron Slabs Separated by 3 in. of Concrete (γ = 15 and 45°).

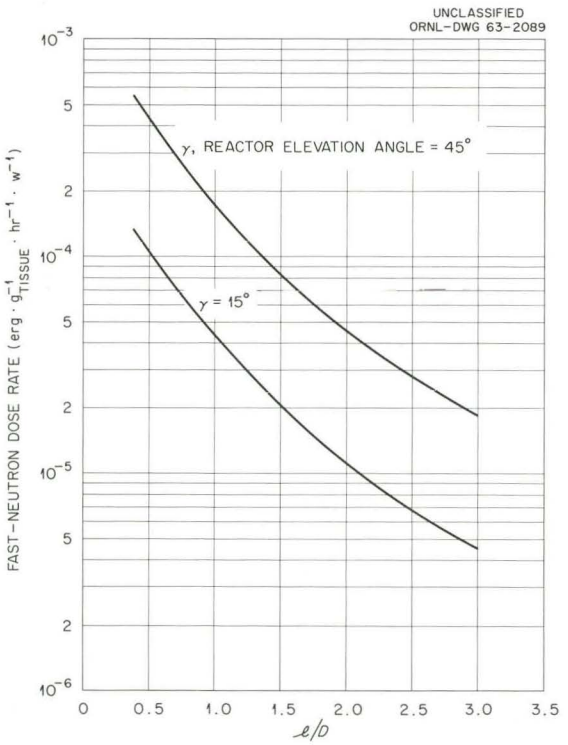

Fig. 29. Fast-Neutron Dose Rate in Hole No. 1 as a Function of ℓ/D for a Shield of Two $3\frac{1}{2}$-in.-Thick Iron Slabs Separated by 6 in. of Concrete (γ = 15 and 45°).

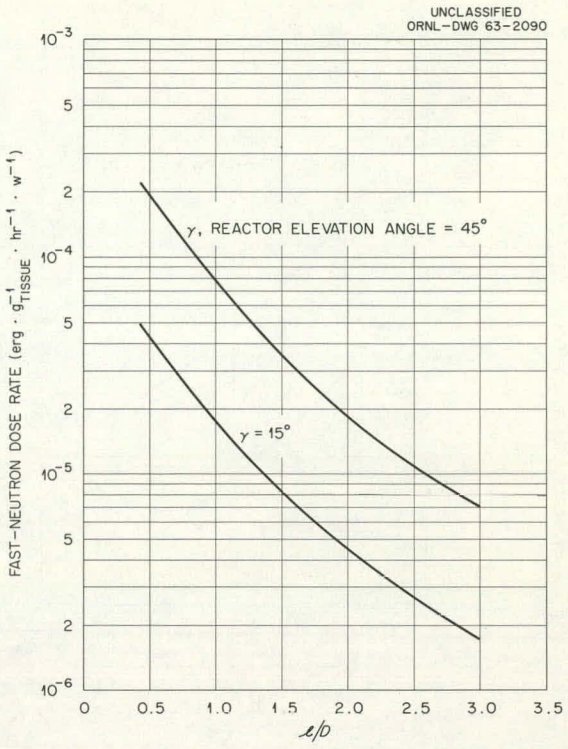

Fig. 30. Fast-Neutron Dose Rate in Hole No. 1 as a Function of ℓ/D for a Shield of Two $3\frac{1}{2}$-in.-Thick Iron Slabs Separated by 9 in. of Concrete (γ = 15 and 45°).

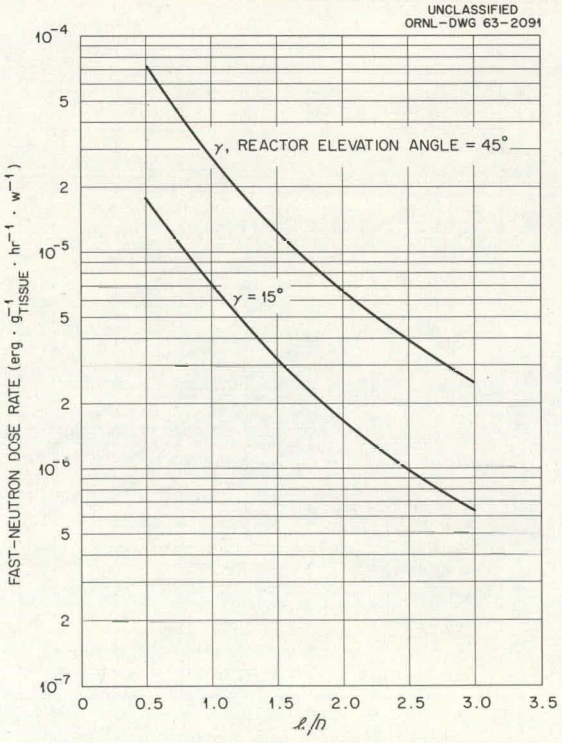

Fig. 31. Fast-Neutron Dose Rate in Hole No. 1 as a Function of ℓ/D for a Shield of Two $3\frac{1}{2}$-in.-Thick Iron Slabs Separated by 12 in. of Concrete (γ = 15 and 45°).

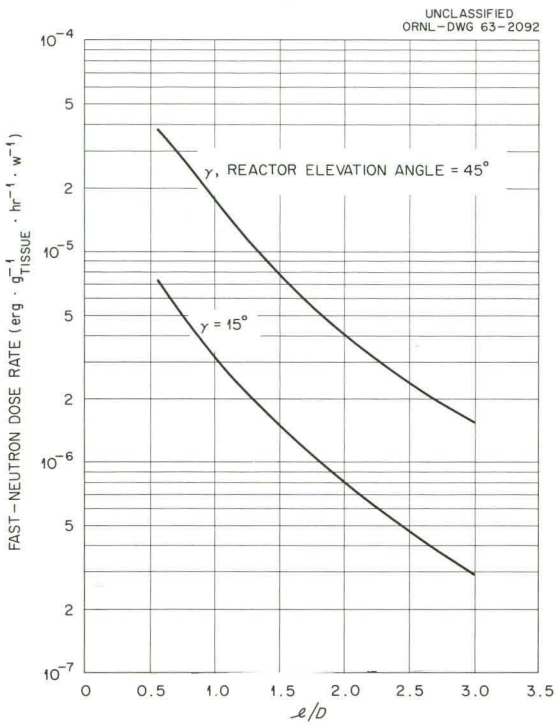

Fig. 32. Fast-Neutron Dose Rate in Hole No. 1 as a Function of ℓ/D for a Shield of Two $3\frac{1}{2}$-in.-Thick Iron Slabs Separated by 15 in. Concrete (γ = 15 and 45°).

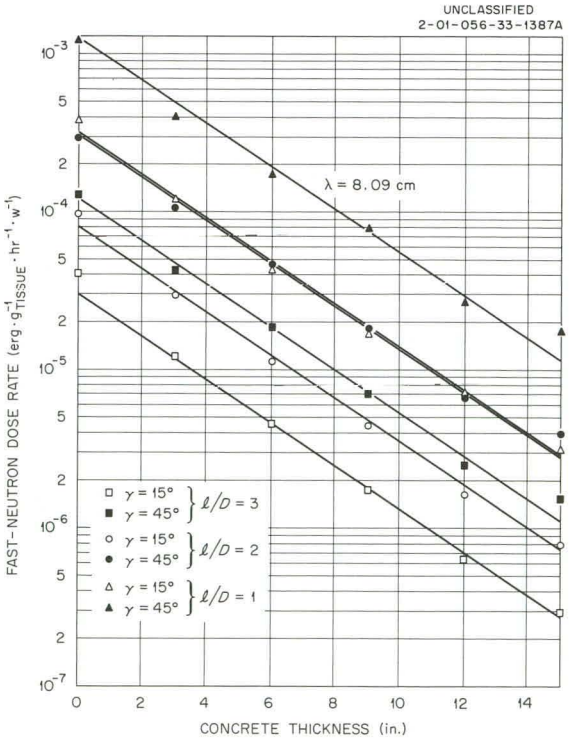

Fig. 33. Fast-Neutron Dose Rate in Hole No. 1 as a Function of the Thickness of Concrete Between Two $3\frac{1}{2}$-in.-Thick Iron Slabs for Various Values of ℓ/D (γ = 15 and 45°).

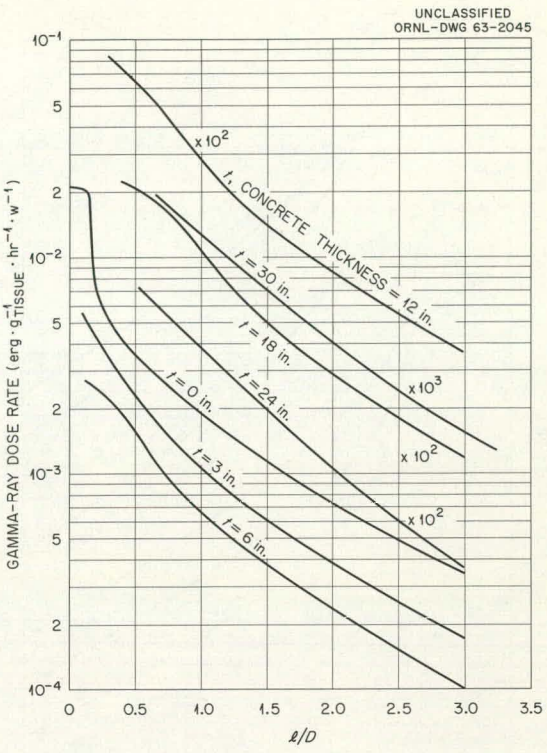

Fig. 34. Gamma-Ray Dose Rate in Hole No. 1 as a Function of ℓ/D for Various Thicknesses of Concrete Shield ($\gamma = 15°$).

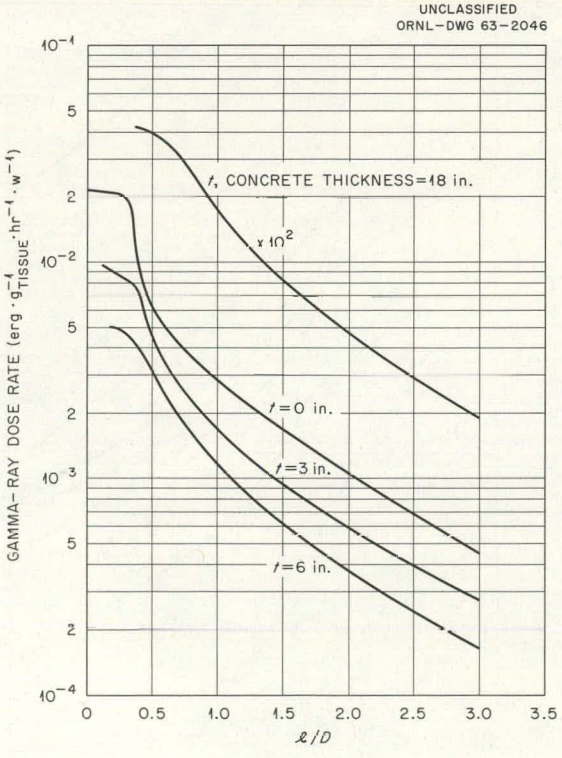

Fig. 35. Gamma-Ray Dose Rate in Hole No. 1 as a Function of ℓ/D for Various Thicknesses of Concrete Shield ($\gamma = 30°$).

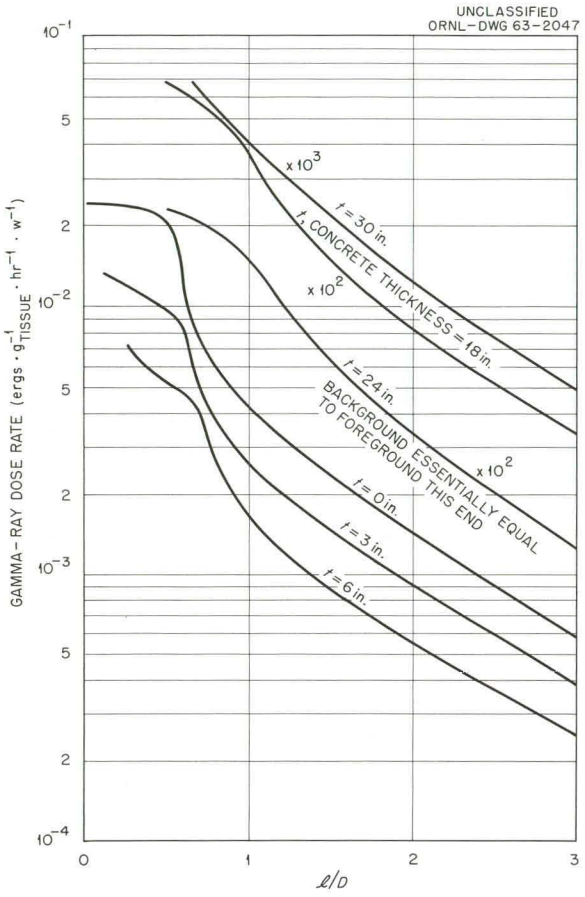

Fig. 36. Gamma-Ray Dose Rate in Hole No. 1 as a Function of ℓ/D for Various Thicknesses of Concrete Shield ($\gamma = 45°$).

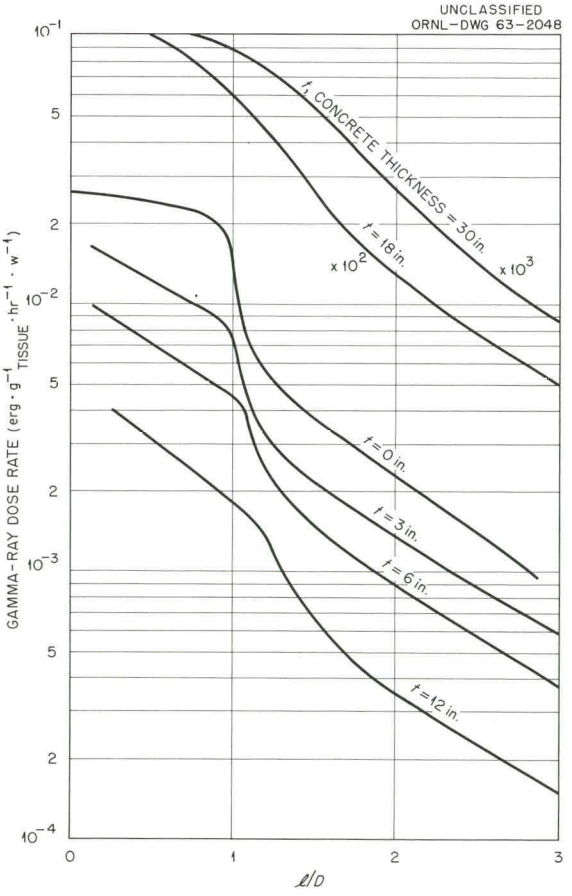

Fig. 37. Gamma-Ray Dose Rate in Hole No. 1 as a Function of ℓ/D for Various Thicknesses of Concrete Shield ($\gamma = 60°$).

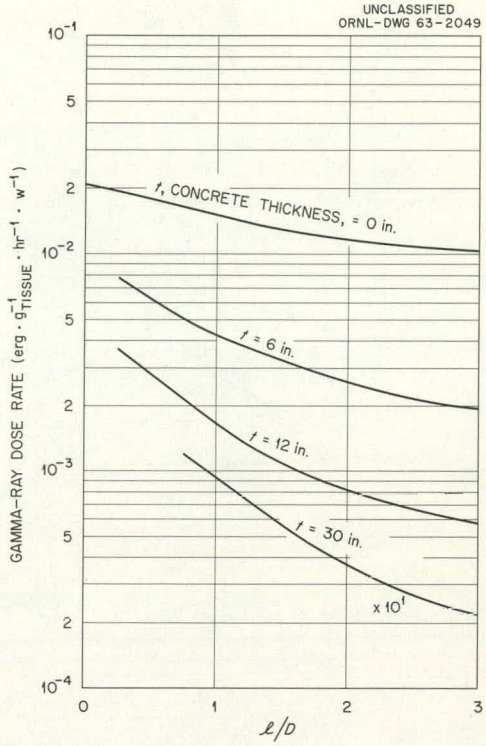

Fig. 38. Gamma-Ray Dose Rate in Hole No. 1 as a Function of ℓ/D for Various Thicknesses of Concrete Shield ($\gamma = 90°$).

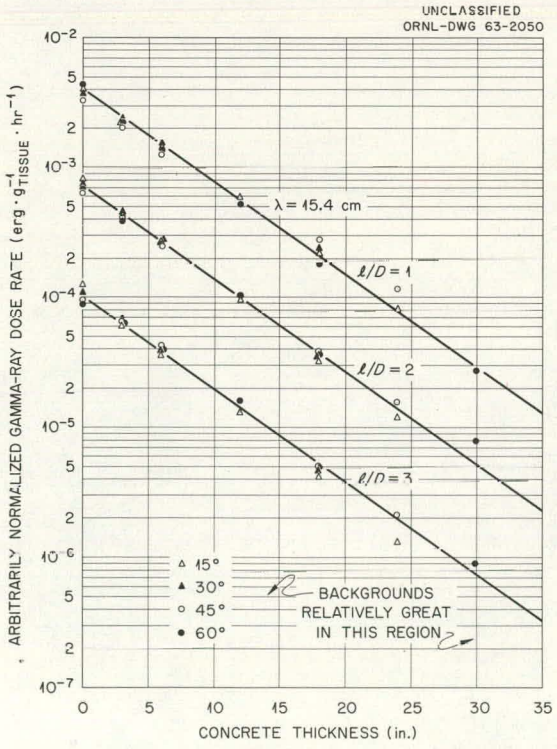

Fig. 39. Arbitrarily Normalized Gamma-Ray Dose Rate in Hole No. 1 as a Function of Thickness of Concrete Shield for Various Values of ℓ/D ($\gamma = 15$, 30, 45, and 60°).

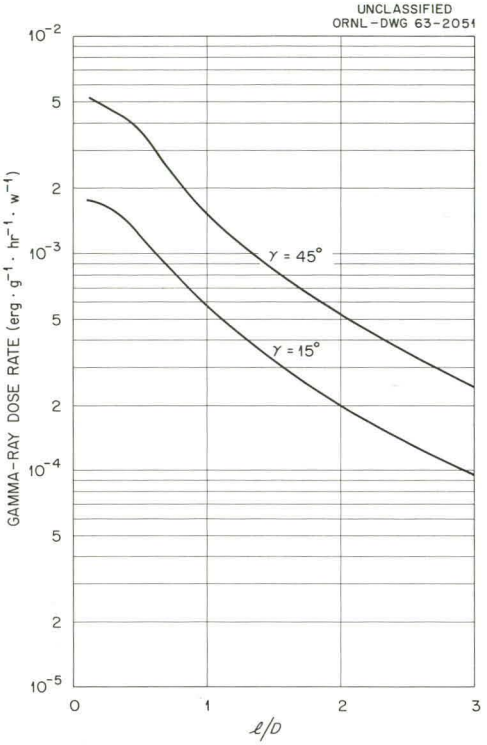

Fig. 40. Gamma-Ray Dose Rate in Hole No. 1 as a Function of ℓ/D for a $3\frac{1}{2}$-in.-Thick Iron Shield (γ = 15 and 45°).

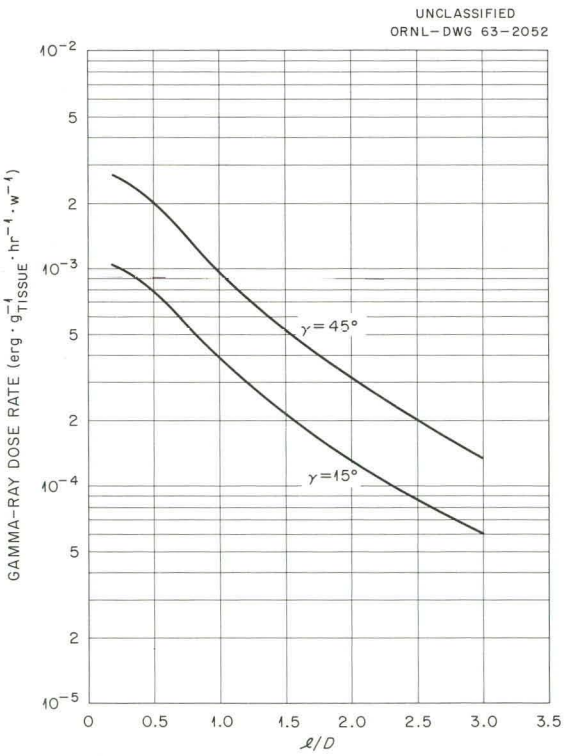

Fig. 41. Gamma-Ray Dose Rate in Hole No. 1 as a Function of ℓ/D for a Shield of $3\frac{1}{2}$ in. of Iron and 3 in. of Concrete (γ = 15 and 45°).

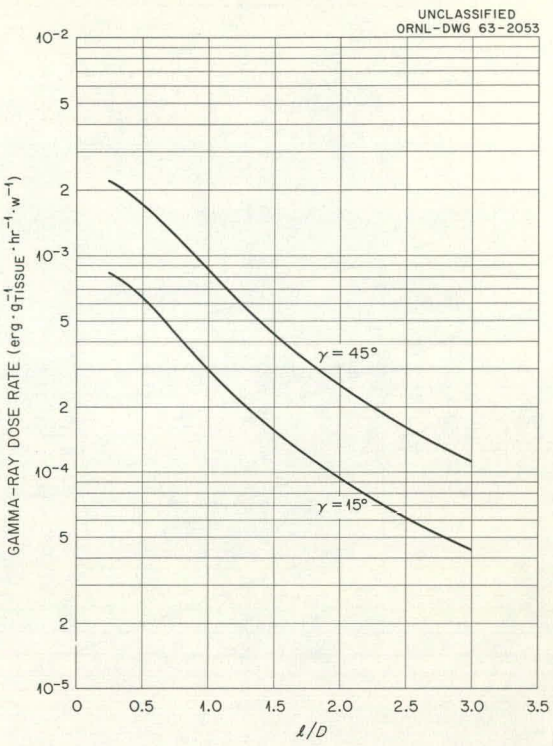

Fig. 42. Gamma-Ray Dose Rate in Hole No. 1 as a Function of ℓ/D for a Shield of $3\frac{1}{2}$ in. of Iron and 6 in. of Concrete (γ = 15 and 45°).

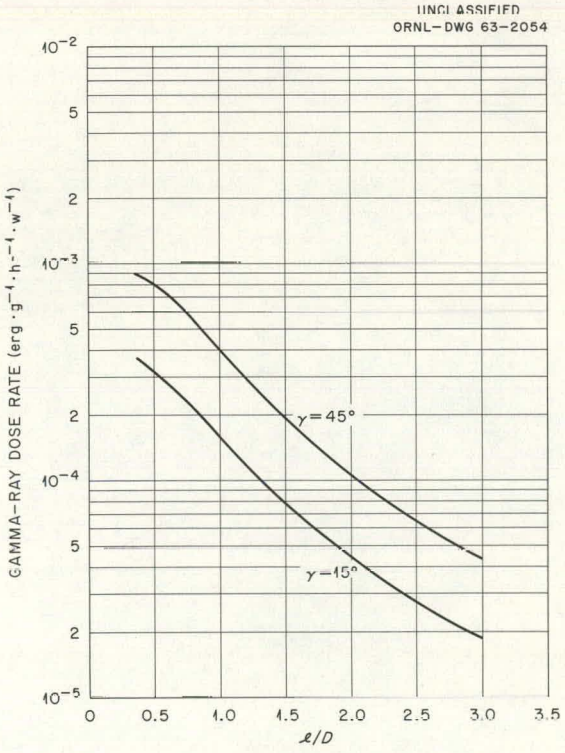

Fig. 43. Gamma-Ray Dose Rate in Hole No. 1 as a Function of ℓ/D for a Shield of $3\frac{1}{2}$ in. of Iron and 12 in. of Concrete (γ = 15 and 45°).

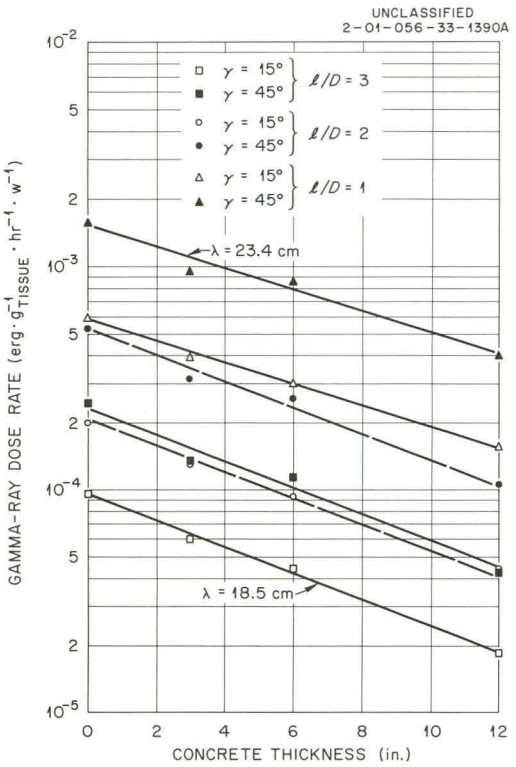

Fig. 44. Gamma-Ray Dose Rate in Hole No. 1 as a Function of the Thickness of Concrete Below $3\frac{1}{2}$ in. of Iron for Various Values of ℓ/D (γ = 15 and 45°).

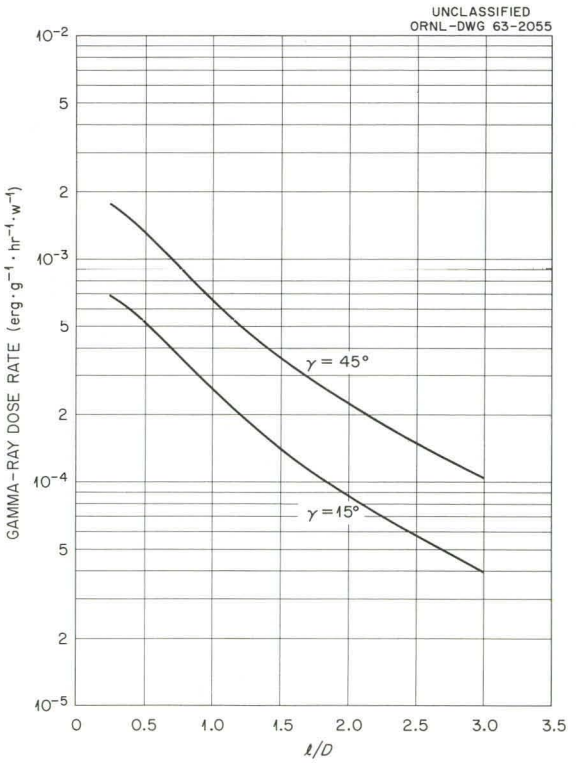

Fig. 45. Gamma-Ray Dose Rate in Hole No. 1 as a Function of ℓ/D for a Shield of $3\frac{1}{2}$ in. of Iron, 3 in. of Concrete, and $1\frac{1}{2}$ in. of Iron (γ = 15 and 45°).

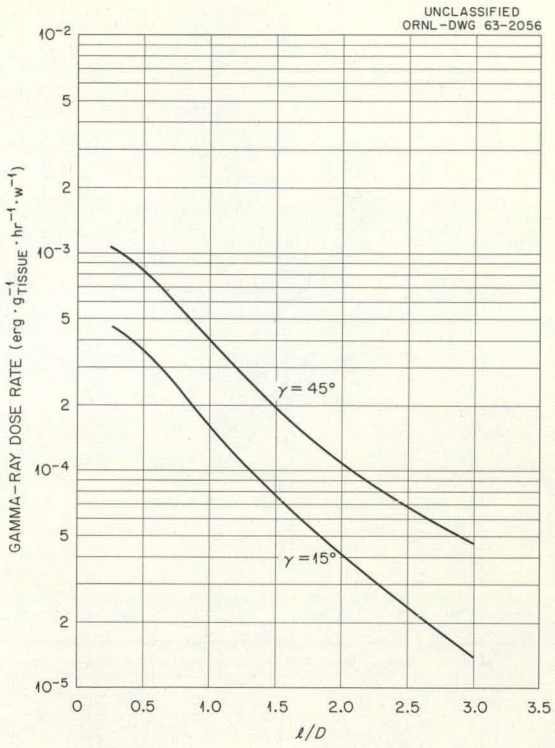

Fig. 46. Gamma-Ray Dose Rate in Hole No. 1 as a Function of ℓ/D for a Shield of $3\frac{1}{2}$ in. of Iron, 6 in. of Concrete, and $1\frac{1}{2}$ in. of Iron (γ = 15 and 45°).

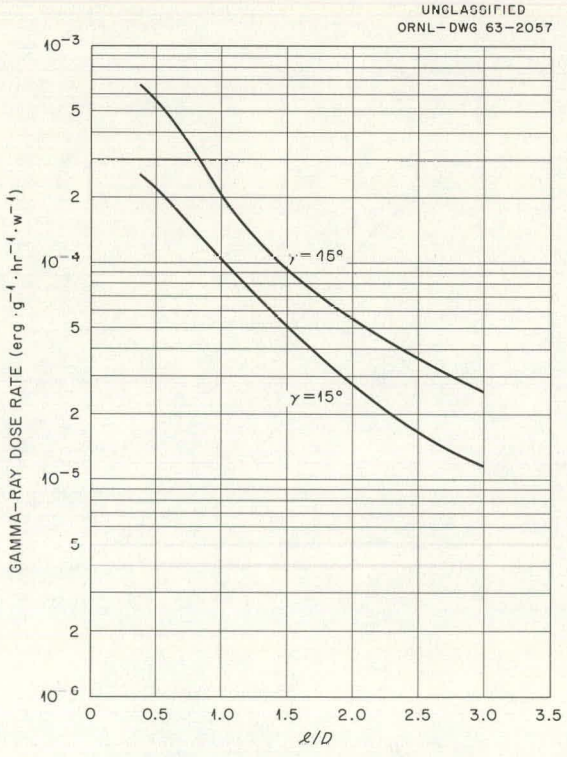

Fig. 47. Gamma-Ray Dose Rate in Hole No. 1 as a Function of ℓ/D for a Shield of $3\frac{1}{2}$ in. of Iron, 9 in. of Concrete, and $1\frac{1}{2}$ in. of Iron (γ = 15 and 45°).

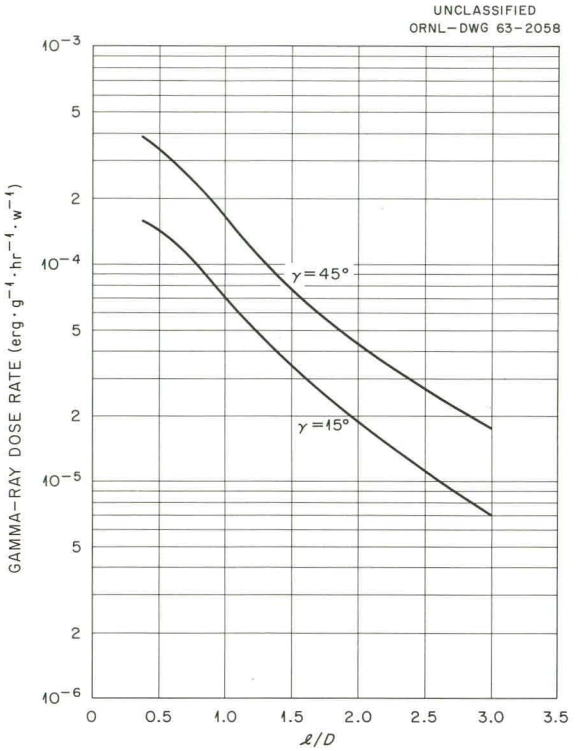

Fig. 48. Gamma-Ray Dose Rate in Hole No. 1 as a Function of ℓ/D for a Shield of $3\frac{1}{2}$ in. of Iron, 12 in. of Concrete, and $1\frac{1}{2}$ in. of Iron (γ = 15 and 45°).

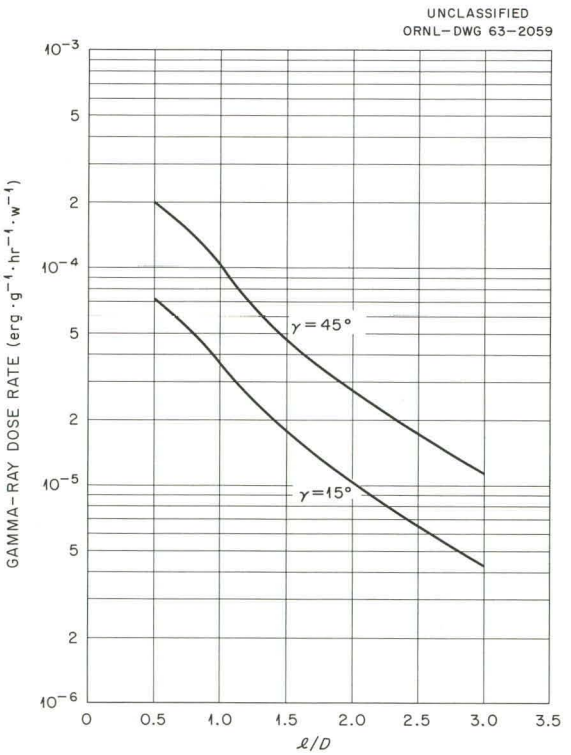

Fig. 49. Gamma-Ray Dose Rate in Hole No. 1 as a Function of ℓ/D for a Shield of $3\frac{1}{2}$ in. of Iron, 15 in. of Concrete, and $1\frac{1}{2}$ in. of Iron (γ = 15 and 45°).

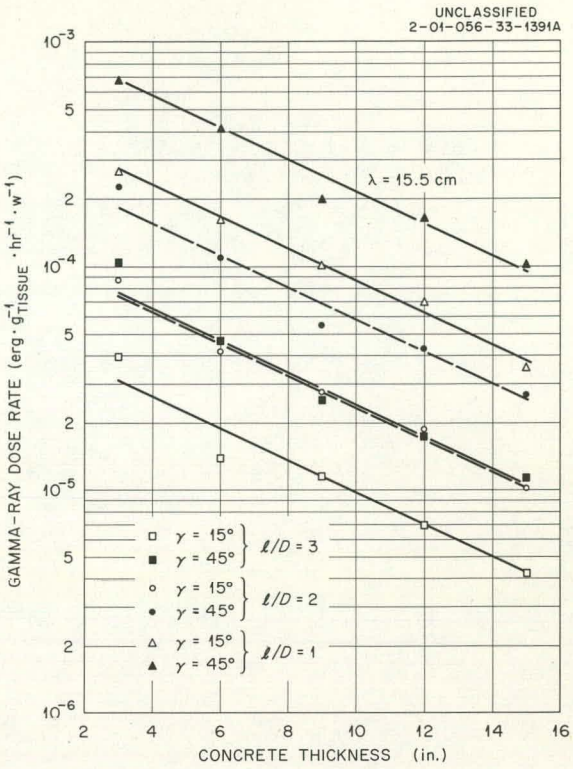

Fig. 50. Gamma-Ray Dose Rate in Hole No. 1 as a Function of the Thickness of Concrete Between $3\frac{1}{2}$-in.-Thick and $1\frac{1}{2}$-in.-Thick Iron Slabs for Various Values of ℓ/D ($\gamma = 15$ and 45°).

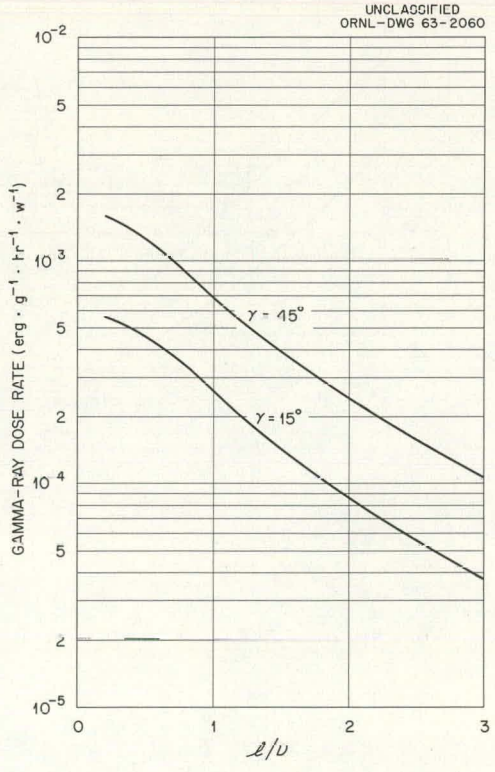

Fig. 51. Gamma-Ray Dose Rate in Hole No. 1 as a Function of ℓ/D for a Shield of Two $3\frac{1}{2}$-in.-Thick Iron Slabs Separated by 12 in. of Air ($\gamma = 15$ and 45°).

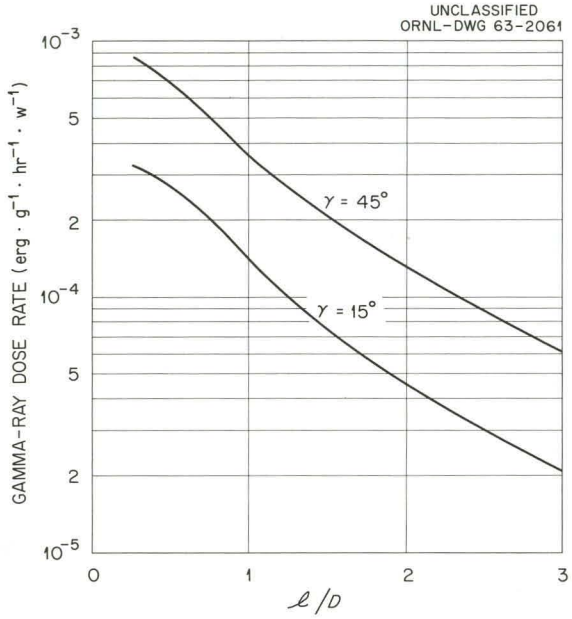

Fig. 52. Gamma-Ray Dose Rate in Hole No. 1 as a Function of ℓ/D for a Shield of Two $3\frac{1}{2}$-in.-Thick Iron Slabs Separated by 3 in. of Concrete ($\gamma = 15$ and 45°).

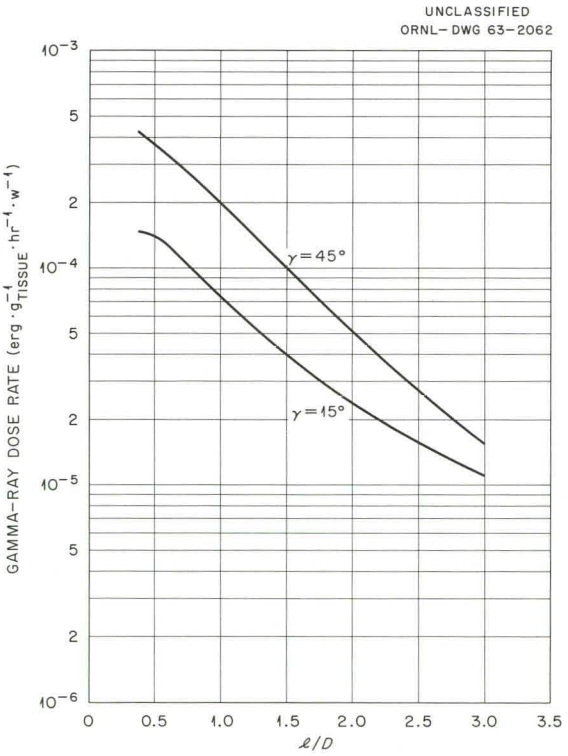

Fig. 53. Gamma-Ray Dose Rate in Hole No. 1 as a Function of ℓ/D for a Shield of Two $3\frac{1}{2}$-in.-Thick Iron Slabs Separated by 6 in. of Concrete ($\gamma = 15$ and 45°).

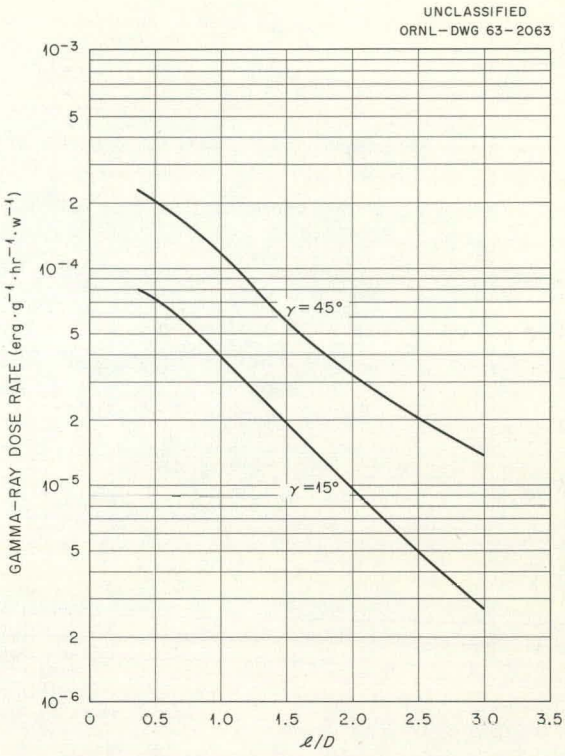

Fig. 54. Gamma-Ray Dose Rate in Hole No. 1 as a Function of ℓ/D for a Shield of Two $3\frac{1}{2}$-in.-Thick Iron Slabs Separated by 9 in. of Concrete ($\gamma = 15$ and $45°$).

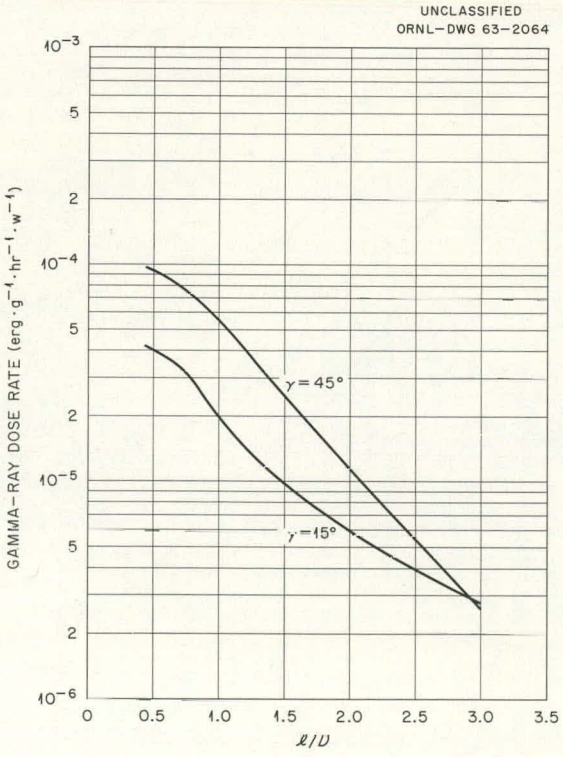

Fig. 55. Gamma-Ray Dose Rate in Hole No. 1 as a Function of ℓ/D for a Shield of Two $3\frac{1}{2}$-in.-Thick Iron Slabs Separated by 12 in. of Concrete ($\gamma = 15$ and $45°$).

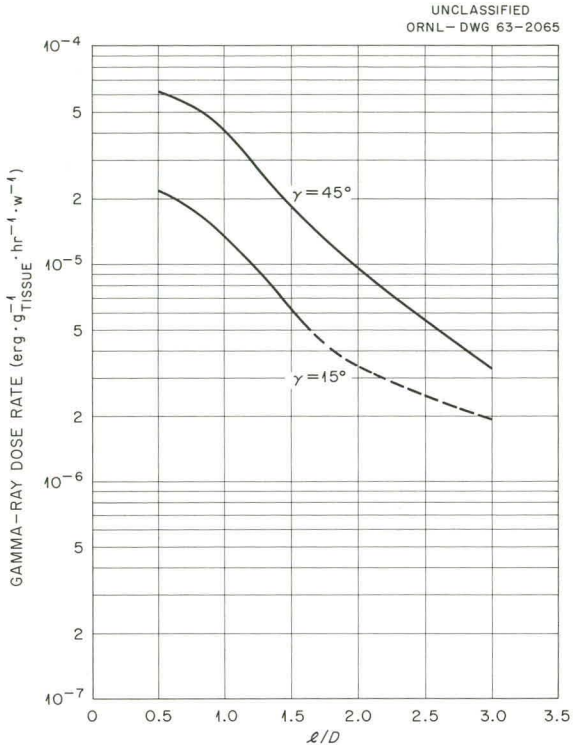

Fig. 56. Gamma-Ray Dose Rate in Hole No. 1 as a Function of ℓ/D for a Shield of Two $3\frac{1}{2}$-in.-Thick Iron Slabs Separated by 15 in. of Concrete ($\gamma = 15$ and 45°).

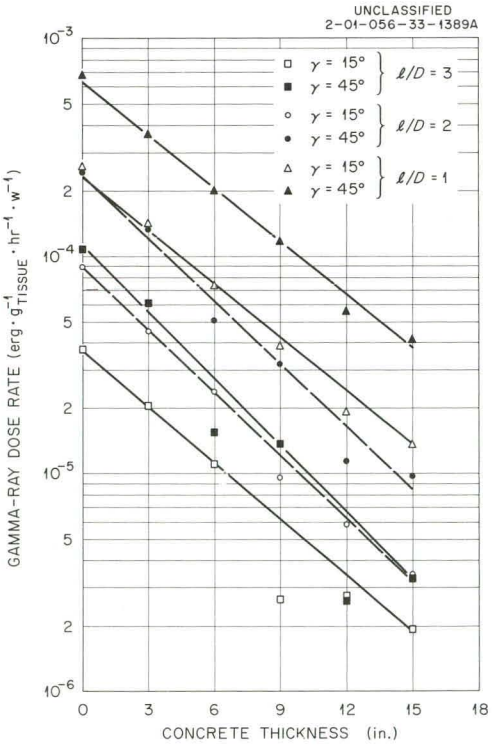

Fig. 57. Gamma-Ray Dose Rate in Hole No. 1 as a Function of the Thickness of Concrete Between Two $3\frac{1}{2}$-in.-Thick Iron Slabs for Various Values of ℓ/D ($\gamma = 15$ and 45°).

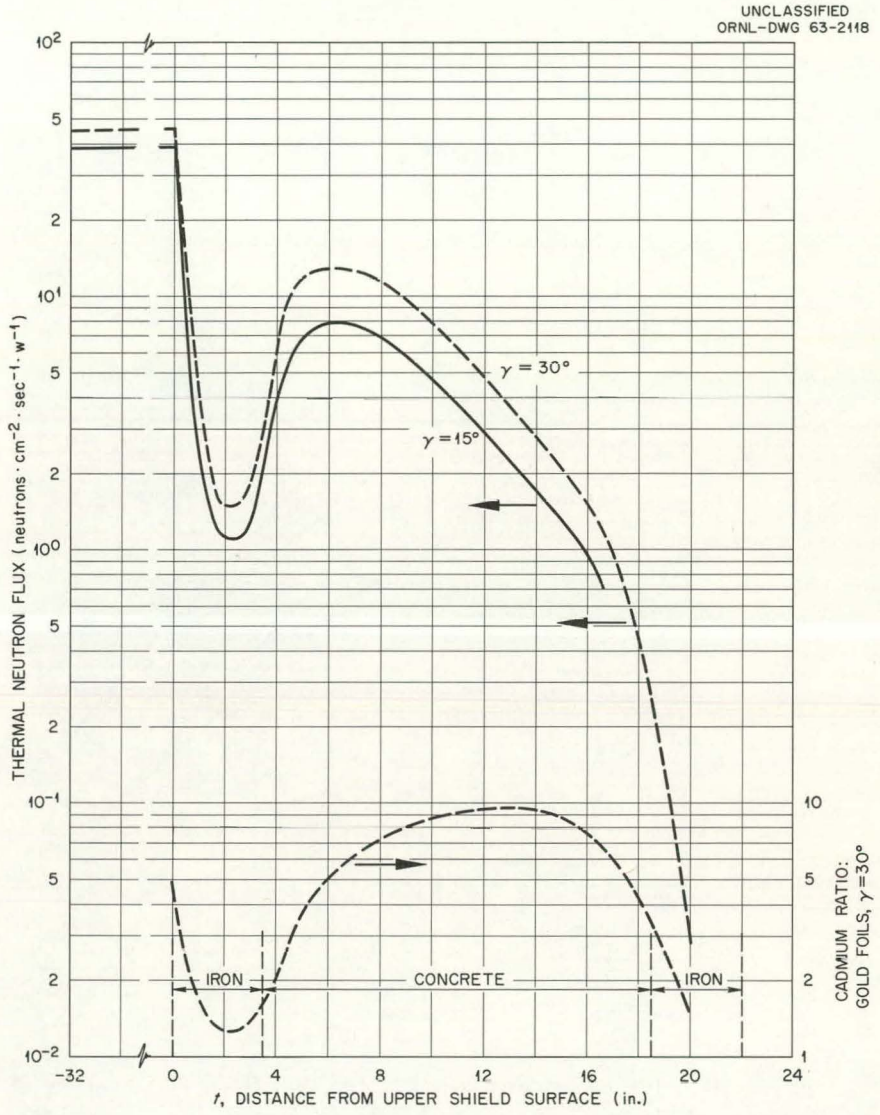

Fig. 58. Thermal-Neutron Flux Within Shield of Two $3\frac{1}{2}$-in.-Thick Iron Slabs Separated by 15 in. of Concrete (γ = 15 and 30°).

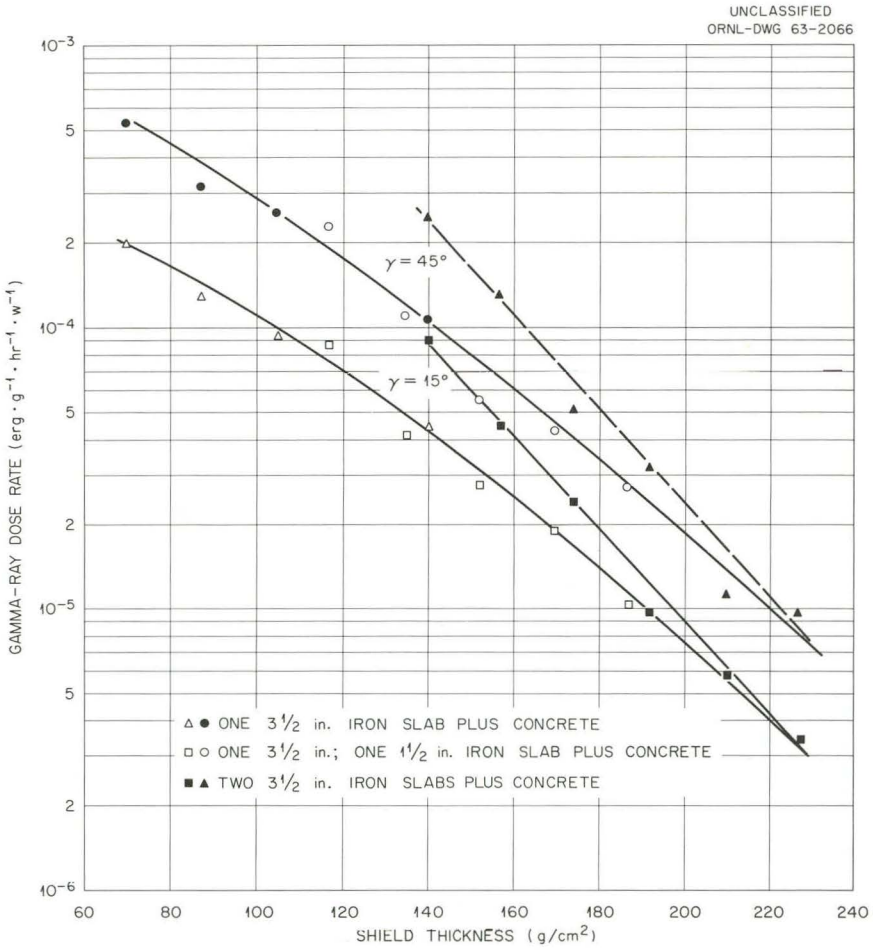

Fig. 59. Gamma-Ray Dose Rate at $\ell/D = 2$ in Hole No. 1 as a Function of the Thickness of Various Multilayer Iron-Concrete Shields (γ = 15 and 45°).

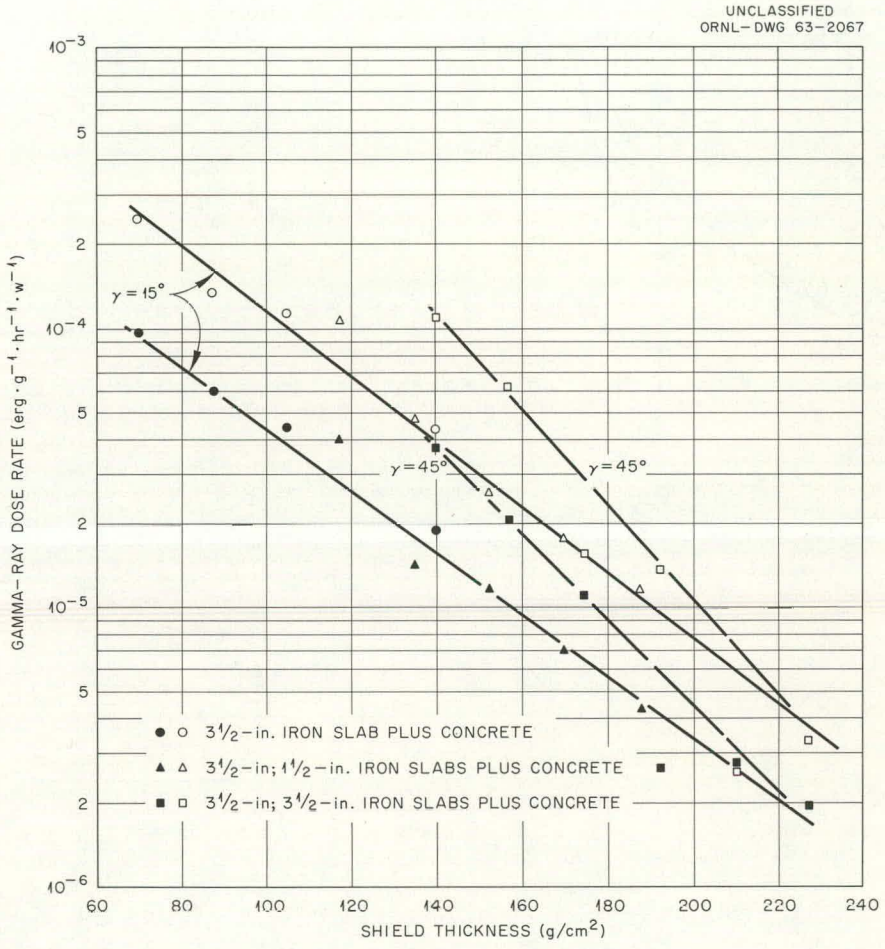

Fig. 60. Gamma-Ray Dose Rate at $\ell/D = 3$ in Hole No. 1 as a Function of the Thickness of Various Multilayer Iron-Concrete Shields (γ = 15 and 45°).

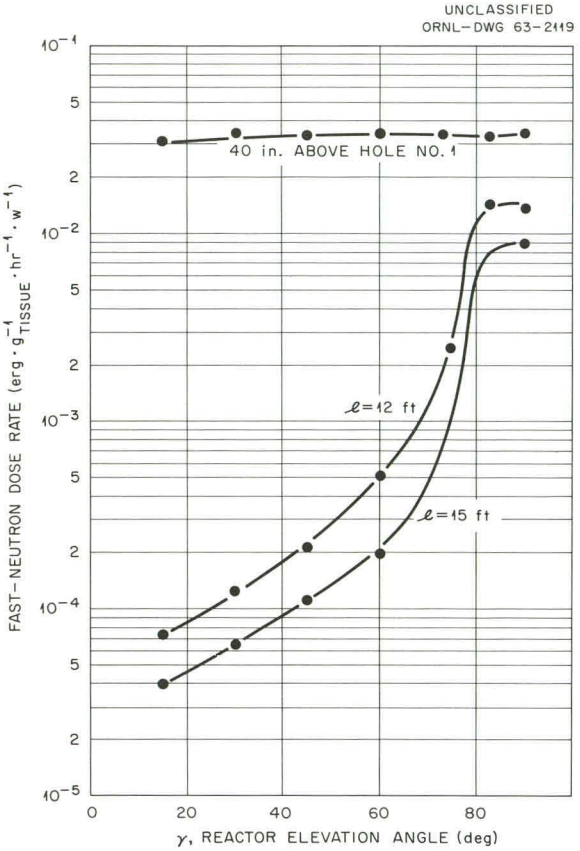

Fig. 61. Variation of Fast-Neutron Dose Rate at $\ell/D = 3$ and 3.75 in Hole No. 1 (No Shield) with Reactor Elevation Angle.

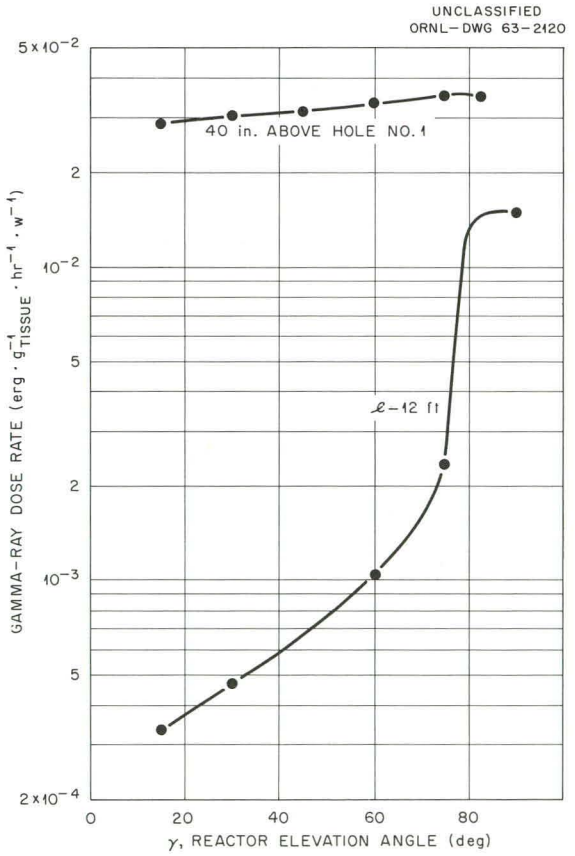

Fig. 62. Variation of Gamma-Ray Dose Rate at $\ell/D = 3$ in Hole No. 1 (No Shield) with Reactor Elevation Angle.

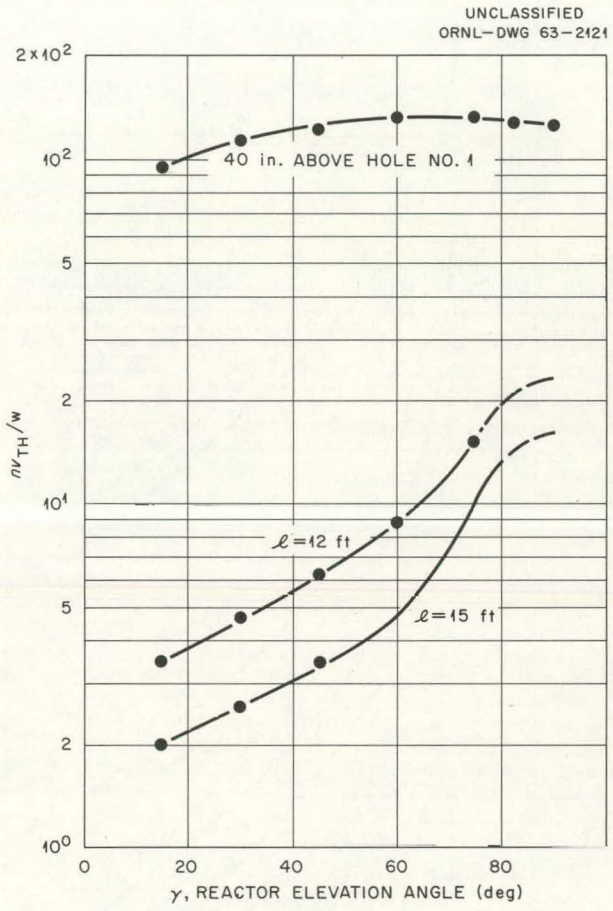

Fig. 63. Variation of Thermal-Neutron Flux at $\ell/D = 3$ and 3.75 in Hole No. 1 (No Shield) with Reactor Elevation Angle.

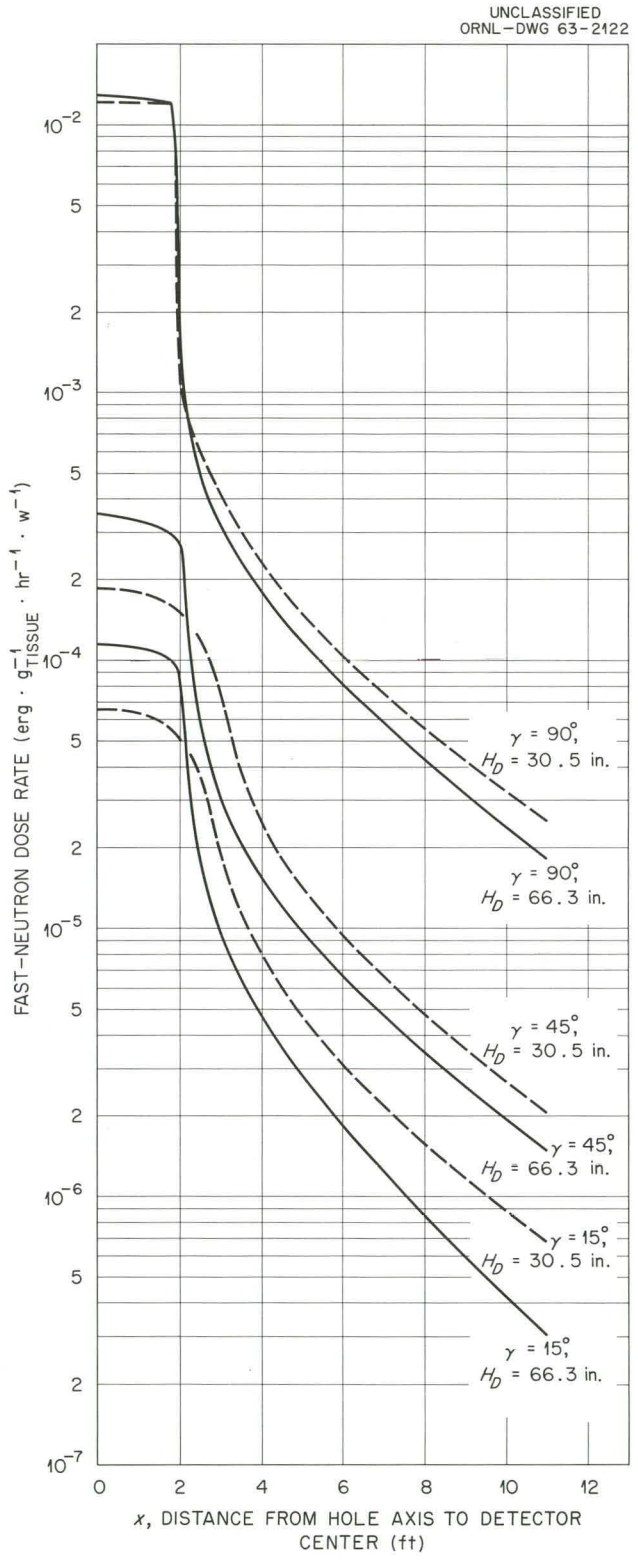

Fig. 64. Fast-Neutron Dose Rate Measured in Tunnel (No Shield over Hole) at Heights of 30.5 and 66.3 in. above Floor (γ = 15, 45, and 90°).

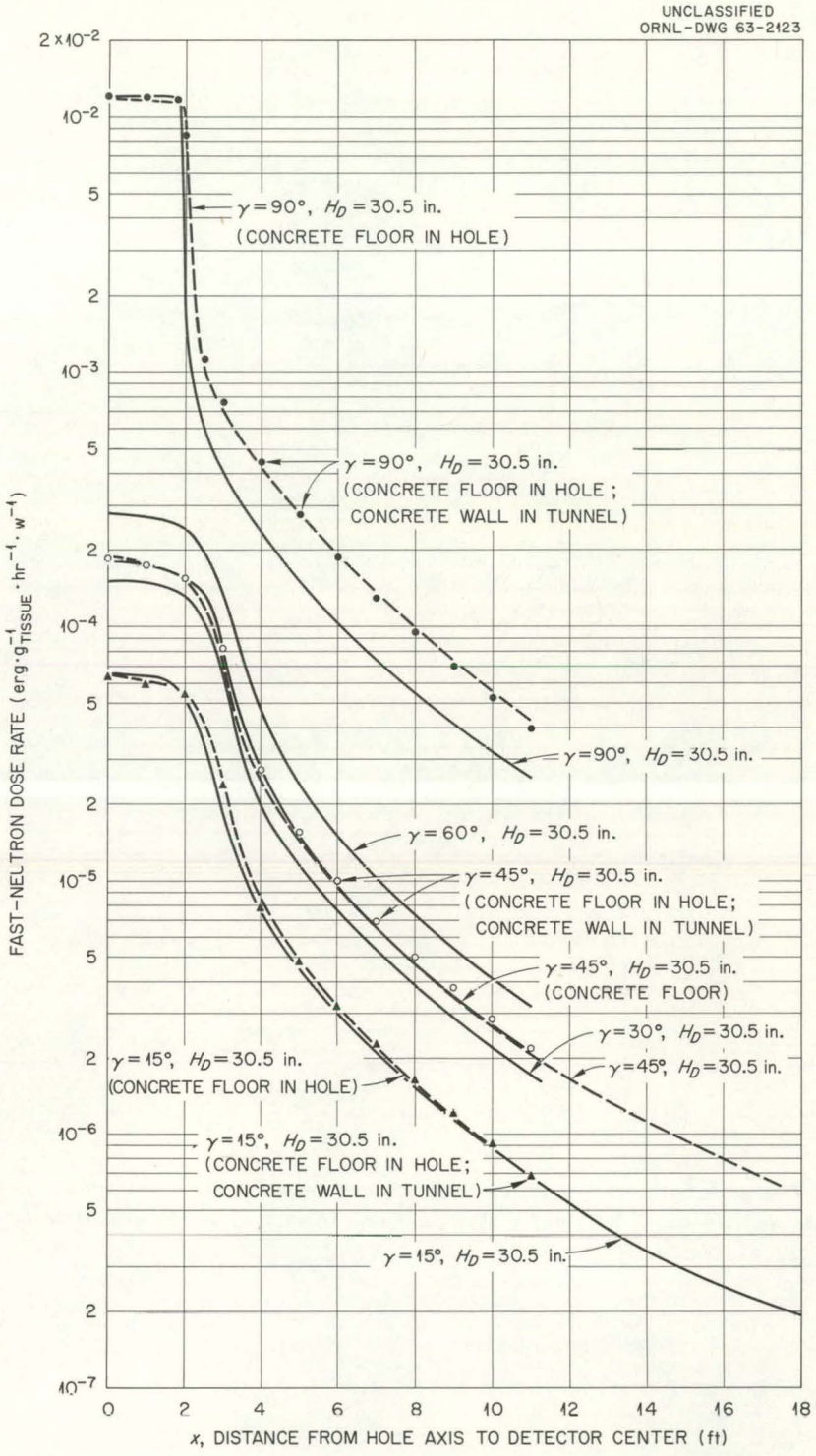

Fig. 65. Fast-Neutron Dose Rate in Tunnel (No Shield over Hole) with and without Modifications to Hole and Tunnel (γ = 15, 30, 45, 60, and 90°).

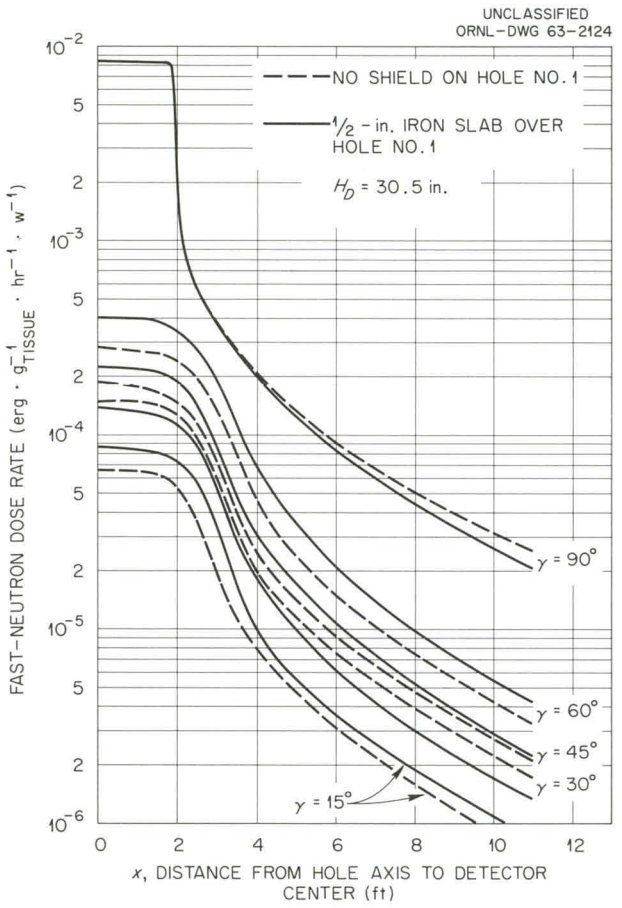

Fig. 66. Fast-Neutron Dose Rate in Tunnel as a Function of Distance from Axis of Hole No. 1 with and without a $\frac{1}{2}$-in.-Thick Iron Shield over Hole (γ = 15, 30, 45, 60, and 90°).

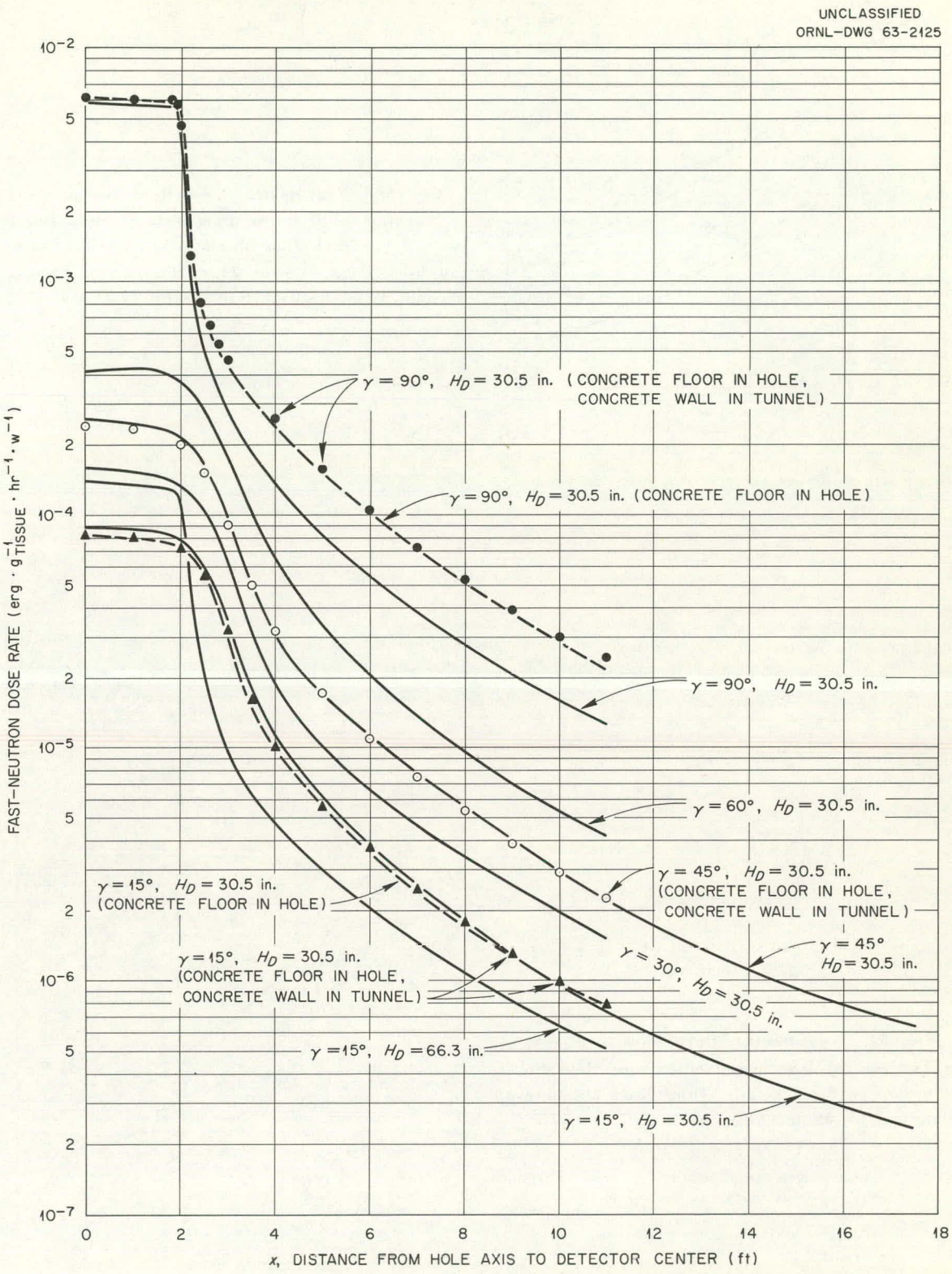

Fig. 67. Fast-Neutron Dose Rate in Tunnel as a Function of Distance from Axis of Hole No. 1 with a 1-in.-Thick Iron Shield over Hole and with Various Modifications to Hole and Tunnel (γ = 15, 30, 45, 60, and 90°).

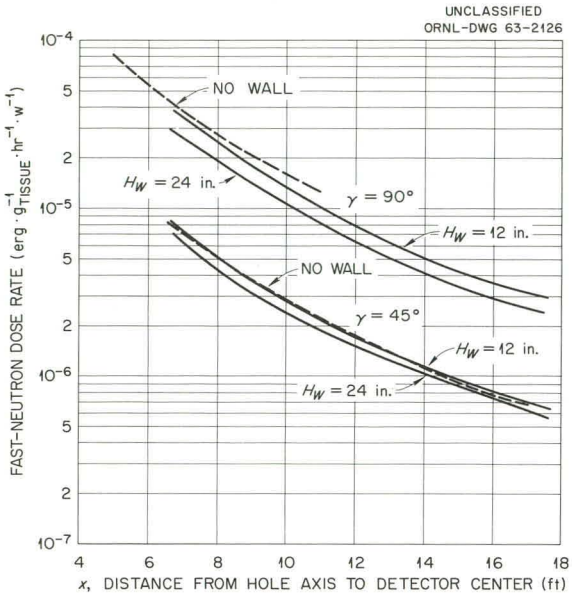

Fig. 68. Fast-Neutron Dose Rate in Tunnel as a Function of Distance from Axis of Hole No. 1 with 1-in.-Thick Iron Shield over Hole and with an 8-in.-Thick, 12- or 24-in.-High Brick Wall in Tunnel 49 in. from the Hole Axis (γ = 45 and 90°).

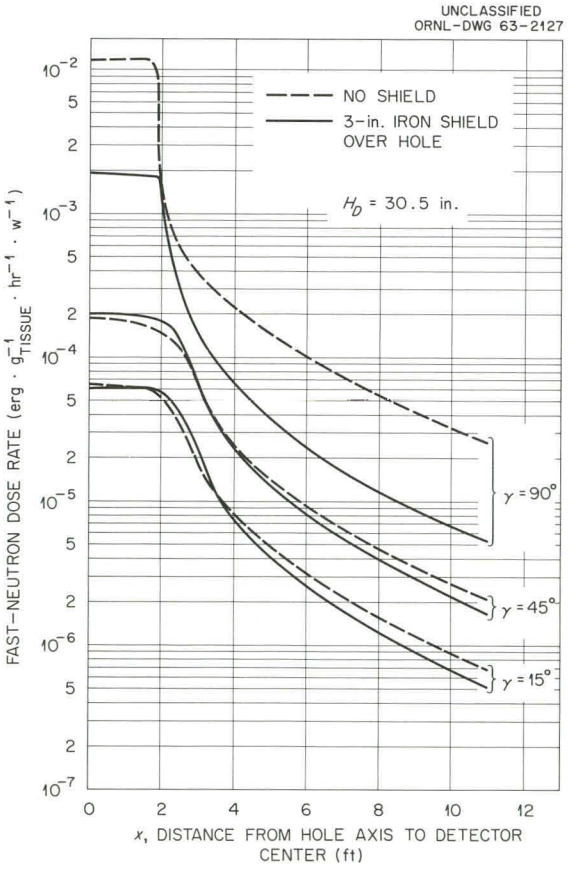

Fig. 69. Fast-Neutron Dose Rate in Tunnel as a Function of Distance from Axis of Hole No. 1 with and without a 3-in.-Thick Iron Shield over Hole (γ = 15, 45, and 90°).

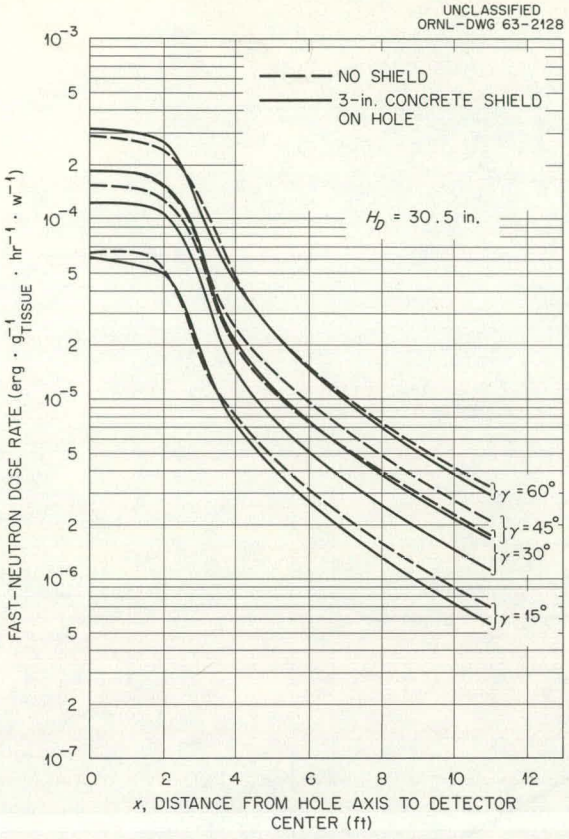

Fig. 70. Fast-Neutron Dose Rate in Tunnel as a Function of Distance from Axis of Hole No. 1 with and without a 3-in.-Thick Concrete Shield on Hole (γ = 15, 30, 45, and 60°).

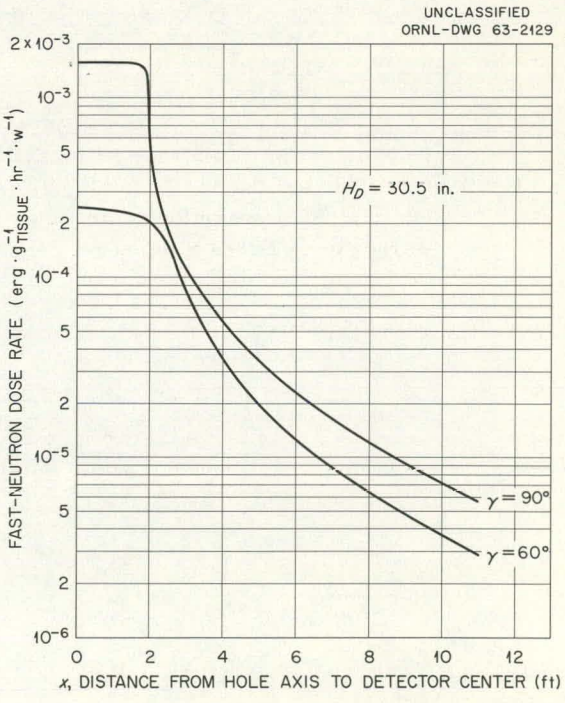

Fig. 71. Fast-Neutron Dose Rate in Tunnel as a Function of Distance from Axis of Hole No. 1 with a Shield of 1 in. of Iron and 3 in. of Concrete over Hole (γ = 60 and 90°).

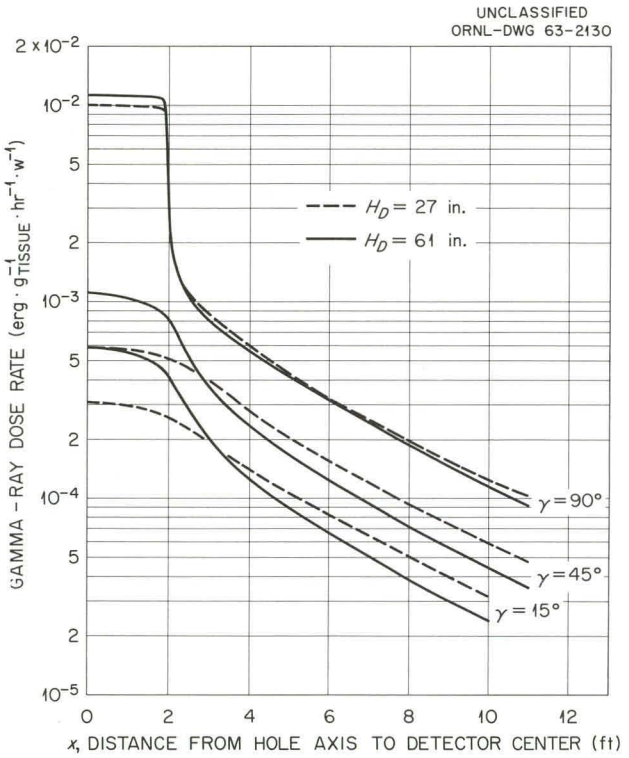

Fig. 72. Gamma-Ray Dose Rates Measured in Tunnel (No Shield on Hole) at Heights of 27 and 61 in. above Floor (γ = 15, 45, and 90°).

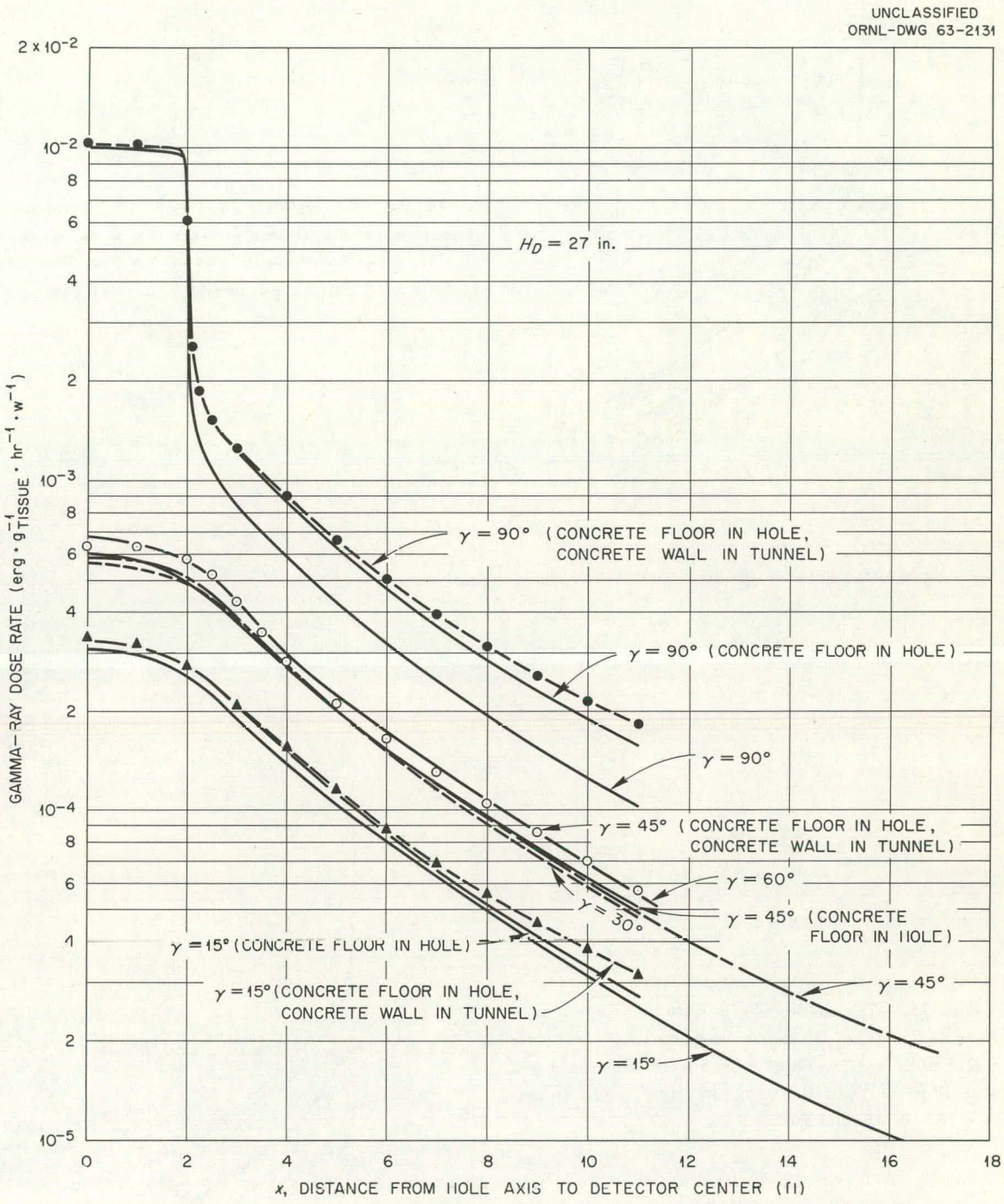

Fig. 73. Gamma-Ray Dose Rate in Tunnel (No Shield over Hole) with and without Modifications to Hole and Tunnel (γ = 15, 30, 45, 60, and 90°).

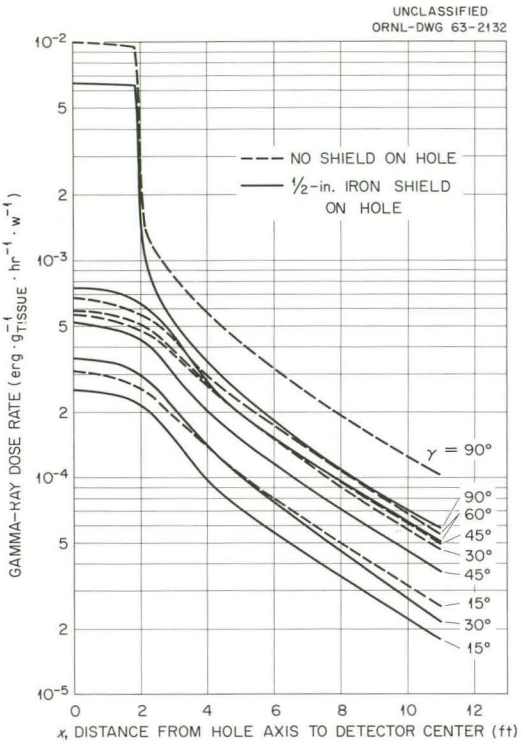

Fig. 74. Gamma-Ray Dose Rate in Tunnel as a Function of the Distance from the Axis of Hole No. 1 with and without a ½-in.-Thick Iron Slab over Hole (γ = 15, 30, 45, 60, and 90°).

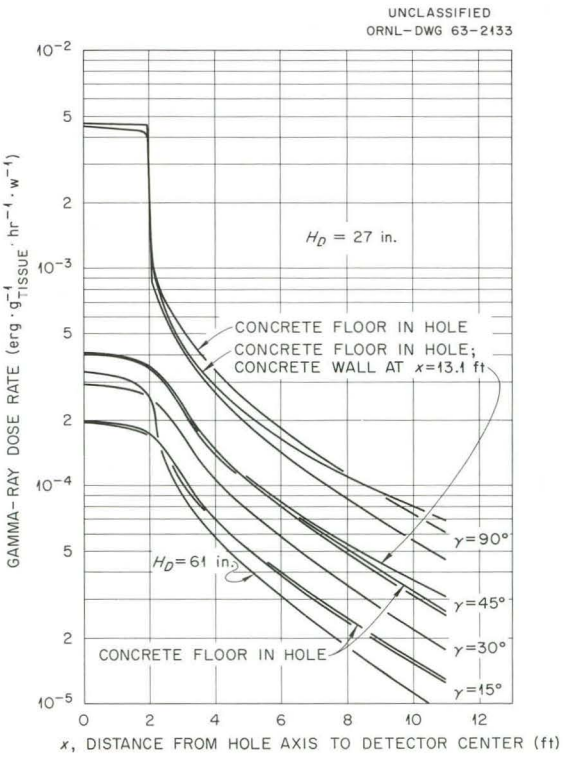

Fig. 75. Gamma-Ray Dose Rate in Tunnel as a Function of the Distance from the Axis of Hole No. 1 with a 1-in.-Thick Iron Shield over Hole and with Various Modifications to Hole and Tunnel (γ = 15, 30, 45, and 90°).

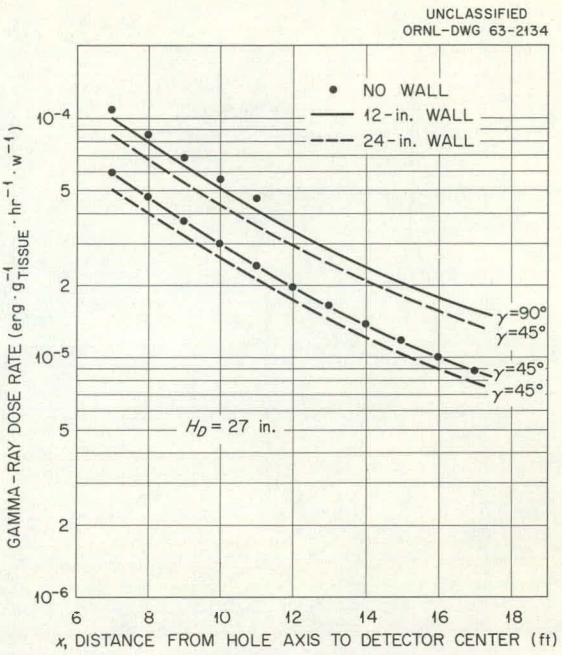

Fig. 76. Gamma-Ray Dose Rate in Tunnel as a Function of Distance from the Axis of Hole No. 1 with a 1-in.-Thick Iron Shield over Hole and with an 8-in.-Thick, 12- or 24-in.-High Brick Wall in Tunnel 49 in. from the Hole Axis (γ = 45 and 90°).

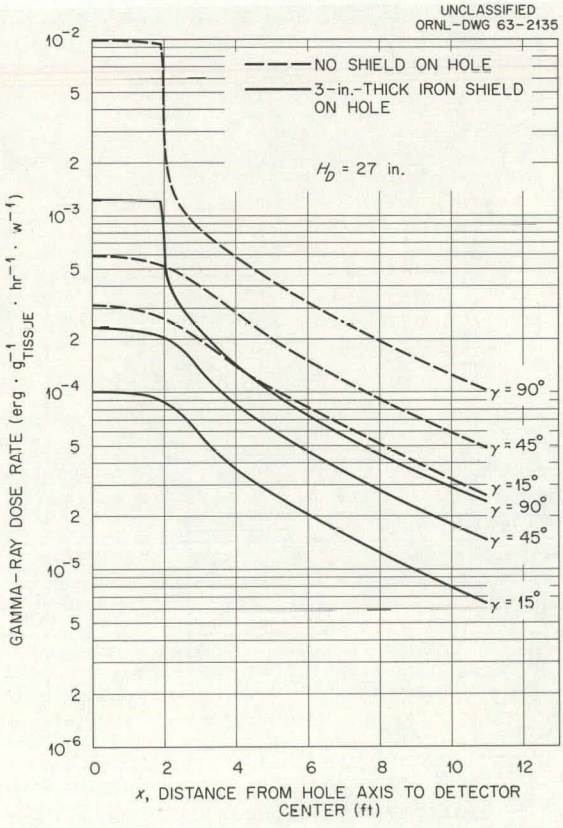

Fig. 77. Gamma-Ray Dose Rate in Tunnel as a Function of Distance from the Axis of Hole No. 1 with and without a 3-in.-Thick Iron Shield over Hole (γ = 15, 45, and 90°).

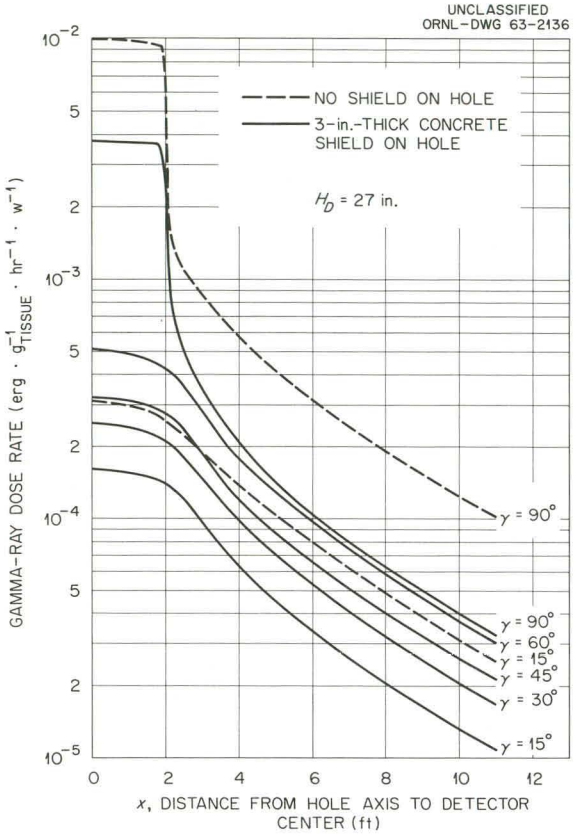

Fig. 78. Gamma-Ray Dose Rate in Tunnel as a Function of Distance from the Axis of Hole No. 1 with and without a 3-in.-Thick Concrete Shield over Hole (γ = 15, 30, 45, 60, and 90°).

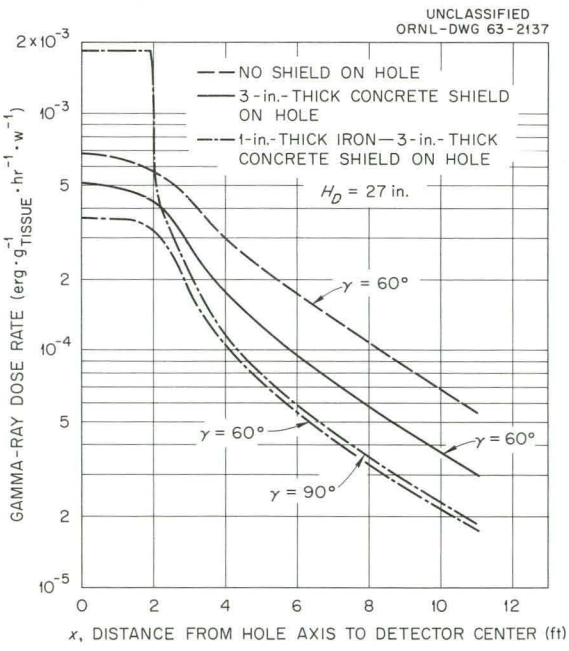

Fig. 79. Gamma-Ray Dose Rate in Tunnel as a Function of Distance from the Axis of Hole No. 1 with and without a 3-in.-Thick Concrete Shield or a Shield of 1 in. of Iron and 3 in. of Concrete over Hole (γ = 60 and 90°).

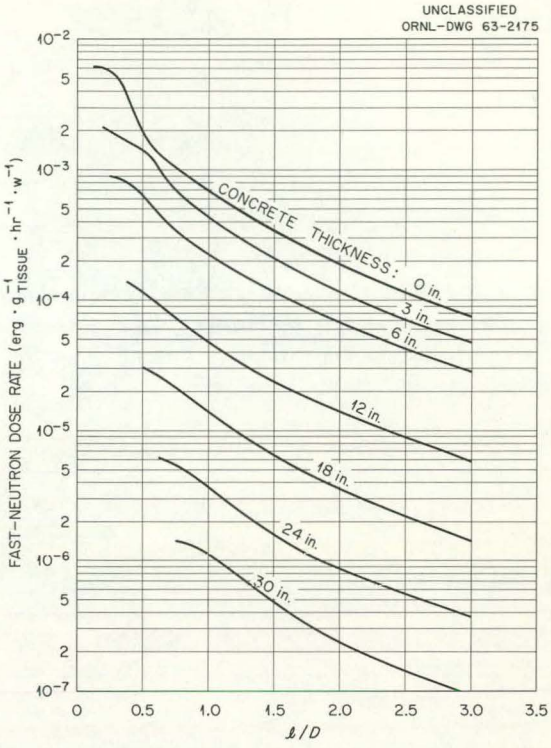

Fig. 80. Fast-Neutron Dose Rate in Hole No. 2 as a Function of ℓ/D for Various Thicknesses of Concrete Shield ($\gamma = 45^{\circ}$).

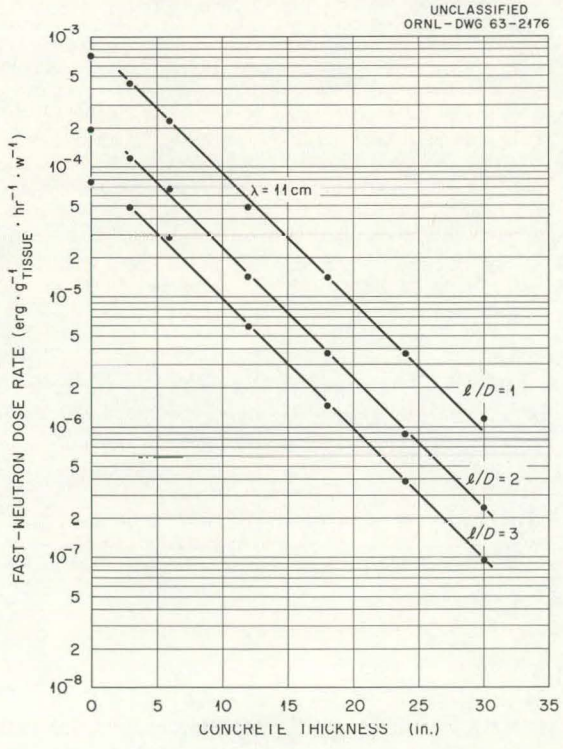

Fig. 81. Fast-Neutron Dose Rate in Hole No. 2 as a Function of the Thickness of Concrete Shield for Various Values of ℓ/D ($\gamma = 45^{\circ}$).

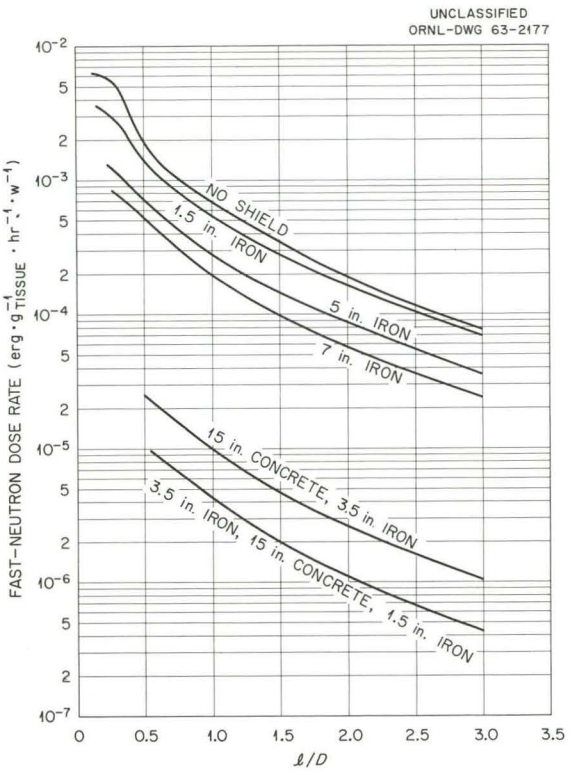

Fig. 82. Fast-Neutron Dose Rate in Hole No. 2 as a Function of ℓ/D for Various Thicknesses of Iron and Iron-Concrete Shields ($\gamma = 45°$).

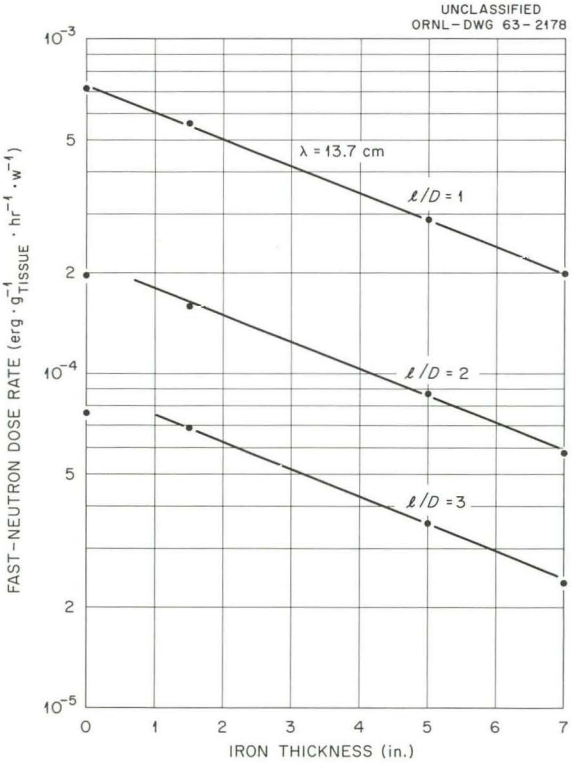

Fig. 83. Fast-Neutron Dose Rate in Hole No. 2 as a Function of the Thickness of an Iron Shield for Various Values of ℓ/D ($\gamma = 45°$).

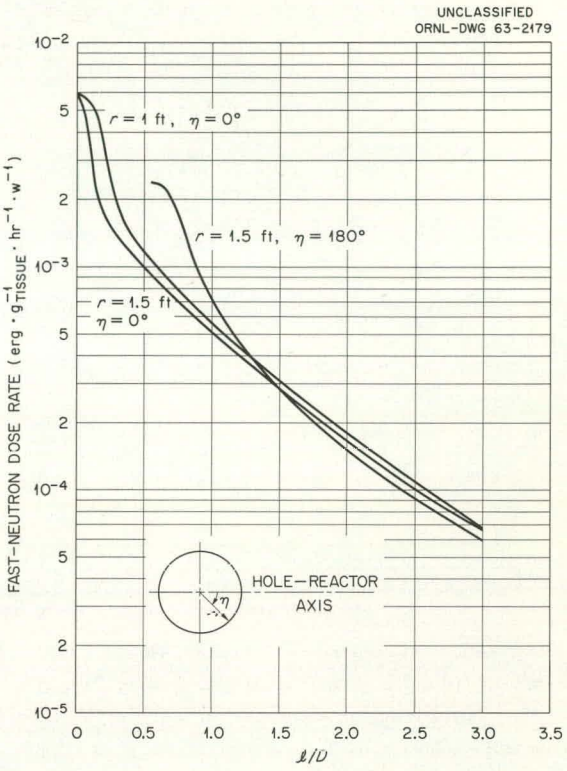

Fig. 84. Variation of Fast-Neutron Dose Rate in Hole No. 2 (No Shield) with Radial Detector Position ($\gamma = 45°$).

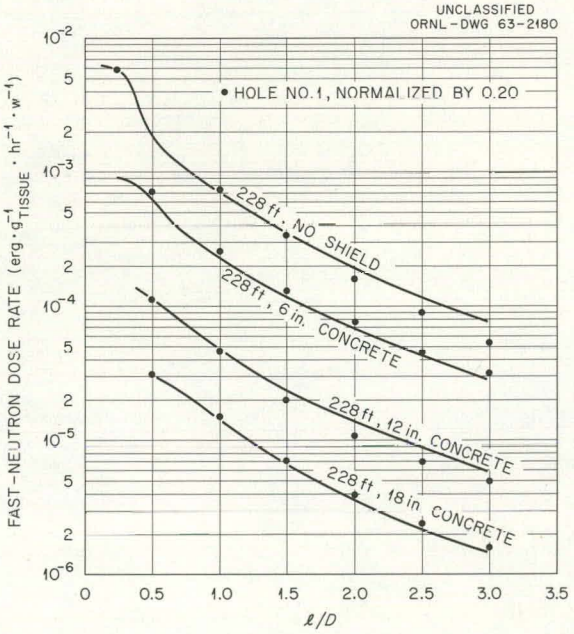

Fig. 85. Comparison of Fast-Neutron Dose Rates in Hole No. 1 and Hole No. 2 as a Function of ℓ/D for Various Thicknesses of Concrete Shield ($\gamma = 45°$).

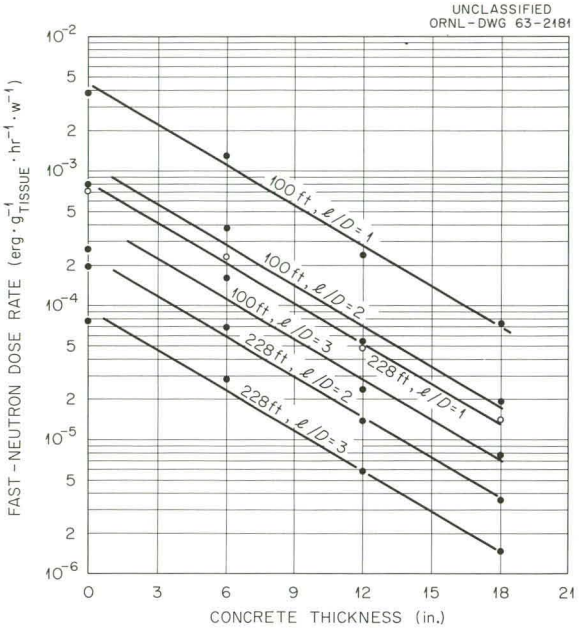

Fig. 86. Comparison of Fast-Neutron Dose Rates in Hole No. 1 and Hole No. 2 as a Function of the Thickness of Concrete Shield for Various Values of ℓ/D ($\gamma = 45^{\circ}$).

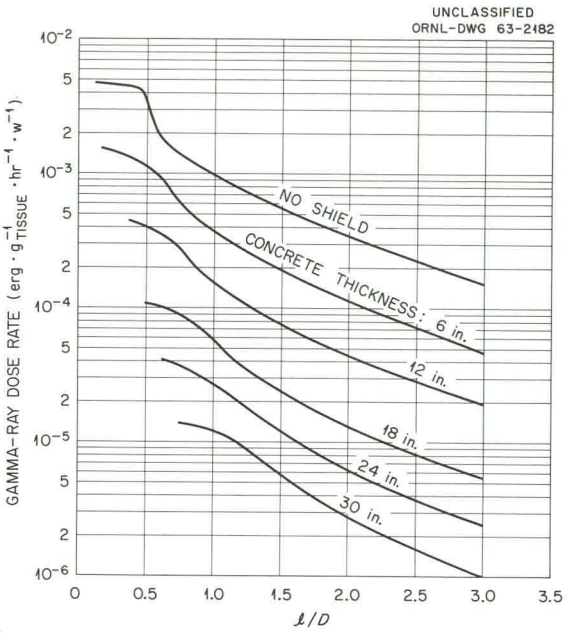

Fig. 87. Gamma-Ray Dose Rate in Hole No. 2 as a Function of ℓ/D for Various Thicknesses of Concrete Shield ($\gamma = 45^{\circ}$).

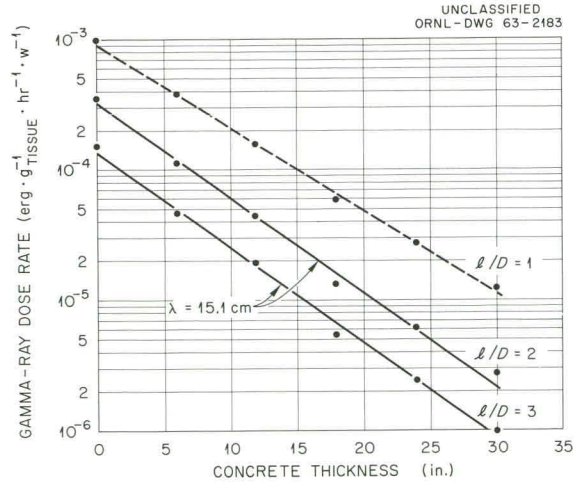

Fig. 88. Gamma-Ray Dose Rate in Hole No. 2 as a Function of the Thickness of Concrete Shield for Various Values of ℓ/D ($\gamma = 45^{\circ}$).

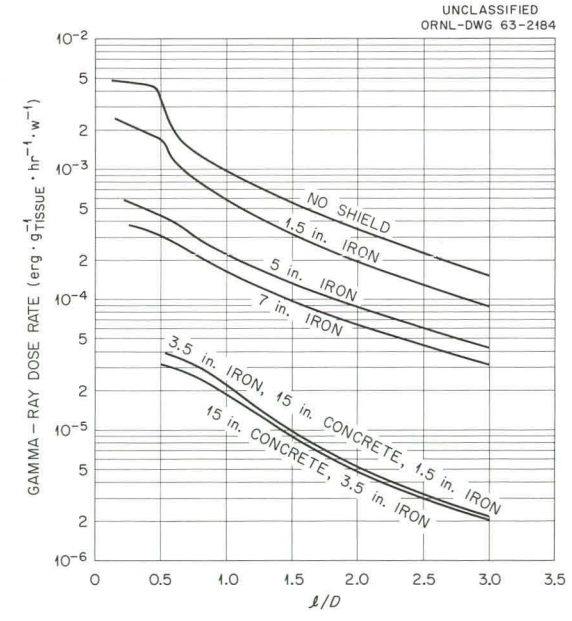

Fig. 89. Gamma-Ray Dose Rate in Hole No. 2 as a Function of ℓ/D for Various Thicknesses of Iron and Iron-Concrete Shields ($\gamma = 45^{\circ}$).

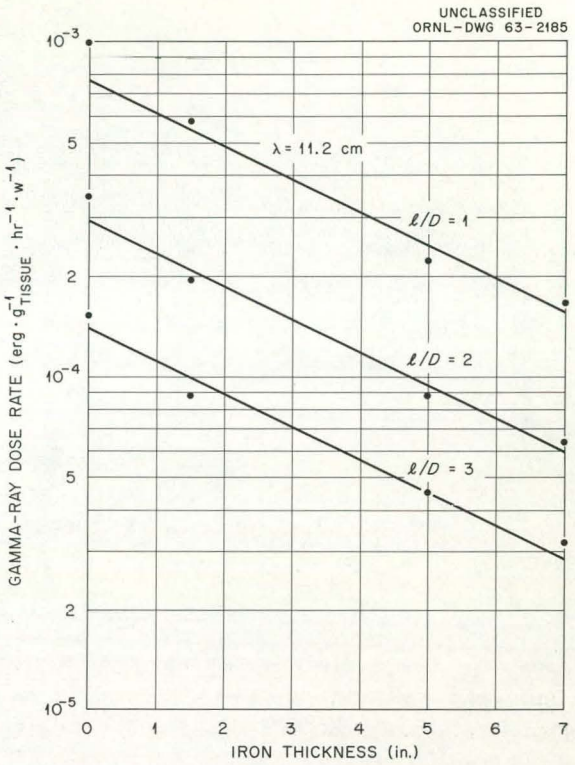

Fig. 90. Gamma-Ray Dose Rate in Hole No. 2 as a Function of the Thickness of Iron Shield for Various Values of ℓ/D ($\gamma = 45^{\circ}$).

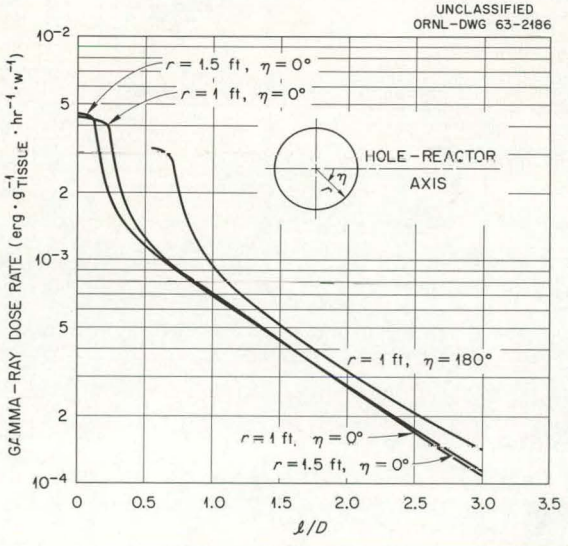

Fig. 91. Variation of Gamma-Ray Dose Rate in Hole No. 2 (No Shield) with Radial Detector Position ($\gamma = 45^{\circ}$).

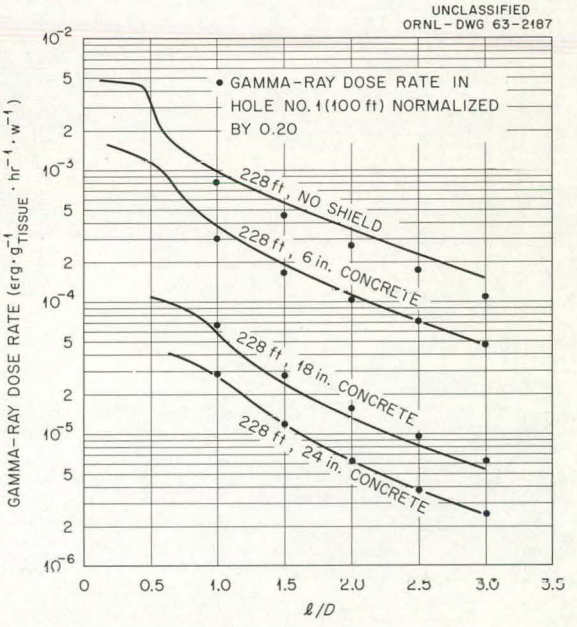

Fig. 92. Comparison of Gamma-Ray Dose Rates in Hole No. 1 and Hole No. 2 as a Function of ℓ/D for Various Thicknesses of Concrete Shield ($\gamma = 45^{\circ}$).

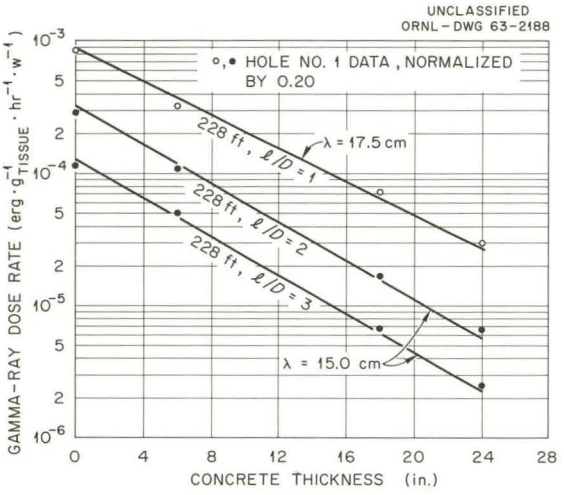

Fig. 93. Comparison of Gamma-Ray Dose Rates in Hole No. 1 and Hole No. 2 as a Function of the Thickness of Concrete Shield for Various Values of ℓ/D ($\gamma = 45°$).

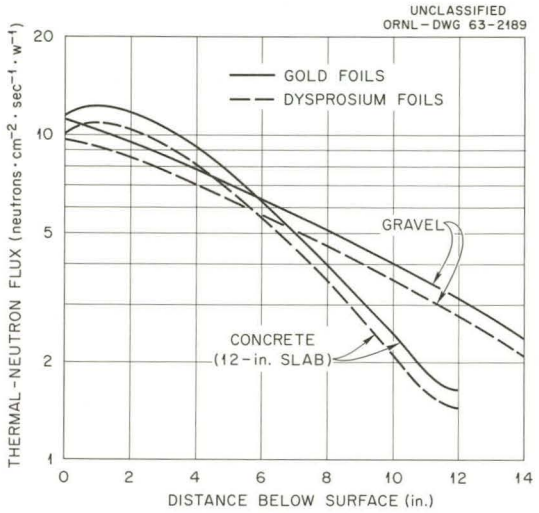

Fig. 94. Thermal-Neutron Fluxes Through Concrete and Gravel at Hole No. 2 ($\gamma = 45°$).

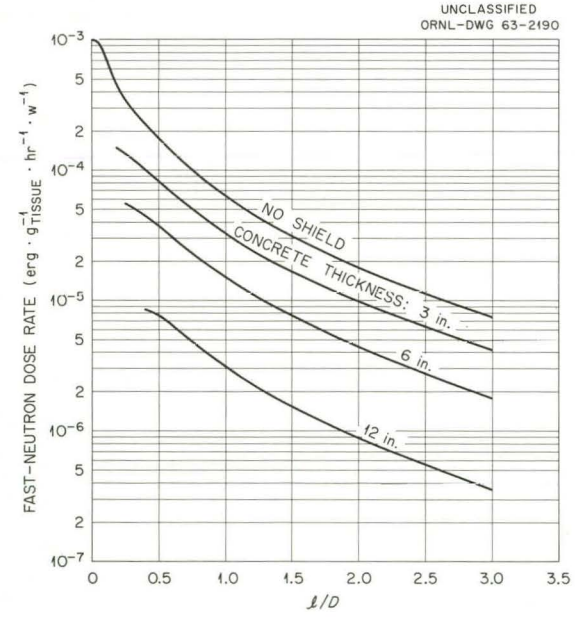

Fig. 95. Fast-Neutron Dose Rate in Hole No. 3 as a Function of ℓ/D for Various Thicknesses of Concrete Shield ($\gamma = 15°$).

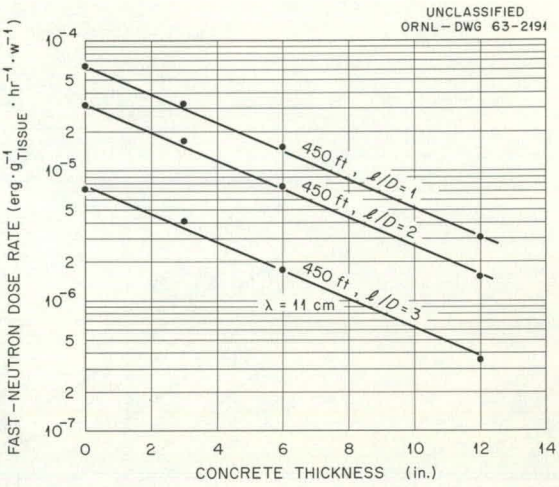

Fig. 96. Fast-Neutron Dose Rate in Hole No. 3 as a Function of the Thickness of Concrete Shield for Various Values of ℓ/D ($\gamma = 15^{\circ}$).

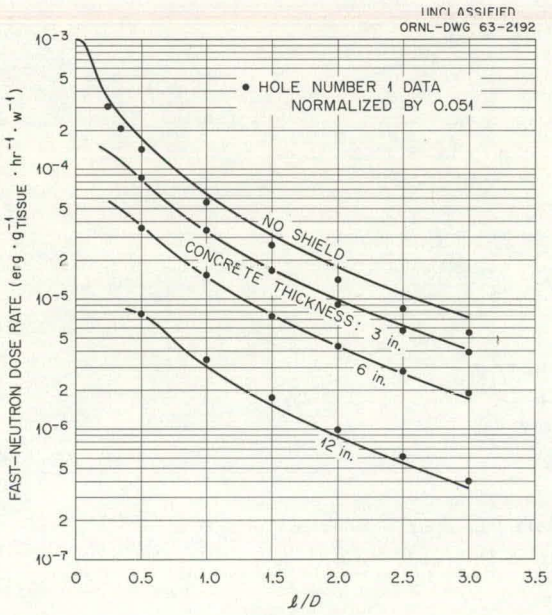

Fig. 97. Comparison of Fast-Neutron Dose Rates in Hole No. 1 and Hole No. 3 as a Function of ℓ/D for Various Thicknesses of Concrete Shield ($\gamma = 15^{\circ}$).

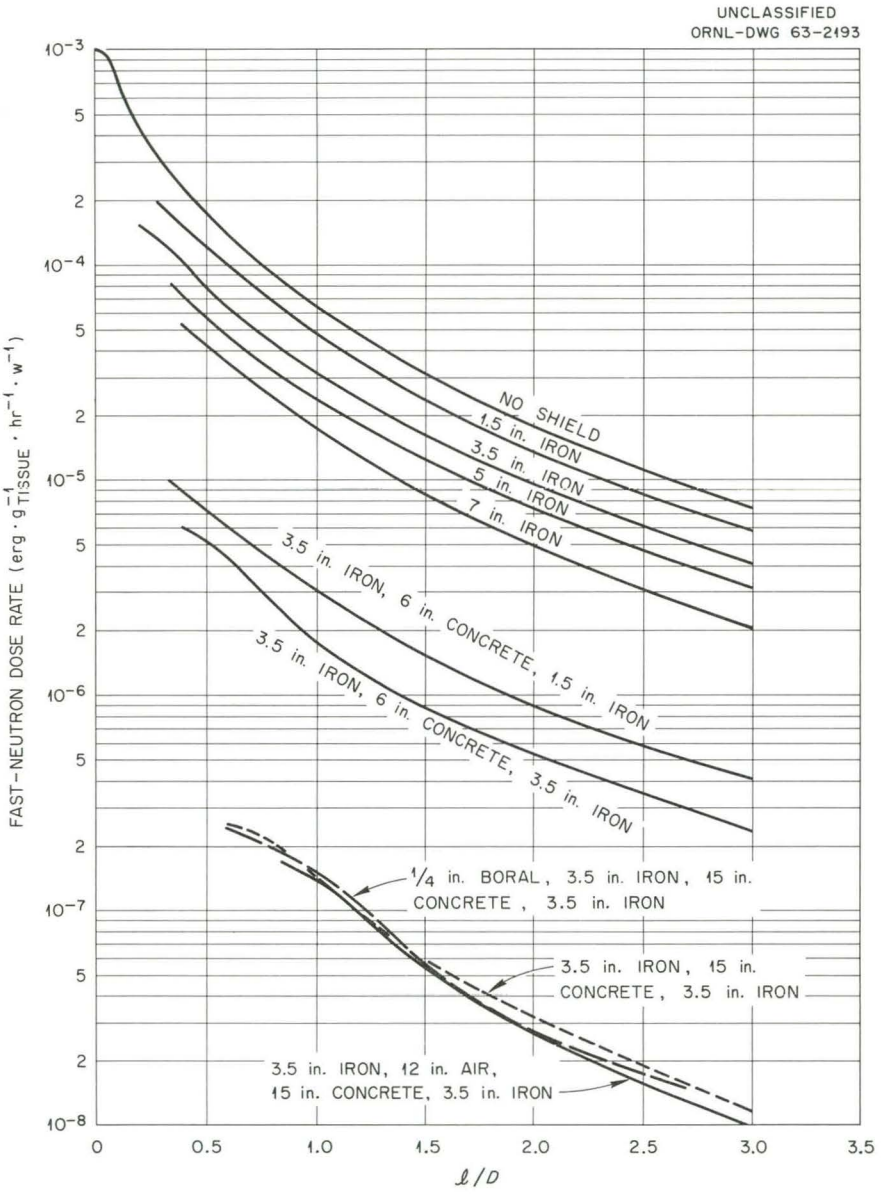

Fig. 98. Fast-Neutron Dose Rate in Hole No. 3 as a Function of ℓ/D for Various Thicknesses of Iron and Iron-Concrete Shields ($\gamma = 15^{\circ}$).

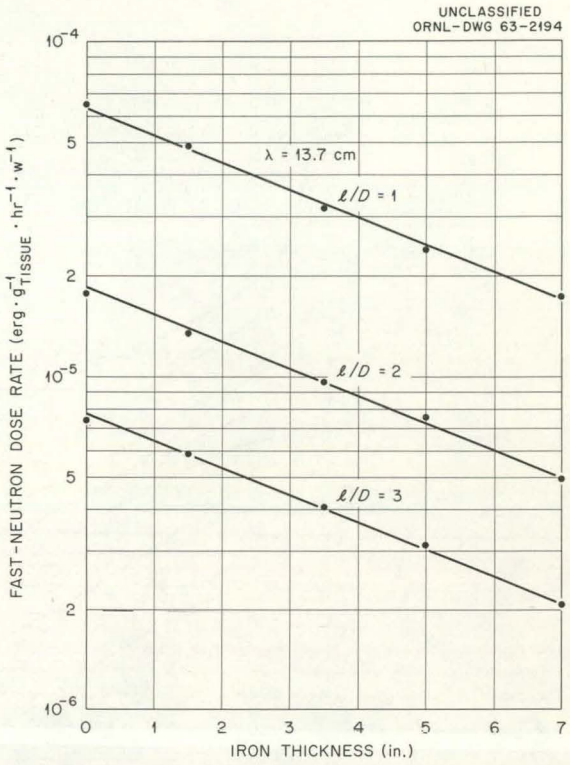

Fig. 99. Fast-Neutron Dose Rate in Hole No. 3 as a Function of the Thickness of an Iron Shield ($\gamma = 15^{\circ}$).

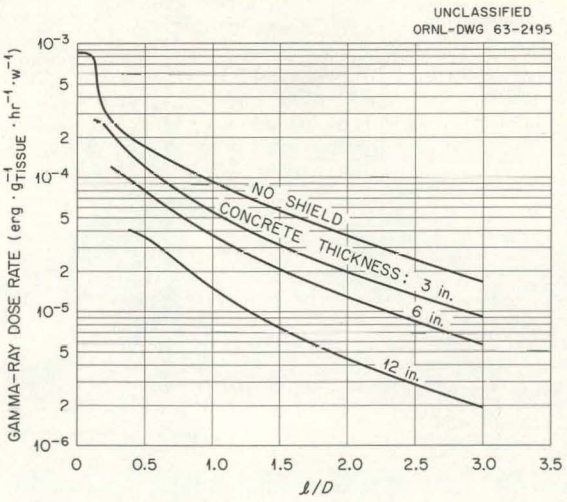

Fig. 100. Gamma-Ray Dose Rate in Hole No. 3 as a Function of ℓ/D for Various Thicknesses of Concrete Shield ($\gamma = 15^{\circ}$).

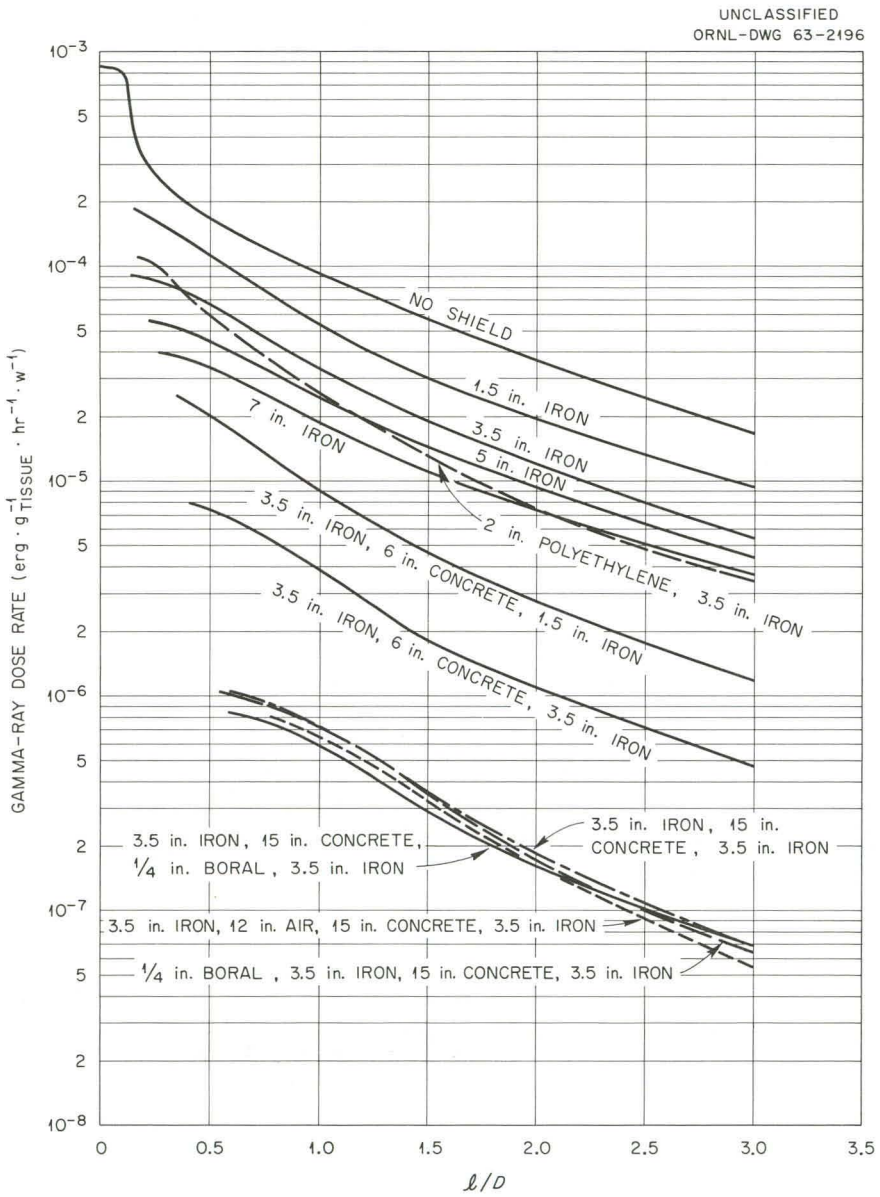

Fig. 101. Gamma-Ray Dose Rate in Hole No. 3 as a Function of ℓ/D for Various Thicknesses of Iron and Iron-Concrete Shields ($\gamma = 15°$).

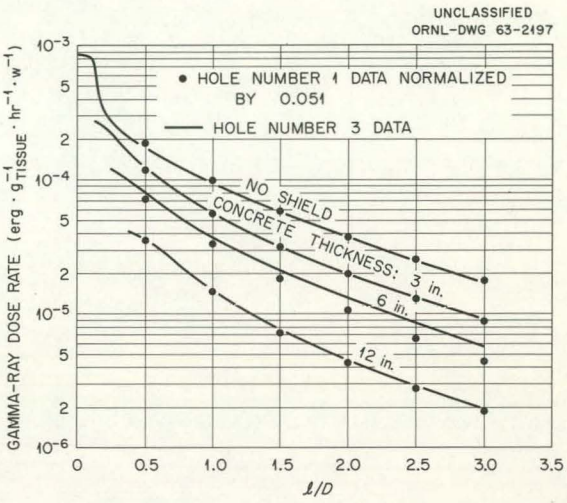

Fig. 102. Comparison of Gamma-Ray Dose Rates in Hole No. 1 and Hole No. 3 as a Function of ℓ/D for Various Thicknesses of Concrete Shield (γ = 15°).

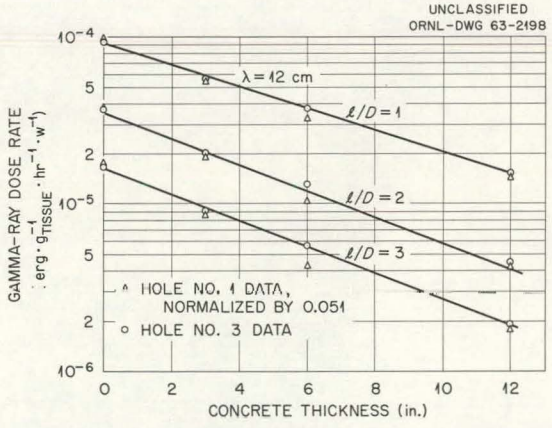

Fig. 103. Comparison of Gamma-Ray Dose Rates in Hole No. 1 and Hole No. 3 as a Function of Concrete Thickness for Various Values of ℓ/D ($\gamma = 15°$).

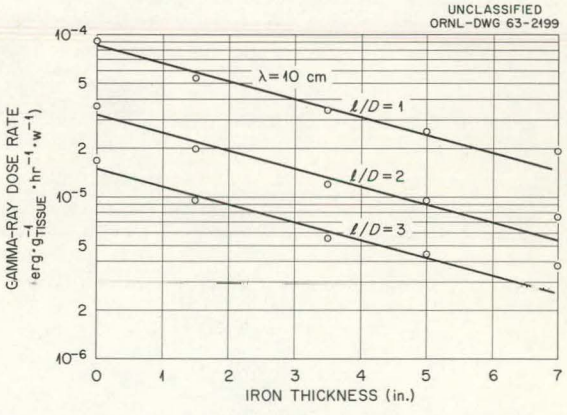

Fig. 104. Gamma-Ray Dose Rate in Hole No. 3 as a Function of the Thickness of an Iron Shield ($\gamma = 15°$).

ORNL-3513
UC-34 – Physics
TID-4500 (26th ed.)

INTERNAL DISTRIBUTION

1. Biology Library
2-4. Central Research Library
5. Reactor Division Library
6-7. ORNL – Y-12 Technical Library Document Reference Section
8-57. Laboratory Records Department
58. Laboratory Records, ORNL R.C.
59. J. A. Auxier
60-61. E. P. Blizard
62-67. V. R. Cain
68. C. E. Clifford
69. B. R. Fish
70. L. B. Holland
71. W. H. Jordan
72. L. Jung
73. C. E. Larson
74. R. T. Santoro
75. M. J. Skinner
76. J. A. Swartout
77. W. E. Thomas
78. A. M. Weinberg
79. R. A. Charpie (consultant)
80. P. F. Gast (consultant)
81. R. F. Taschek (consultant)
82. T. J. Thompson (consultant)
83. M. L. Goldberger (consultant)

EXTERNAL DISTRIBUTION

84. M. Leimdorfer, Forsvarets Forskningsanstalt, Avdelning 4, Research Institute of National Defense, Stockholm 80, Sweden
85. Douglas Bynum, 5311 Wellington Drive, Austin, Texas
86. H. L. Callahan, Black and Veatch, Consulting Engineers, 114 West Gregory Boulevard, Kansas City, Missouri
87-126. Ben Sussholz, Systems Engineering Division, Space Technology Laboratories, A Division of the Ramo-Woolridge Corporation, Post Office Box 45564, Airport Station, Los Angeles, California
127. Neal FitzSimons, Office of Civil Defense, Washington, D.C.
128. Chief of Naval Operations, Navy Department, Attn: OP-754, Washington, D.C.
129-130. Assistant Secretary of Defense (Civil Defense), Attn: Director of Research, Washington, D.C. (1 copy each to W. E. Strope and J. O. Buchanan)
131. Commanding Officer, U.S. Army Combat Developments Command, Nuclear Group, Attn: Major Joseph T. Gibson, Fort Bliss, Texas
132. Chief of Research and Development, Department of the Army, Attn: Lt. Col. D. Baker, Washington, D.C.
133. Chief, Bureau of Ships, Navy Department, Attn: Code 362, Lorenz E. Sieffert, Washington, D.C.
134. Technical Operations, Inc., South Avenue, Burlington, Massachusetts, Attn: E. Clarke
135. R. L. French, Radiation Research Associates, Fort Worth, Texas
136. M. B. Wells, Radiation Research Associates, Fort Worth, Texas
137. H. E. Hungerford, Nuclear Engineering Department, Purdue University, Lafayette, Indiana
138. R. Aronson, Radioptics, Inc., 28 Pilgrim Avenue, Yonkers, New York
139. Defense Atomic Support Agency, TP, Washington, D.C.
140. Defense Atomic Support Agency, CT, Washington, D.C.

141. Defense Atomic Support Agency, ST, Washington, D.C.
142. V. B. Bhanot, Physics Department, Panjab University, Chandigarh-3, India
143. Jacobo Rapaport, University of Chile, Box 2777, Institute of Science, Santiago, Chile
144-203. Office of Civil Defense, DoD, Pentagon, Attn: Director for Research, Washington, D.C.
204-206. Army Library, Civil Defense Unit, Pentagon, Washington, D.C.
207. Assistant Secretary of the Army (R&D), Attn: Assistant for Research, Washington, D.C.
208. Chief of Naval Research (Code 104), Department of the Navy, Washington, D.C.
209. Chief of Naval Operations (Op-07T10), Department of the Navy, Washington, D.C.
210. Chief, Bureau of Naval Weapons (Code RRRE-5), Department of the Navy, Washington, D.C.
211. Chief, Bureau of Medicine and Surgery, Department of the Navy, Washington, D.C.
212. Chief, Bureau of Supplies and Accounts (Code L12), Department of the Navy, Washington, D.C.
213. Chief, Bureau of Yards and Docks, Office of Research (Code 74), Department of the Navy, Washington, D.C.
214. Commanding Officer and Director, U.S. Naval Civil Engineering Laboratory, Attn: Document Library, Port Hueneme, California
215. Advisory Committee on Civil Defense, National Academy of Sciences, Attn: Richard Park, 2101 Constitution Avenue, N.W., Washington, D.C.
216-235. Defense Documentation Center, Arlington Hall Station, Arlington, Virginia
236. Chief of Naval Personnel (Code Pers M12), Department of the Navy, Washington, D.C.
237. Coordinator, Marine Corps Landing Force, Development Activities, Quantico, Virginia
238. Director of Research and Development, Office of Emergency Planning, Washington, D.C.
239-240. Chief, Defense Atomic Support Agency, Attn: Document Library, Washington, D.C.
241-244. Chief, Defense Atomic Support Agency, Attn: Major F. A. Verser, Washington, D.C.
245. Ottawa University, Department of Physics, Attn: L. V. Spencer, Ottawa, Kansas
246. Principal Investigator, Office of Civil Defense, Contract OCD-OS-62-241, National Bureau of Standards, Washington, D.C.
247. Principal Investigator, Office of Civil Defense, Contract OCD-OS-62-145, Atomic Energy Commission, Oak Ridge, Tennessee
248. University of Illinois, Department of Civil Engineering, Attn: A. B. Chilton, Urbana, Illinois
249. Commanding Officer and Director, U.S. Naval Radiological Defense Laboratory, Attn: W. E. Kregar, San Francisco, California
250-251. Commanding Officer, U.S. Army Nuclear Defense Laboratory, Attn: H. Donnert and H. Tiller, Army Chemical Center, Edgewood, Maryland

252. Director, U.S. Army Ballistic Research Laboratory, Attn: F. Allen, Aberdeen Proving Ground, Maryland
253. Charles Eisenhauer, Neutron Physics Division, Brookhaven National Laboratory, Upton, Long Island, New York
254. Kansas State University, Department of Nuclear Engineering, Attn: W. Kimel, Manhattan, Kansas
255. Director of the Reactor Facility, University of Virginia, Attn: T. C. Williamson, Charlottesville, Virginia
256-257. Chemical Laboratories, Defense Research Board, Attn: E. E. Massey and C. E. Clifford, Ottawa, Canada
258. A&M College of Texas, Department of Chemical Engineering, College Station, Texas
259. U.S. Naval Post Graduate School, Department of Physics, Attn: E. Milne, Monterey, California
260. University of Maryland, Department of Chemical Engineering, Attn: J. Silverman, College Park, Maryland
261. Commanding Officer and Director, U.S. Naval Civil Engineering Laboratory, Attn: C. M. Huddleston, Port Hueneme, California
262. Director, Civil Effects Test Group, Atomic Energy Commission, Attn: L. J. Deal, Washington, D.C.
263. Director, U.S. Army Materials Research Agency, Watertown Arsenal, Attn: Dorothy Weeks, Watertown, Massachusetts
264. Commanding General, Tank Automotive Command, Detroit Arsenal, Attn: J. Brooks, Centerline, Michigan
265. Director, U.S. Army Ballistic Research Laboratory, Attn: Document Library, Aberdeen Proving Ground, Maryland
266. Commanding Officer, U.S. Army Nuclear Defense Laboratory, Attn: Document Library, Army Chemical Center, Maryland
267. Commanding Officer and Director, U.S. Naval Radiological Defense Laboratory, Attn: Document Library, San Francisco, California
268. Principal Investigator, Office of Civil Defense, Contract OCD-OS-62-144, Research Triangle Institute, P. O. Box 490, Durham, North Carolina
269. Principal Investigator, Stanford Research Institute, Office of Civil Defense, Contract OCD-OS-62-135, 1915 University Avenue, Palo Alto, California
270. Armour Research Foundation of Illinois Institute of Technology, 10 West 35th Street, Attn: C. Terrell, Chicago, Illinois
271. Brookhaven National Laboratory, Nuclear Engineering Department, Attn: L. P. Hatch, Upton, Long Island, New York
272. Brookhaven National Laboratory, Attn: Document Library, Upton, Long Island, New York
273. U.S. Public Health Service, Attn: Radiological Health Division, Rockville, Maryland
274. Los Alamos Scientific Laboratory, Attn: Document Library, Los Alamos, New Mexico
275. Edgerton, Germeshausen, and Grier, Inc., Attn: Z. Gu. Burson, 300 West Wall Street, Las Vegas, Nevada
276. Headquarters, United States Air Force, AFRDC/NU, Attn: Major E. C. Lowry, Washington, D.C.
277. Chief, Bureau of Yards and Docks, Navy Department, Attn: C-400, Washington, D.C.

278. North Carolina State University, Attn: W. Doggett, Chapel Hill, North Carolina
279. United Nuclear Corporation, Attn: M. Kalos, 5 New Street, White Plains, New York
280. Principal Investigator, General Dynamics/Fort Worth, Fort Worth, Texas
281. Principal Investigator, Technical Research Group, 2 Aerial Way, Syossett, New York
282. Lockheed Missiles and Space Division, Technical Information Center, 3251 Hanover Street, Palo Alto, California
283. Principal Investigator, Office of Civil Defense, Contract OCD-OS-62-14, Technical Operations Research, Burlington, Massachusetts
284. Principal Investigator, Office of Civil Defense, Contract OCD-OS-62-219, Technical Operations Research, Burlington, Massachusetts
285. Research and Development Division, AEC, ORO
286-925. Given distribution as shown in TID-4500 (26th ed.) under Physics category (75 copies – OTS)